Selenoxo Modulation of Oligopeptide Backbone: Synthesis, Photoisomerization and Electronic Effects

Dissertation

zur Erlangung des akademischen Grades

doctor rerum naturalium (Dr. rer. nat.)

vorgelegt der

Naturwissenschaftlichen Fakultät I

der Martin-Luther-Universität Halle-Wittenberg

von

Yun Huang

geboren am 13.06.1982 in Ganzhou, P. R. China

Gutachter:

1. Prof. Dr. Gunter. Fischer, Halle
2. Prof. Dr. Mike. Schutkowski, Halle
3. Prof. Dr. Franz. X. Schmid, Bayreuth

Halle (Saale), 21.02.2013

Table of Content

List of abbreviations

Ac	Acetyl
ACN	Acetonitrile
AIM	Atoms in molecules
AU	Absorption Unit
ART	Attenuated total reflectance
BBO	Broadband probe
Bz	Benzoyl
UV/Vis	Ultraviolet visible
FTIR	Fourier transform infrared spectroscopy
Boc	*tert*-Butyloxycarbonyl
Cyp	Cyclophilin
DCM	Dichloromethane
DIPEA	N,N-Diisopropylethylamine
DMF	Dimethylformamide
DMSO	Dimethylsulfoxide
DTT	Dithiothreitol
equiv.	Equivalent
EtOAc	Ethyl acetate
FKBP	FK506-binding proteins
Fmoc	9-fluorenylmethoxycarbonyl
HATU	1-[Bis(dimethylamino)methylene]-1*H*-1,2,3-triazolo[4,5-*b*] pyridinium 3-*oxid* hexafluorophosphate
hCyp18	Human cyclophilin 18
HPLC	High-performance liquid chromatography
MS	Mass spectrometry
Me	Methyl
NAIP	N-Alkylated indanylidene pyrroline
NMM	N-Methylmorpholine
NMR	Nuclear magnetic resonance
p-HPLC	Preparative high-performance liquid chromatography
PG	Protecting group
PE	Petroleum ether

Ph	Phenyl
PPIase	Peptidyl-prolyl *cis/trans* isomerase
ppm	Parts per million
PSS	Photostationary state
PyBOP	(Benzotriazol-1-yloxy)tripyrrolidinophosphonium hexafluorophosphate
rt	room temperature
Sec	Selenocysteine
SKIE	Solvent deuterium kinetic isotope
SPPS	Solid phase peptide synthesis
tBu	*tert*-Butyl
THF	Tetrahydrofuran
TIS	Triisopropyl silane
TLC	Thin layer chromatography
TFA	Trifluoroacetic acid
Xaa	Amino acids

1. Introduction

1.1 Peptide bond *cis/trans* isomerization

1.1.1 Peptide bond structure and conformation

Peptide bond (amide bond) is the linkage between amino acid residues in peptides and proteins. It plays a fundamental role in protein folding and structure. An electronic interaction between the amide nitrogen lone pair and the carbonyl π system results in a partial double bond character for the C–N linkage such that only two conformations are energetically preferred (Scheme 1.1) (1). The conformations where the dihedral angle ω (C_α-C-N-C_α') is restricted to either 180° or 0° are designated to *trans* and *cis*, respectively. Other properties of the amide group, like a shortened C–N distance, reduced C=O stretching frequency, and reduced nitrogen basicity are also satisfactorily explained by this resonance model (2).
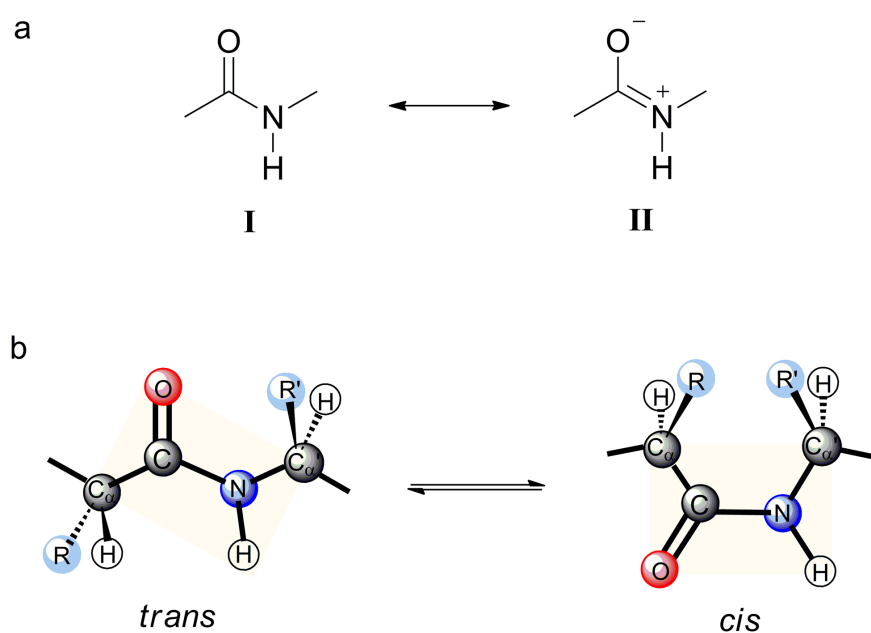
Scheme 1.1 Resonance structures (a) and preferred conformations (b) of a peptide bond

A large number of experimental and theoretical work supports that the spontaneous isomerization of amide bonds occur via a C–N rotation pathway but not via nitrogen inversion (3, 4). The rotational pathway defines transition states that feature a twisted structure with $\omega \approx 90°$, thus disrupting resonance stabilization (Scheme 1.2). The atomic motions involved in the rotation process include C–N bond lengthening, nitrogen and carbon pyramidalization, solvent cage reorganization and bond rotation. Based on

population analysis using the AIM model, Wiberg *et al*. reported that charge redistribution during C−N rotation occurs mainly at the nitrogen and carbonyl carbon atoms, while the charge density at the carbonyl oxygen varies very little (5), indicating the complexity of the amide bond structure.
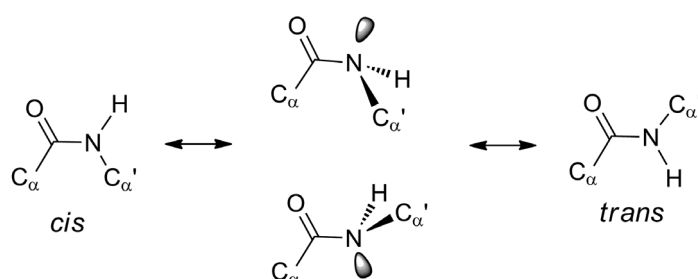
Scheme 1.2 Transition states of peptide bond rotational *cis/trans* isomerization

The majority of the peptide bonds in protein structures are constrained to the *trans* conformation (6) due to a steric repulsion between the alkyl substituents of both sides of the amide moiety in *cis* conformation (Scheme 1.1b). However, surveying the protein structure database has identified a very small part of peptide bonds adopting the *cis* conformation ($\omega \approx 0°$). More precisely, about 6% Xaa-Pro peptide bonds were found in *cis* form (7-10), while only 0.03% of the Xaa-nonPro peptide bonds in *cis* conformation (9). Aromatic residues are highly favored to flank the *cis* peptide bond, where the *cis* conformation is additionally stabilized by CH···π interactions (11-16). The high propensity of peptidyl-prolyl bonds (prolyl bonds) to adopt *cis* conformation is due to the dialkyl substitution on the imide nitrogen, which results in a similar environment of the carbonyl in *cis* and *trans* conformation. Actually, in aqueous solution the prolyl peptide bond populates 6-20% *cis* conformation with a *cis*→*trans* rotational barrier range from 16 to 22 kcal/mol depending on the sequential context (17, 18). For secondary amide peptide bonds, the *cis* population in aqueous solution is generally lower than 0.1%, with a *cis*→*trans* rotational barrier of ~ 16 kcal/mol (19, 20). Free energy differences between the *cis* and *trans* conformations have been reported to be only ~ 0.5 kcal/mol for Xaa−Pro bonds and ~ 2.5 kcal/mol for Xaa−nonPro bonds (7). Based on these values and assuming thermodynamic equilibrium at 20 °C, Xaa−Pro bonds should populate about 30% *cis* conformation (21), and Xaa−nonPro bonds should populate about 1.5% *cis* conformation (22). These numbers are much larger than the values obtained from statistical analysis of protein structure database. Notably, the *cis* peptide bond was found more abundant in high resolution crystal structures, indicating

that the *cis* peptide bond is probably under-accounted due to inappropriate refinement in the low resolution structures (9).
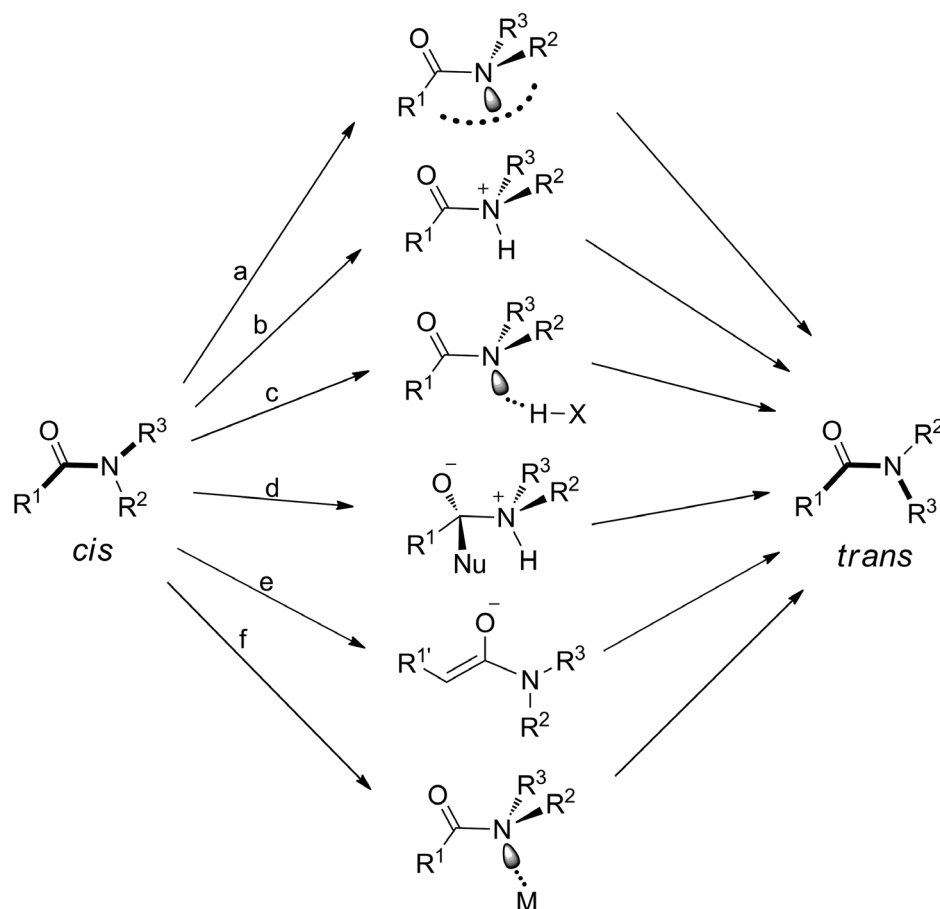
Figure 1.1 Nonenzymatic catalysis of peptide bond *cis/trans* isomerization. Catalysis by a hydrophobic environment that stabilizes a more apolar twisted transition state (a), by N-protonation (b), by intramolecular H-bonding to N (c), by nucleophilic attack on carbonyl carbon (d), by base via an enolate anion (e), and by metal coordination (f).

1.1.2 Chemical and enzymatic catalysis of *cis/trans* isomerization

The *cis/trans* rotational barrier is strongly influenced by the solvent. For instance, by changing the environment from a nonpolar aprotic solvent to water, the rotational barrier increased by up to 3 kcal/mol (23). This effect was rationalized by a selective stabilization of the more polar ground states in water. In addition, several ways are found to catalyze the amide bond *cis/trans* isomerization (Figure 1.1). Brønsted acids are able to catalyze amide *cis/trans* isomerization through a small but kinetically significant quantity of N-protonated intermediate (24), although the oxygen atom is the preferred site of protonation in amides (25). Intramolecular hydrogen bonding to the amide nitrogen has also been shown to catalyze the *cis/trans* isomerization (26). Furthermore, nucleophilic attack was found to

catalyze the *cis*/*trans* isomerization (27) and has been proposed to be involved in the catalytic cycle of PPIases (28). In addition, strong bases like sodium methoxide can catalyze the *cis*/*trans* isomerization by deprotonation of the C_α proton (29). Finally, metal ions are also able to catalyze the *cis*/*trans* isomerization in case the nitrogen coordinates to metal ions (30).

Hindered peptide bond rotation (ω) along with mobile single bonds (φ, ψ) on either side of the peptide unit is fundamental to the formation of the three-dimensional structure of proteins. Due to the considerably slow *cis*/*trans* isomerization of peptide bonds compared with the single bond rotation, the presence of a *cis* peptide bond remarkably retards the folding process. A general possibility to accelerate peptide bond *cis*/*trans* isomerization in bioorganisms is enzyme catalysis. In fact, nature has devised ingenious enzymes to catalyze the peptide bond rotation. The first family was found to catalyze the *cis*/*trans* isomerization with substrate specific to peptidyl-prolyl bonds (PPIase) (31, 32). Currently, the PPIase family comprises three members: cyclophilins, FK506 binding proteins (FKBP), and parvulins (33). These three PPIase members have distinct substrate specificities and are sensitive to different types of inhibitors. The second family (APIase) has been identified in the Hsp70 protein DnaK, which selectively accelerates the *cis*/*trans* isomerization of secondary amide bonds (34). PPIases are widely distributed throughout all living organisms including *Mycoplasma genitalium*, a bacterium that possesses the smallest known genome of any freely self-replicating organism (35). The high diversity and ubiquitous occurrence of PPIases suggest that they have multiple cellular functions. The APIase function of Hsp70 molecular chaperones is considered to allow kinetic proofreading of folding by rapid scanning of APIase-sensitive sites of unfolded polypeptide chains (18).
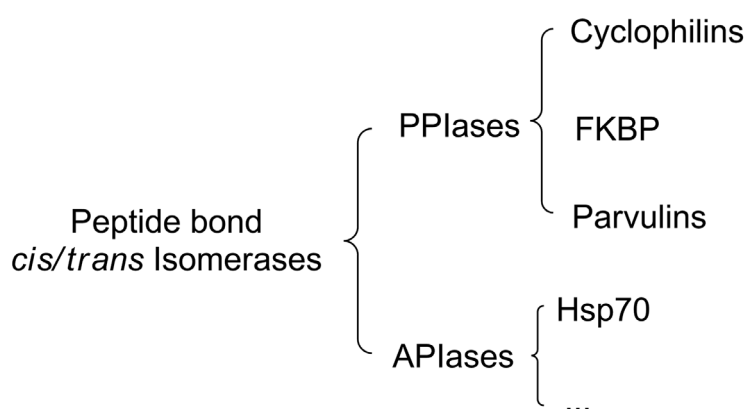
Scheme 1.3 Enzymes found to catalyze peptide bond *cis*/*trans* isomerization

1.2 *Cis*/*trans* isomerization in protein folding and function

The prolyl bond *cis*/*trans* isomerization, due to its rather slow rate, has long been recognized as a rate-limiting step in the folding/unfolding pathway of many proteins (36-40).

$$U \xrightarrow{\text{fast folding}} I \xrightarrow{\substack{\text{slow proline} \\ \text{isomerization}}} N$$
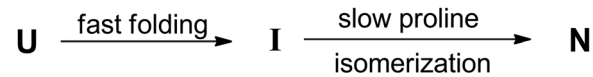
With the discovery of PPIases, those slow folding and unfolding processes were found to be enzymatically catalyzed (41-44). Mutation of the proline to a non-proline residue showed a decrease of the conformational stability and a change of the folding kinetics (45-47). A *cis* peptide bond was also reported to speed up the fast folding phase in phosphoglycerate kinase, probably due to the restriction of conformational space accessible to the molecule (48). Using the Pro39Ala variant of ribonuclease T1, which retains a *cis* peptide bond between Tyr[38] and Ala[39] in the native state, Schmid *et al.* showed that slow *cis*/*trans* isomerization of this secondary amide peptide bond is also a rate-limiting step in protein folding and unfolding (49).

The *cis* conformation reverses the local orientation of the main chain and leads to a significant shrinking of the atom distance between C_{i-1}^{α} and C_{i}^{α} (Xaa_{i-1}–Pro_i) compared to the *trans* conformation. Moreover, this one bond-mediated conformational change could be amplified by a lever-arm effect (50). On the molecular scale, the *cis*/*trans* isomerization has been found to be able to trigger a conformational switch, by which it functions like a molecular switch or timer to regulate protein function (51). For example, in the cell signaling protein Interleukin-2 tyrosine kinase (Itk), Pro287 undergoes CypA-catalyzed *cis*/*trans* isomerization. The *cis*-Pro-containing SH2 conformer exhibits a 3.5-fold higher affinity to the Itk SH3 domain compared with the *trans* conformer binding to the same ligand, while the *trans*-Pro-containing SH2 conformer binds phosphopeptides with a 4-fold greater affinity than the *cis* conformer (Figure 1.2). Thus, the *cis* and *trans* prolyl bonds of the Itk SH2 domain mediate separate, specific binding events that may have functional implications in T cell signaling (52, 53). Moreover, *cis*/*trans* isomerization has been shown to be implicated in neurodegeneration (54), amyloid formation (55), channel gating (56) and phage infection (57). Interestingly, peptide bond *cis*/*trans* isomerization has been suggested as a key stage in the chemo-mechanical cycle of motor proteins (58).
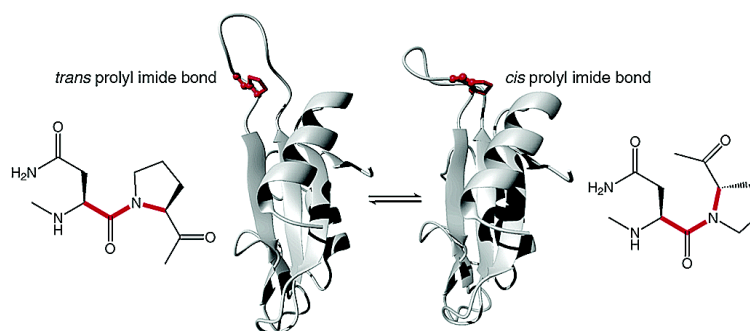
Figure 1.2 Proline-driven conformational switch in the Itk SH2 domain. The prolyl bond in the loop adopts different conformations thus regulates the molecular recognition of Itk (52).

1.3 Photocontrol of backbone conformation in peptides and proteins

The ability of proteins to undergo conformational switching is central to protein function (59, 60). Such a conformational change can be initiated by many factors such as a change in temperature, pH, voltage, ion concentration, phosphorylation, reduction potential, binding of a ligand, etc. (61, 62). Interestingly, nature has already used light as a trigger to control protein structures. For instance, rhodopsin uses light-triggered *cis/trans* isomerization of retinal to induce the conformational movement of the opsin, which is coupled with a neuron action potential (63). The phytochrome can also undergo conformational switch by light (64).

Photoisomerization, which conducts a conformational switch of a chromophore by light, is an appealing approach because the light of appropriate wavelength may not damage the system under study and can be used remotely and noninvasively. The high resolution with which light can be manipulated both temporally (fs) and spatially (μm) makes it possible to investigate fast processes such as protein folding. Methods of photocontrol from molecule to cell level have seen explosive growth (65-68). Photocontrol of protein backbone conformation is of great interest, due to its unique roles in protein folding and function. While a large number of studies conducted photocontrol by introducing a chromophore to protein side chain (69-73), much less attention was paid on photomodulation of the protein backbone, due to the difficulty of incorporating a chromophore into the backbone and the concomitant worse structural compatibility of the large chromophores with the protein conformation.

To photocontrol the polypeptide backbone, the chromophores have to meet the following requirements: (i) the photoswitchable moiety has to show two different isomeric forms that can be transformed into each other using different wavelengths of light; (ii) the wavelengths

should be no less than the absorption of the peptide bond itself; (iii) the photoreaction should be reversible and the reaction rate has to be fast if a light-induced chemical transformation is used in time-resolved experiments; (iv) the molecular switch should be able to induce strong force on the attached peptide chain to exert a conformational rearrangement upon irradiation; (v) the photochemical quantum yield should be sufficiently high and the side reactions should be negligible; (vi) importantly, the trigger molecule should be structure-compatible, which means that at least one of the conformations of the chromophore can adopt a similar structure as the unmodified one.

Azobenzene and stilbene derivatives are prominent examples used to design backbone photoswitchable peptides (74, 75). For instance, the azobenzene (Figure 1.3a) has been used to mimic a turn structure and study the folding and refolding of the beta-hairpin (76, 77). It has also been incorporated to the amyloid-β to study the turn nucleation in amyloid-β self-assembly (78, 79). Moreover, a computational designed N-alkylated indanylidene pyrroline (NAIP) moiety (Figure 1.3b) has also been used to photoswitch a cyclic peptide (80). Very recently, thehemithioindigo–hemistilbene system (Figure 1.3c) has been incorporated to the backbone of linear and cyclic peptides and their photoproducts were formed in the range of 10-30 ps (81, 82).
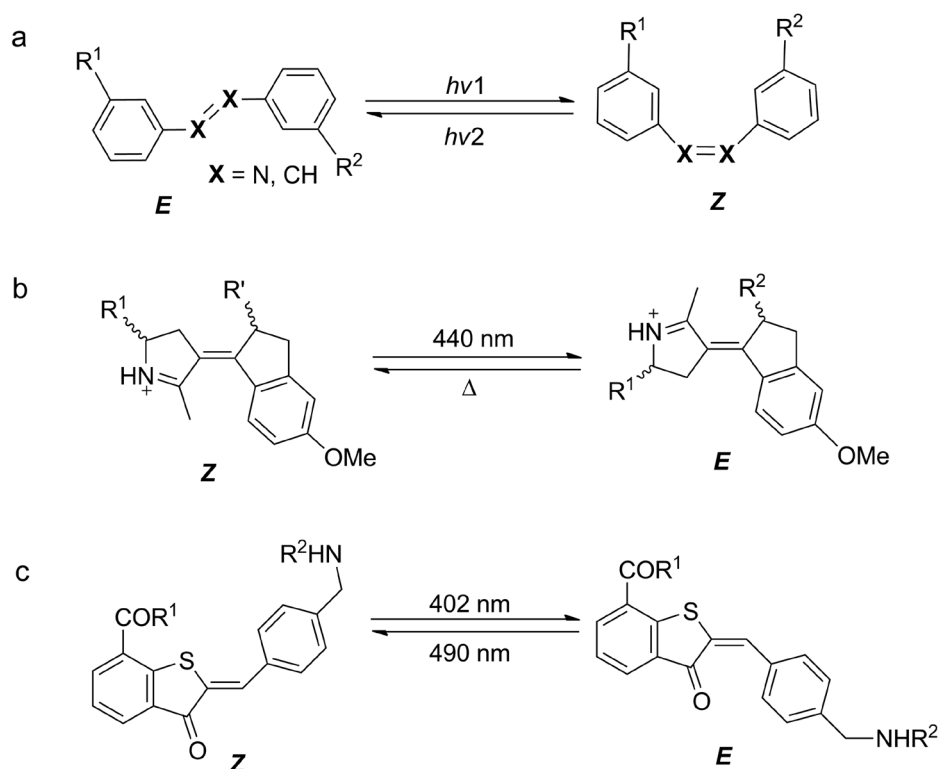
Figure 1.3 Photoswitching of the peptide backbone via azobenzene (X = N) or stilbene (X = CH) derivatives (a), N-alkylated indanylidene pyrroline (NAIP) derivatives (b) and hemithioindigo-based derivatives (c).

1.4 Thioxo peptide bonds and their application on photocontrol of peptide backbone conformations

Unfortunately, all azobenzene, stilbene, NAIP and hemithioindigo-based moieties are rather large compared to the amide bond in the peptide backbone and thus disrupt the hydrogen bonding network of the original amide bond. Moreover, their large aromatic systems may cause a poor aqueous solubility, which may be an issue for biochemical applications. Therefore, photoswitches with better structural compatibility are needed. Notably, the peptide backbone itself could be switched from *trans* conformation to *cis* by UV light irradiation (83, 84). However, the high energy of the excitation light (206 nm), which leads to a photo-decomposition, and the non-selectivity render it not applicable for site-specific protein conformational control. Remarkably, a simple oxygen to sulfur one-atom substitution allows the resulted thioxo peptide bond [CS–NH] to be selectively switched from the *trans* conformation to *cis* by using UV light near 260 nm, without any influence on the non-modulated peptide bonds (85, 86).
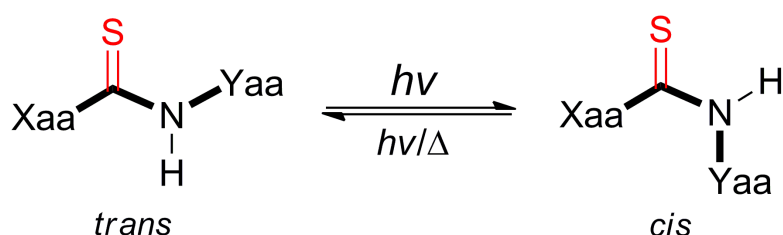
Scheme 1.3 Photoisomerizatoin of the thioxo peptide bond. The *trans* conformation can be stimulated to *cis* by ~260 nm irradiation. The *cis* conformation can return to *trans* by thermal decay or 291 nm irradiation (86).

The thioxo peptide bond is an isostere of the regular amide bond. It preferentially adopts a *trans*-planar conformation featuring shorter C–N distance but longer C=S distance, resulting in an increased C–N rotational barrier by ~3 kcal/mol (87). The thioxo amide proton is more acidic than regular amide and hence is a stronger hydrogen bond donor, whereas the thioxo carbonyl sulfur is a slightly weaker hydrogen bond acceptor than regular amide (Scheme 1.4) (88-90). Hence, the special hydrogen bond accepting and donating ability of the thioxo peptide bond makes it very useful to probe molecular interactions. For example, a thioxo scan has been employed to investigate the backbone interactions in the transition state of a coupled protein folding and binding reaction (91). Therefore, it is not surprising that the thioxo peptide bond is shown to be compatible for helix (92-95), turn (96-99) and hairpin (100) secondary structures, though a slight destabilizing effect of an α-

helix has been observed (101). The thioxo analogues of bioactive peptides showed a generally enhanced resistance toward proteases (102-105) and diverse biological effects (106-110). Conformational energy and free energy calculations of thioxo peptide bonds suggest that they are conformationally more restricted than the regular peptide bonds (111, 112). Therefore, the excellent bio-compatibility of the thioxo group renders it an excellent photoswitch to backbone conformational control.

Amides

bond length *ca.* 1.24 Å
bond energy *ca.* 170 kcal/mol
VDW radius 1.52 Å

$$O$$
$$R_1 \quad N^{-R_2}$$
$$H \longleftarrow pK_a \, ca. \, 17$$

170-195 nm (π-π* transition)
210-220 nm (n-π* transition)

Thioxo amides

250-280 nm (π-π* transition)
340-400 nm (n-π* transition)

VDW radius 1.80 Å
slightly weaker H-bond acceptor than O

bond length *ca.* 1.65-1.68 Å

$$S$$
$$R_1 \quad N^{-R_2}$$
$$H \longleftarrow$$ stronger acid (pK_a 11-13)
stronger H-bond donor

increased barrier of rotation
by 2-3 kcal/mol

-enhanced stability towards various proteases
-restriction of conformational freedom
-enhanced polarity

Scheme 1.4 Comparison between amides and thioxo amides (Ref. 92).

An oxygen to sulfur substitution leads to a drastic red shift of the π-π* and n-π* transition to ~260 and ~330 nm, respectively. The *trans→cis* photoisomerization can be efficiently triggered by UV light at 254 nm, resulting in a red shift of the UV absorption (Figure 1.4a). The *cis→trans* thermal decay lasts from minutes in thioxo amide bonds to hours in thioxo imide bonds (85, 86). The *cis→trans* isomerzation can be accelerated by 290 nm irradiation and further by 310 nm irradiation (Figure 1.4b) (86). Quantum efficiency for *trans→cis* photoisomerization is 30-40% without wavelength dependence, while the *cis→trans* photoisomerization proceeds with 60-70% quantum efficiency (113).
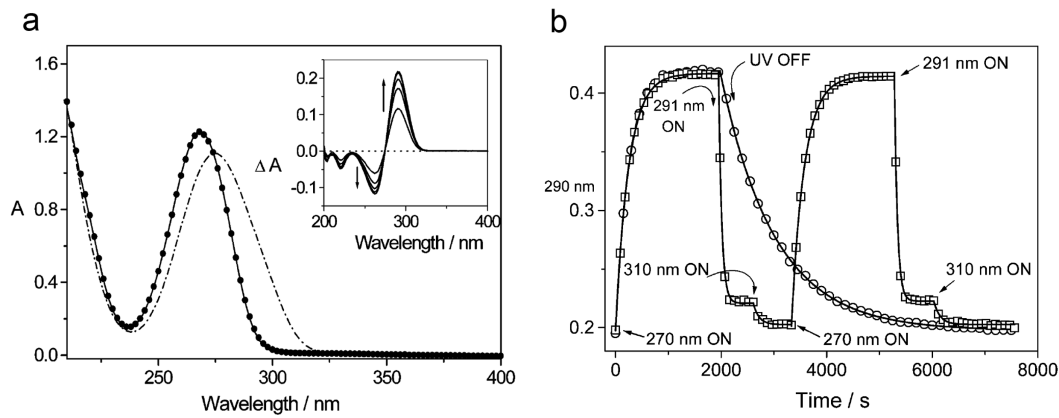
Figure 1.4 UV/Vis spectroscopic behavior of thioxo peptide bond upon photoisomerization (114). (a). UV/Vis spectrum of Phe-ψ[CS-NH]Ala before irradiation (solid line), after irradiation (254 nm, 3 min) (dot-dash line) and after re-equilibration (dots). Inset: the difference spectrum during irradiation (*cis* isomer has a stronger absorbance in the 275–325 nm region, which was a maximum at 290). (b). Dual-directional photoswitching monitored at 290 nm. Two runs are presented (270 nm irradiation and UV switch off: circles; 270 nm irradiation, 291 nm irradiation, 310 nm irradiation: squares). Irradiation wavelength changes are marked on the curves. The solid lines represent nonlinear single exponential fits. Measurements are performed in sodium phosphate buffer, pH 7.0, 16 °C. Figures are taken from Ref. (114).

The *cis/trans* photoswitching of the thioxo group finishes within a few hundred picoseconds (115) and has been applied to probe the ultrafast breaking and formation of hydrogen bonds as well as conformational dynamics (116-119). Wildemann et al. have shown that reversible photoswitching the thioxo peptide bond in ψ[CS–NH]^4-S peptide bound to S-protein leads to a reversible control of the ψ[CS–NH]^4-RNase S enzyme activity (Figure 1.5) (120). A similar approach provided clear evidence for a *cis*-prolyl-preferred binding of Phe-Tyr-ψ[CS–NH]Pro-Trp-Gly-NH$_2$ with the insect kinin receptor (121). The unique hydrogen bonding ability of thioxo peptide bond coupled with a photoswitchable property makes it a promising tool for the study of protein structure and function. However, the high-energy 254 nm UV light used for photoswitching and the relatively fast *cis* to *trans* decay may limit the application of thioxo photoswitch in some cases.
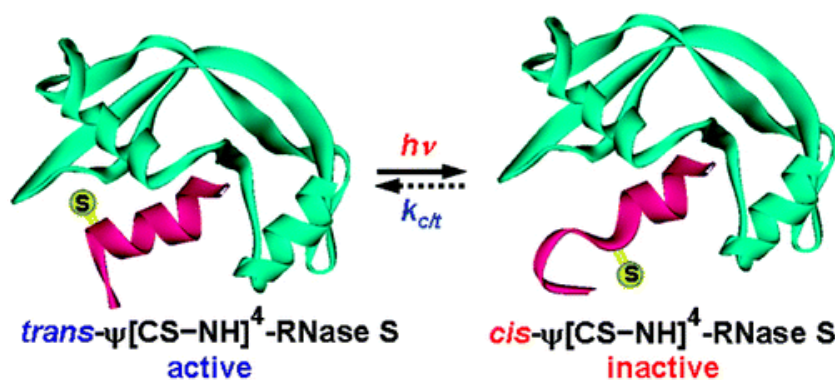

Figure 1.5 Reversible control of ψ[CS-NH]^4-RNase S enzymatic activity by photoswitching the ψ[CS-NH]^4-S peptide conformations (120).

1.5 Selenoxo amides and their potential as a photoswitch

Selenium is a heavier element than sulfur in the chalcogen group and represents an essential trace element in animals, including humans. The selenium-substituted analogue of cysteine, selenocysteine (Sec or U), was identified as the 21st proteinogenic amino acid (122, 123). Selenocysteine is often found in enzymatic active sites, where the selenol group functions either as a nucleophile, as a metal ligand or as a redox element (124, 125). For instance, glutathione peroxidase was the first selenoprotein identified in mammals (126). It protects cells from oxidative damage by catalyzing the reduction of H_2O_2 and other organic peroxides (125, 127). The catalytic cycle of glutathione peroxidase is considered to include an oxidation of a Sec selenol group by hydroperoxide to form a selenenic acid, which is further converted to a selenenylsulfide by glutathione. The selenenylsulfide bond is then reduced by an additional glutathione and thus regenerates a selenol group at the Sec residue of the enzyme (Scheme 1.5) (128).
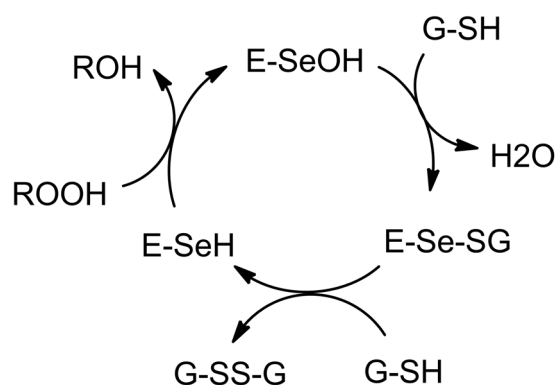
Scheme 1.5 The general mechanism of glutathione peroxidases (128).

Table 1.1 Comparison of chalcogen atomic properties

Properties	Oxygen	Sulfur	Selenium	Tellurium
Van der Waals radius r_{VDW} (in Å) (129)	1.52	1.80	1.90	2.06
Electronegativity χ (Pauling scale) (1)	3.44	2.58	2.55	2.1
Polarizability α (in Å^3) (129)	0.80	2.90	3.77	5.5
Redox potential (mV) [a] (130)	n.a.[c]	-233	-488	n.a.[c]
pK_a [b] (131)	n.a.[c]	8.3	5.2	n.a.[c]

[a] versus the normal hydrogen electrode (NHE)

[b] values from Cys and Sec

[c] not available

While the special role of selenol functional group of Sec in peptides and proteins is well documented, the selenoxo carbonyl C=Se has never been studied in polypeptide systems. Due to the weak double bond character and strong nucleophilicity of selenium, the selenoxo carbonyl group is unstable and prone to polymerization (132). Steric or resonance stabilization from neighboring groups is required to form stable selenoxo compounds (133). Selenoxo amides for example have proved to be very useful compounds in organic transformations, but the high reactivity makes them unstable in solution especially in case of the aliphatic selenoxo amides (134-136). Thus, the compatibility between selenoxo substitution and peptide synthesis protocols has never been investigated, and selenoxo peptides have not been reported so far.

Despite the difficulty to construct selenoxo amide bonds and the reported instability, the unique features of thioxo peptides prompted us to explore the world of the selenium-substituted peptide bond analogue (i.e. selenoxo peptide bond or selenoxo amide bond). Fortunately, the recent development of a new selenation reagent, Woollins' reagent (137, 138), has provided great benefit to the synthesis of selenoxo amides (139, 140). Previous theoretical and experimental work of selenoxo amides has shown that the C–N bond is shorter than that in thioxo amides, whereas the C–Se bond is longer than that in thioxo amides. Moreover, the selenoxo amides favor a *Z* conformation but more planar than thioxo amides (141-145). These features were explained by an increased partial double bond character in the C–N bond, owing to an enhanced delocalization of the nitrogen lone pair electrons to the C=Se group (146). The structural properties of chalcogen-substituted amides indicated an increased C–N double bond character in the order of O < S < Se < Te (Figure 1.6). However, the extreme instability of the telluroxo amides makes them unfeasible for biochemical application.
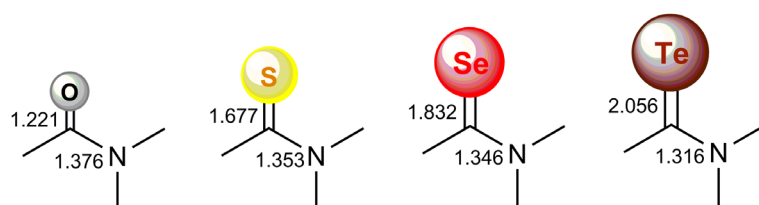
Figure 1.6 Bond lengths of chalcogen-substituted amides (141, 142)

The rotational barrier of selenoxo amide is generally ~1 kcal/mol higher than that of thioxo amides (146-148). The UV absorption wavelengths of the selenoxo amides are located

around 290 nm and 350 nm for the $\pi-\pi^*$ and $n-\pi^*$ transitions, respectively (149), which are shifted to longer wavelengths compared to thioxo amides. As the thioxo amide bonds in peptides have shown a reversibly photoswitchable property, the selenoxo amide bonds are expected to be photoswitchable as well. Moreover, a longer excitation wavelength and a longer lifetime of the *cis* isomer compared to the corresponding thioxo congeners are anticipated.

2. Aims and objectives

In order to investigate the photoswitching activity of selenoxo peptide bonds and their influence on peptide structure, this work focuses on:

- synthesizing selenoxo peptides with high enantiopurity and studying their chemical properties including the stability in aqueous solution;

- characterizing the photoswitching properties of selenoxo peptides, such as excitation wavelength, *cis* content in the photostationary state, thermodynamic parameters of *cis*→*trans* decay, and comparing them to the corresponding thioxo peptides;

- evaluating the electronic effects of selenoxo substitution imposed on peptides, such as nuclear shielding of the surrounding atoms, amide proton acidity, C−N rotational barrier, n···π* interaction and NH···π interaction.

3. Materials and methods

3.1 General information

Reagents: All reagents, amino acids, and solvents were purchased from commercial suppliers and used without further purification. Amino acids were purchased from Merck-Novabiochem or Bachem. Acetonitrile (HiPerSolv CHROMANORM® isocratic grade) was purchased from VWR. Other chemicals including Woollins' reagent were purchased from Sigma Aldrich (p.a. grade). Resins were purchased from Merck-Novabiochem. Human Cyp18 was laboratory-produced.

Thin layer chromatography (TLC) was carried out with Merck TLC silica gel 60 F_{254}.

Column chromatography was conducted with Merck silica gel 60 (0.040–0.063 mm, 230–400 mesh ASTM).

Analytic HPLC was performed on a SYKAM HPLC system equipped with LiChroCART® (Merck) 125-4 RP8 (5 μm) column; flow rate: 1 ml/min; standard linear gradient from 5% to 100% B (A: 0.05% TFA/H_2O, B: 0.05% TFA/ACN) in 30 min; detection wavelength: 220 nm. In the case of enantiopurity analysis, a GRACE Vydac® 208TP54, C8, 5 μm, 4.6 × 250 mm column and isocratic elution were used.

Preparative HPLC was performed on a SYKAM HPLC system equipped with LiChrosorb® (Merck) 250-25 RP8 (7 μm) column; flow rate: 15 ml/min; (A: 0.05% TFA/H_2O, B: 0.05% TFA/ACN)

Solid phase peptide synthesis (SPPS): Standard Fmoc protocol and PyBOP/DIPEA coupling system were used. In the case of thioxo peptides, a modified protocol was employed. Peptide amides were synthesized on Sieber amide resin or 2-Chlorotrityl resin. Peptide acids were synthesized on Sasrin resin or Wang resin.

NMR spectroscopy: Spectra were recorded using Bruker DRX 500 spectrometer equipped with a 5 mm ^{1}H/^{13}C/^{15}N triple-resonance probe or a 5 mm BBO probe. ^{1}H and ^{13}C chemical shifts were referenced to external 2,2-dimethyl-2-silapentane-5-sulfonate; ^{77}Se chemical shifts were referenced to external selenous acid at 1300.0 ppm (150). For chemical shift assignments, standard 2D ^{1}H/^{1}H-TOCSY, ^{1}H/^{1}H-ROESY and ^{1}H/^{13}C-HSQC spectra were collected with the carrier placed in the center of the spectrum on the water resonance, which

was suppressed by applying either presaturation or a WATERGATE sequence. Standard 1D ^{77}Se-NMR spectra were collected with a relaxation delay of 3 s.

Mass spectrometry

The identity of the peptides and intermediates was verified by electrospray ionization mass spectrometry on a VG-BIO-Q Triple Quadrupole Tandem Electrospray mass spectrometer (Fisons Instruments, San Carlos, CA) and a MALDI-Tof Reflex mass spectrometer (Bruker Daltronik)

Infrared spectroscopy

ATR-FTIR spectra were recorded using FTIR Tensor 27 spectrometer (Bruker) equipped with a BIOATR II cell and a MCT detector that was cooled with liquid nitrogen. 10 µl of the peptide samples in THF solution (peptide concentration: 1-5 mg/ml) were placed onto the crystal of the ATR cell. Collected spectra represent averages of 64 scans (resolution 2 cm^{-1}).

UV/Vis spectroscopy

Measurements were performed on a Hewlett Packard 8453 Diode Array UV/Vis spectrophotometer where an integration time of 0.2 s was set for spectra acquisition, or on a Perkin Elmer Lambda 900 UV/Vis/NIR spectrometer where the slit width was set to 0.2 nm and the integration time was set to 1 s. Quartz UV cells of 1 cm path length were used for all measurements. The temperature was controlled by water circulating through a thermostat.

Photoisomerization

Peptide solution in a quartz cuvette (1 cm) was irradiated by UV light using a home-assembled monochromatic light source (Figure 3.1). The optical building block includes a Hamamatsu L2423 200 W Mercury-Xenon lamp housed in a E7356 lamp housing (Hamamatsu Photonics, Japan) and a PTI 101 monochromator (Photon Technology International, Inc. USA). Slit width of the monochromator was set to 6 mm. The temperature of the sample holder was controlled by water circulating through a thermostat. In the case of thioxo peptides, direct irradiation using a 254 nm UV lamp was sometimes applied. (Care must be taken since the high-energy UV light is harmful to eyes and skin!)
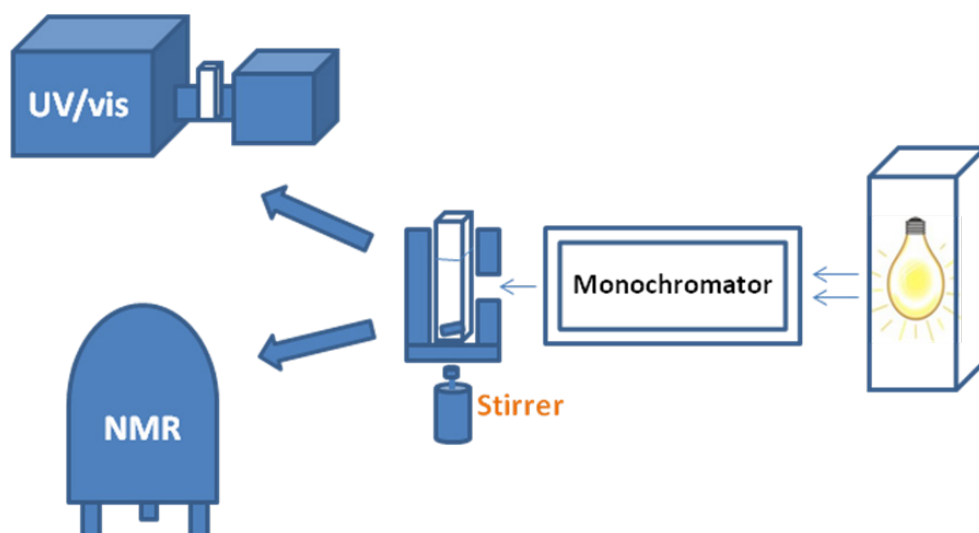
Figure 3.1 Apparatus used for photoirradiation

3.2 Experimental part

3.2.1 Solution phase synthesis

3.2.1.1 Synthesis of Fmoc-Ala-ψ[CS-NH]-6-nitro-benzotriazole

Fmoc-Ala-2-amino-5-nitroanilide (The same procedure as dipeptide synthesis)

N-Methylmorpholine (2.2 ml, 20 mmol) was added to a solution of Fmoc-Ala-OH·H_2O (3.2 g, 10 mmol) in THF (100 ml) at -20 °C, followed by dropwise addition of isobutyl chloroformate (2.6 ml, 20 mmol). The mixture was stirred for 10 min, then 4-nitro-1,2-phenylenediamine (1.53 g, 10 mmol) was added, and the resulting slurry was stirred at -20 °C for 1 h and at rt for 3 h. The precipitate was filtered off and the filtrate was evaporated to dryness. The residue was washed with EtOAc (250 ml) and the insoluble yellow solid was collected as pure product. The eluate was collected and washed successively with 1 M NaH_2PO_4, brine, 5% $NaHCO_3$, and brine again, and then dried with $MgSO_4$ and evaporated to dryness. The yield was 72%.

Fmoc-Ala-ψ[CS-NH]-2-amino-5-nitrothioanilide

P_4S_{10} (0.44 g, 1 mmol) was mixed with Na_2CO_3 (0.108 g, 1 mmol) in THF (100 ml). The mixture was stirred under an argon atmosphere for 1 h at rt and then cooled to 0 °C. To this clear solution was added Fmoc-Ala-2-amino-5-nitroanilide (2 mmol), and the reaction

mixture was stirred at 0 °C for 30 min and then at rt for 2.5 h. The mixture was filtered and the filtrate was evaporated to dryness. The residue was dissolved in EtOAc and washed with 5% NaHCO$_3$ (2 × 30 ml) and the aqueous layers were back-extracted with EtOAc (75 ml). The combined organic layers were washed with brine, dried over MgSO$_4$, and evaporated to yellow solid. Further purification could be conducted with silica gel column chromatography.

Fmoc-Ala-ψ[CS-NH]-6-nitrobenzotriazole

To a solution of Fmoc-Ala-ψ[CS-NH]-2-amino-5-nitrothioanilide (0.5 mmol), dissolved by gentle warming at 40 °C and then cooled to 0 °C in glacial acetic acid (30 ml), NaNO$_2$ was added (0.052 g, 0.75 mmol) in portions over 5 min under constant stirring. After 30 min, ice-cold water (100 ml) was added and the precipitated product was filtered and washed thoroughly with water. The orange solid was dried in vacuo at rt overnight and used in coupling without further purification.

3.2.1.2 Synthesis of Bz-Val-Gly-OH

Bz-Val-Gly-OtBu solid was treated with 50% TFA/DCM for 30 min and evaporated to oil. To this flask was added cold Et$_2$O and the white precipitate was washed 3 times with cold Et$_2$O. After evaporation under reduced pressure, the pure product was obtained.

3.2.1.3 Synthesis of thioxo peptides (Representative procedure)

Boc-Ala-ψ[CS-NH]Ala-OMe

Boc-Ala-Ala-OMe (137 mg, 0.5 mmol) was dissolved in 10 ml dry benzene and, after addition of Lawesson's reagent (0.5 equiv.), the resulting heterogeneous mixture was refluxed for 2 h under argon atmosphere. The solvent was evaporated under reduced pressure. The residue was dissolved in EtOAc and washed with NaHCO$_3$ and brine. The organic layer was dried with MgSO$_4$ and then evaporated to oil. Further purification was performed by p-HPLC with a yield of 75%.

Procedure for Boc deprotection

To a flask containing Boc-Ala-ψ[CS-NH]Ala-OMe (109 mg), ZnCl$_2$·Et$_2$O solution (1 mol/l, 5 ml) was added. The mixture was stirred for 5 hours at rt and then evaporated to oil under reduced pressure. To this flask was added 1 ml acetonitrile and the precipitate was extracted

with additional acetonitrile (1 ml × 2). The extract was collected and evaporated to oil. The product was purified by p-HPLC (RP18) with a yield of 53%.

Procedure for coupling

38 mg (0.2 mmol) H-Ala-ψ[CS-NH]Ala-OMe and 57 mg (0.21 mmol) Bz-Val-Gly-COOH were dissolved in dichloromethane. To this solution 104 mg (0.2 mmol) PyBOP were added, followed by 69 μl (0.4 mmol) DIPEA to trigger the coupling reaction. The product was isolated by p-HPLC (RP8) with a yield of 66%.

3.2.1.4 H-Trp-ψ[CS-NH]Leu-OH

Boc-Trp(Boc)-Leu-OtBu (863 mg, 1.5 mmol) was dissolved in 15 ml dry benzene and, after addition of Lawesson's reagent (610 mg), the resulting heterogeneous mixture was refluxed for 2 h under argon atmosphere. The solvent was evaporated under reduced pressure. The residue was dissolved in EtOAc and washed with $NaHCO_3$ and brine. The organic layer was dried with Na_2SO_4 and then evaporated to oil. To this flask was added 10 ml 50% TFA/2.5% TIS/2.5% H_2O/DCM. After 30 min, the solution was evaporated to oil and subjected to p-HPLC purification (RP8). After lyophilization, the pure product H-Trp-ψ[CS-NH]Leu-OH was obtained as white solid with an overall yield of 41%.

3.2.1.5 Synthesis of selenoxo peptides (representative procedure)

Boc-Ala-ψ[CSe-NH]Ala-OMe

Boc-Ala-Ala-OMe (300 mg, 1.1 mmol) was dissolved in dry toluene and, after addition of 190 mg Woollins' reagent (0.5 equiv.), the resulting heterogeneous mixture was refluxed for 2 h under argon atmosphere. The solvent was evaporated under reduced pressure. After p-HPLC (RP8) purification and lyophilization, the pure product was obtained as brown solid with a yield of 37%.

H-Ala-ψ[CSe-NH]Ala-OMe

To a flask containing Boc-Ala-ψ[CSe-NH]Ala-OMe (25 mg) was added 1 ml $ZnCl_2 \cdot Et_2O$ solution (1 mol/l). The reaction mixture was stirred under argon atmosphere for 5 h at rt and then evaporated to oil under reduced pressure. To this flask was added 0.5 ml acetonitrile and the precipitation was extracted with additional acetonitrile (1 ml × 2). The extract was

collected and evaporated to oil. The product was isolated by p-HPLC (RP18) with a yield of 69%.

Bz-Val-Gly-Ala-ψ[CSe-NH]Ala-OMe

Bz-Val-Gly-OH (14 mg) was dissolved in THF and cooled down to -20 °C. To this solution N-methylmorpholine (11.2 µl) was added, followed by isobutyl chloroformate (6.7 µl). After 3 min, a precooled solution of H-Ala-ψ[CSe-NH]Ala-OMe (12 mg) in THF was added. The mixture was stirred 1h at -20 °C and then 1 h at rt. The precipitate was removed by filtration and the filtrate was evaporated under reduced pressure. The product was purified by p-HPLC (RP8) and lyophilized to yield 16 mg light yellow floccules.

3.2.1.6 H-Trp-ψ[CSe-NH]Leu-OH

Boc-Trp(Boc)-Leu-OtBu (863 mg, 1.5 mmol) was dissolved in dry toluene and, after addition of 450 mg Woollins' reagent (0.53 mmol), the resulting heterogeneous mixture was refluxed for 2 h under argon atmosphere. The reaction mixture was filtered and the solvent was evaporated under reduced pressure. The slurry was re-dissolved with EtOAc and washed with $NaHCO_3$ and brine. The organic layer was dried and evaporated to oil, to which 30 ml 50% TFA/5% TIS/DCM was added. After 30 min, the solution was evaporated to oil and subjected to p-HPLC purification (RP8). After lyophilization, the pure product H-Trp-ψ[CSe-NH]Leu-OH was obtained as yellow solid with an overall yield of 30%.

3.2.1.7 Elongation of the selenoxo dipeptide at the C-terminus

Bz-Val-Gly-Ala-ψ[CSe-NH]Ala-Ala-NH₂

Bz-Vla-Gly-Ala-ψ[CSe-NH]Ala-OMe (5 mg) was dissolved in NaOH solution (0.1M, 4 ml). After 30 min, the solution was neutralized by 1 M HCl to pH ~6. The solution was extracted with 10 ml EtOAc and the organic phase was washed with water and brine. The organic layer was dried and evaporated at reduced pressure. After p-HPLC purification, 2 mg pure Bz-Val-Gly-Ala-ψ[CSe-NH]Ala-OH was obtained. The product was re-dissolved in 1 ml DCM and cooled to 0 °C. To this solution was added 1 equiv. H-Ala-NH₂·HCl, 1 equiv. HATU and 3 equiv. DIPEA. The reaction mixture was stirred for 1 h and then the solvent was evaporated under reduced pressure. The product was separated by p-HPLC, which gave rise to 1.5 mg pure solid after lyophilization.

3.2.1.8 Alkylation of the selenoxo amide group

Boc-Ala-ψ[CSe-NH]Ala-OMe (10 mg) was dissolved in 1 ml NaOH (0.1 M) at 0 °C (ice bath). To this solution was added methyl iodide (6 μl). After 1 h stirring, the reaction flask was placed to refrigerator (-20 °C) for 5 days and then analyzed by p-HPLC. The peaks were collected for mass spectrometric analysis.

3.2.2 Synthesis of thioxo peptides by SPPS

200 mg Fmoc-Sieber amide resin (0.71 mmol/g) was swelled for 2 h in DCM. After deprotecting the Fmoc group (20% piperidine/DMF, 5 min × 3), the amino acids were coupled with the standard Fmoc strategy with 3-fold excess of amino acid activated with PyBOP in the presence of DIPEA. Thioxylation was performed by adding 2.5 equiv. Fmoc-Ala-ψ[CS-NH]-6-nitrobenzotriazole in DCM to the free peptidyl-resin at 4 °C for 1 h and then at rt overnight. The resin was then washed thoroughly and treated with 2% piperidine/1% HOBt/98% DMF (v/w/v, 4 × 2 min). Further elongation was identical to the normal Fmoc peptide chemistry. The peptide was cleaved from the resin by treatment with 2% TFA/DCM for 30 min. The solution was evaporated to oil and then purified by RP-HPLC.

3.2.3 pK$_a$ determination

The peptide water solution was titrated with KOH solution. pH values were read from a pH meter, with the exception that values > 12 were calculated by the amount of KOH added and transformed to proton activity by Davies equation:

$$-\lg f_{\pm} = 0.5 z_1 z_2 \left(\frac{\sqrt{I}}{1+\sqrt{I}} - 0.15I \right)$$

($f_{\pm}$ is the mean molar activity coefficient of an electrolyte that dissociates into ions having charges z_1 and z_2 as a function of the ionic strength I).

The change of absorbance was monitored at 296 nm for selenoxo peptides and at 266 nm for thioxo peptides. The pK$_a$ values were obtained by fitting the absorbance vs. pH plots according to the Henderson-Hasselbalch equation.

For measurements in deuterated water, peptides were dissolved in 99.9% deuterated water and the pD was adjusted by adding DCl or KOD solution in D_2O. The pD values were calculated by pD = $pH_{reading}$ + 0.4.

3.2.4 UV/Vis spectroscopic characterization of photoisomerization

The ground state spectrum of peptide samples in buffer solution was collected in the dark. After 5 min irradiation with UV light at appropriate wavelength (thioxo peptide: ~260 nm, selenoxo peptide: ~290 nm) to achieve the photostationary state (PSS), a spectrum was recorded immediately. The difference spectrum was obtained by subtracting the spectrum in the ground state from the spectrum in the PSS. The irradiation wavelength was optimized based on the wavelength in the trough of the difference spectrum.

In order to obtain the time course of *cis* to *trans* decay, the peptide solution was irradiated for 5 min in a cuvette at the desired temperature and then moved to the cuvette holder of the UV/Vis spectrophotometer (Figure 3.1). The monitoring at the appropriate wavelength was then started immediately. The typical time for the cuvette transfer was 2-3 s. The temperature was controlled by water circulating through a thermostat.

### 3.2.5 NMR spectroscopic characterization of photoisomerization

A 600 µl peptide sample was irradiated (in a 1 cm quartz cuvette) at the appropriate wavelength and then transferred immediately to the NMR tube and placed in the magnet of the NMR spectrometer. The first spectrum was generally recorded 2-3 min after termination of the irradiation.

4. Results

4.1 Synthesis and characterization of selenoxo peptides

4.1.1 Synthesis

To build the selenoxo peptide bond, we chose the selenation strategy by using Woollins'
reagent (2,4-diphenyl-1,3,2,4-diselenadiphosphetan-2,4-diselenide), which has been
employed to selenate amides very efficiently (139, 151). The selenated dipeptides were then
elongated at the N- or C-terminus (Scheme 4.1).
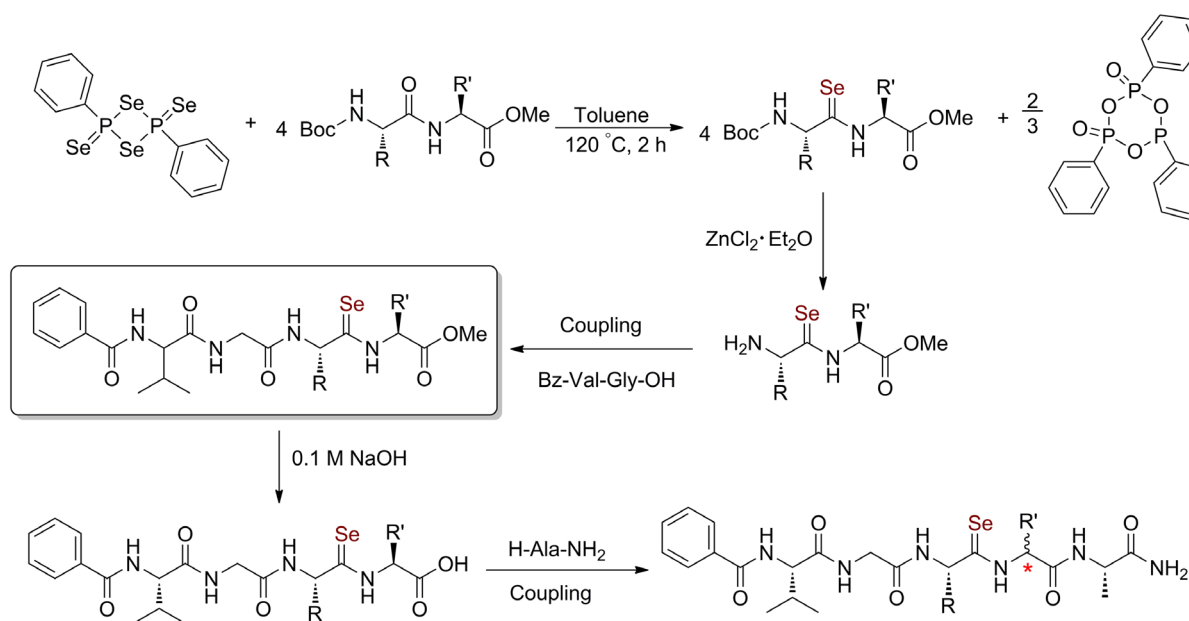
**Scheme 4.1** Synthesis of selenoxo peptides.
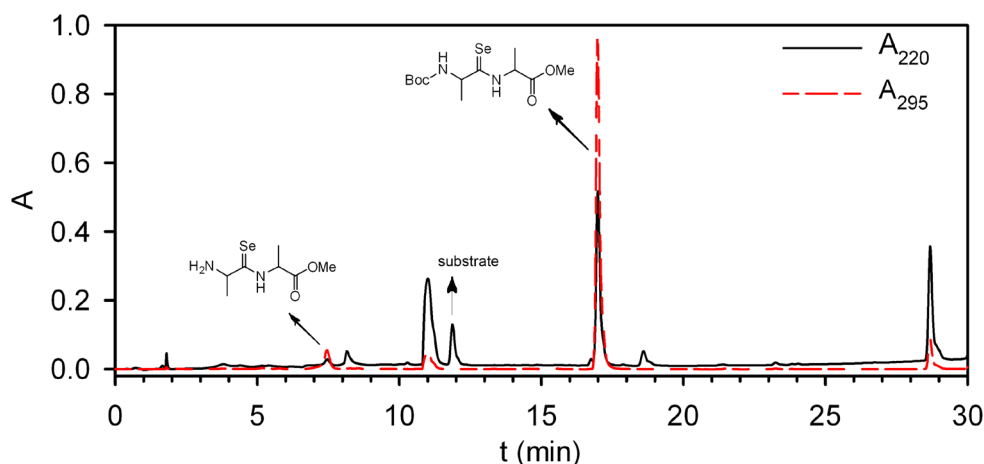
Figure 4.1 HPLC analysis of the selenating reaction mixture. The sample was taken from the reaction mixture
after 2 h refluxing in the presence of 0.5 equiv. Woollins' reagent. Solvent gradient: 5-100% B, 30 min. The
black line and dashed line are chromatograms monitored at 220 and 295 nm, respectively.

The peptide bond of the fully protected dipeptides was selenated successfully by using Woollins' reagent. The selenated products were obtained with a moderate yield for the secondary amide peptide bonds, but a very low yield for the imidic peptide bond in Boc-Ala-Pro-OMe. Fmoc-Ala-Pro-OMe, on the other hand, could be selenated with a much better yield (Table 4.1). Due to the strong acidity of H_2Se released from the reaction mixture, a small part of Boc-deprotected product was also observed (Figure 4.1). The selenated products are less polar than the substrates and could thus be easily purified by p-HPLC.

The Boc protecting group was deprotected by 1 M $ZnCl_2$ ether solution without observable side reactions. Alternatively, 50% TFA could also be used to deprotect the Boc group. In the case of Fmoc deprotection, 5% piperidine/DMF was used. All products were able to be purified by preparative HPLC using acetonitrile/water eluting system. Coupling of the N-terminal segment Bz-Val-Gly-OH with the free amino group of the dipeptide ester was carried out by mixed anhydride method with a yield above 60%. The resulting selenoxo peptides were obtained as light yellow solid after HPLC purification and lyophilization.

Table 4.1 Synthesis of protected selenoxo dipeptides and selenoxo amide[a]

Entry	Product	Reaction time (h)	Yield (%)
1	Boc-Ala-ψ[CSe–NH]Ala-OMe	2	37
2	Boc-Ala-ψ[CSe–NH]Ala-OMe	2	92 [b]
3	Boc-Ala-ψ[CSe–NH]Phe-OMe	1.5	45
4	Boc-Ala-ψ[CSe–N]Pro-OMe	1.5	3
5	Fmoc-Ala-ψ[CSe–N]Pro-OMe	6	55 [c]
6	Fmoc-Ala-ψ[CSe–NH]Ala-OMe	3.5	30 [c]
7	Boc-Leu-ψ[CSe–NH]Trp(Boc)-OtBu	3	> 50
8	CH3-ψ[CSe–NH]CH3	2	> 50

[a] Reactions were conducted under argon atmosphere, subsequent operations were performed in air. A mixture of substrate and 0.5 equivalent Woollins' reagent in anhydrous toluene was heated to 125 °C. The resulting orange solution was cooled to room temperature and the solvent was removed under reduced pressure. The product was separated by HPLC.
[b] 0.3 equivalent of Woollins' reagent was used.
[c] 3 equivalent of Woollins' reagent was used.

For the synthesis of the endo-selenoxo peptides, the C-terminal ester of the selenoxo peptides was hydrolyzed by 0.1 M NaOH. The resulting selenoxo peptide acid was coupled with H-Ala-NH$_2$ by using HATU in the presence of DIPEA. Like the case of thioxo dipeptides, where the C-terminal elongation always encounters a problem of epimerization (152), extension at the C-terminus of the selenoxo dipeptide also resulted in partial epimerization. For example, Bz-Val-Gly-Ala-ψ[CSe–NH]Ala*-Ala-NH$_2$ was obtained with ~ 40% D-Ala^4 epimer. Fortunately, the epimers of Bz-Val-Gly-Ala-ψ[CSe–NH]Phe*-Ala-NH$_2$ could be separated by preparative HPLC.

4.1.2 General characterization

4.1.2.1 Mass spectrometry

Mass spectrometry was used to identify the peptides and intermediates. It should be noted that the positive mode did not work well for some selenoxo compounds, while the negative mode could show the molecular ions. The list of the retention times (t_R) and mass-to-charge ratios (m/z) of all peptides is shown in Table 4.2. A typical isotope pattern on the mass spectrum of a mono-selenoxo peptide is shown in Figure 4.2.
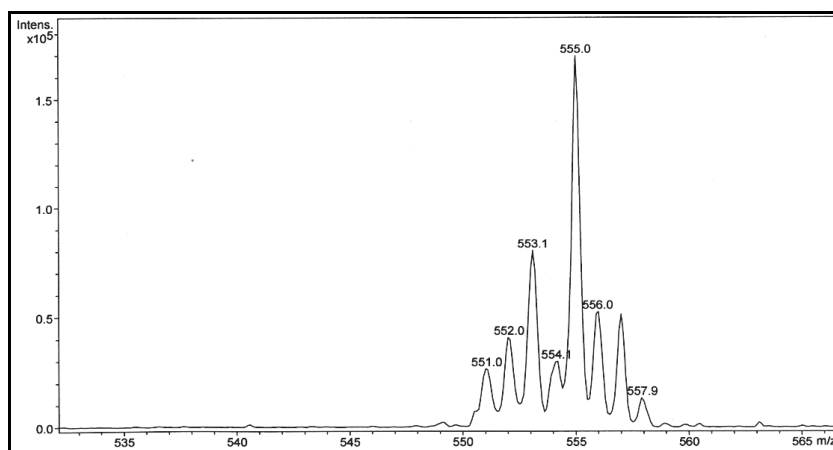

Figure 4.2 Isotope pattern in the mass spectrum of a mono-selenoxo peptide.

Table 4.2 Analytical data for the synthesized peptides

Name [a]	Peptide	t_R (min) [b]	m/z [c] Calculated	Found
1a	Bz-Val-Gly-Ala-Ala-OMe	12.7	435.2 [M+H]$^+$	435.0
2a	Bz-Val-Gly-Ala-Phe-OMe	16.4	511.3 [M+H]$^+$	511.0
3a	Bz-Val-Gly-Ala-Pro-OMe	12.7	461.2 [M+H]$^+$	461.1
1b	Bz-Val-Gly-Ala-ψ[CS−NH]Ala-OMe	14.4	451.2 [M+H]$^+$	451.0
2b	Bz-Val-Gly-Ala-ψ[CS−NH]Phe-OMe	19.2	527.2 [M+H]$^+$	527.1
3b	Bz-Val-Gly-Ala-ψ[CS−N]Pro-OMe	15.5	461.2 [M+H]$^+$	461.0
4b	Bz-Val-Gly-Ala-ψ[CS−NH]Ala-Ala-NH$_2$	11.8	507.2 [M+H]$^+$	507.1
5b	Bz-Val-Gly-Ala-ψ[CS−NH]Phe-Ala-NH$_2$	15.4	583.3 [M+H]$^+$	583.1
6b	Ac-Gly-Ala-ψ[CS−NH]Phe-NH$_2$	10.5	351.1 [M+H]$^+$	350.9
7b	Ac-Val-Ala-ψ[CS−NH]Phe-Gly-Gly-Ala-Phe-OMe	15.3	762.3[M+Na]$^+$	762.2
8b	Ac-Val-Ala-ψ[CS-NH]Phe-Gly-Gly-OH	11.9	508.2 [M+H]$^+$	508.1
9b	H-Leu-ψ[CS−NH]Trp-OH	*trans*:13.1 *cis*: 12.6	334.2 [M+H]$^+$	334.0
1c	Bz-Val-Gly-Ala-ψ[CSe−NH]Ala-OMe	15.5	497.1 [M-H]$^−$	496.8
2c	Bz-Val-Gly-Ala-ψ[CSe−NH]Phe-OMe	20.1	573.2 [M-H]$^−$	572.9
3c	Bz-Val-Gly-Ala-ψ[CSe−N]Pro-OMe	*trans*:15.2 *cis*: 15.8	525.2 [M-H]$^−$	525.0
4c	Bz-Val-Gly-Ala-ψ[CSe−NH]Ala-Ala-NH$_2$	11.5	555.2[M+H]$^+$	555.0
5c	Bz-Val-Gly-Ala-ψ[CSe−NH]Phe-Ala-NH$_2$	15.2	629.2 [M-H]$^−$	629.0
10c	Boc-Val-Gly-Ala-ψ[CSe−NH]Ala-OMe	16.0	495.2 [M+H]$^+$	495.1
11d	Ac-Val-Ala-Phe-Gly-Gly-Ala-ψ[CSe−NH]Phe-OMe	15.8	810.3[M+Na]$^+$	810.1
12c	Ac-Val-Ala-ψ[CS-NH]Phe-Gly-Gly-Ala-ψ[CSe−NH]Phe-OMe	17.3	804.3 [M+H]$^+$	804.1
13c	Ac-Gly-Ala-ψ[CSe−NH]Ala-OMe	8.4	338.1 [M+H]$^+$	337.9
9c	H-Leu-ψ[CSe−NH]Trp-OH	*trans*:12.7 *cis*: 13.8	382.1 [M+H]$^+$	381.9

[a] **a**, **b**, **c**, refers to oxo peptide, thioxo peptide, selenoxo peptide, respectively; **d** refers to the thioxo and selenoxo dual-labeled peptide.

[b] RP-HPLC conditions: LiChroCART® (Merck) 125-4 RP8 (5 μm) column; flow rate: 1 ml/min; linear gradient from 5% to 100% B (A: 0.05% TFA/H$_2$O, B: 0.05% TFA/ACN) in 30 min; detection wavelength: 220 nm.

[c] the m/z of the selenoxo peptides was calculated based on ^{80}Se.

4.1.2.2 Hydrophobicity and HPLC analysis

Compared with the regular peptides, the selenoxo congeners were considerably more hydrophobic, as manifested by their decreased aqueous solubility and retention behavior in HPLC. In the analytic RP-HPLC, the retention times of selenoxo peptides were 2-3 min longer than the oxo congeners, but only 1 min longer than the thioxo congeners (Figure 4.3, Table 4.2).
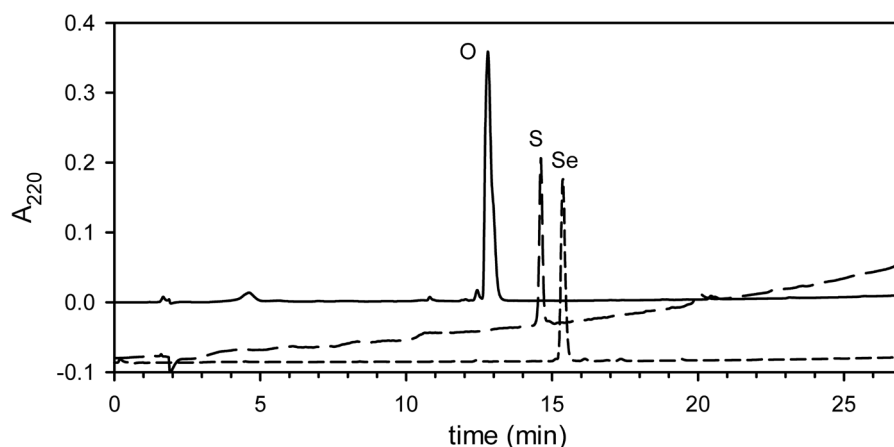

Figure 4.3 Superposition of the HPLC chromatograms of the Bz-Val-Gly-Ala-ψ[C**X**–NH]Ala-OMe peptide series (**X** = O, S, Se). Solvent gradient: 5% to 100% B in 30 min.

4.1.2.3 Stability of selenoxo peptides

The selenoxo peptides were stable in neutral aqueous solution for several days without any observable change. Under basic (pH 9.0) conditions, partial ester hydrolysis and an accelerated selenium to oxygen exchange was observed (Figure 4.4). Hence, the selenoxo peptides are much more stable than the smaller selenoxo amides, which have been reported to decompose under oxygen-containing conditions and should be handled in a moisture- and oxygen-free environment (134, 151, 153).
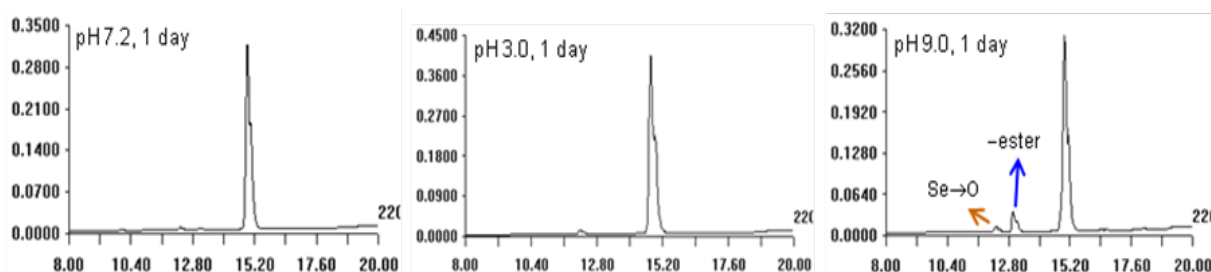
Figure 4.4 Stability of Bz-Val-Gly-Ala-ψ[CSe–NH]Ala-OMe in aqueous solution. A small amount of peptide was dissolved in 30 mM phosphate buffer (pH 7.2), 50 mM sodium acetate buffer (pH 3.5) or 20 mM Gly-NaOH (pH 9.0) buffer. After 1 day of incubation, the purity was analyzed by HPLC with the detection wavelength set to 220 nm. Blue arrow indicates the C–terminal ester hydrolyzed peptide. Orange arrow indicates the peptide undergone selenium to oxygen exchange.

Interestingly, the C-terminal ester in selenoxo peptides was found to be more labile to alkaline hydrolysis than that in thioxo and oxo peptides (Table 4.3).

Table 4.3 C-terminal ester hydrolysis in oxo, thioxo, and selenoxo peptides [a]

Peptide	time (d)	Ester hydrolysis (%)
Bz-Val-Gly-Ala-Ala-OMe	2	2.5
Bz-Val-Gly-Ala-ψ[CS–NH]Ala-OMe	2	4.6
Bz-Val-Gly-Ala-ψ[CSe–NH]Ala-OMe	2	5.8

[a] Measurements were conducted in 30 mM phosphate buffer (pH 8.0) for 2 days at rt.

4.1.2.4 Enantiopurity

Because of the stronger hyperconjugation with the selenoxo carbonyl group, the alpha carbon might encounter epimerization during selenation. By comparison with the synthesized D-epimer, epimerization occurred at about 7% in Bz-Val-Gly-Ala-ψ[CSe–NH]Ala-OMe (Figure 4.5a, b). However, the oxo peptide was found to also contain a similar amount of D-epimer (Figure 4.5c), which should be resulted from the Boc-Ala-Ala-OMe substrate. Therefore, the selenation reaction itself is nearly free of epimerization, and no epimerization occurs in the coupling step in N-terminal elongation.
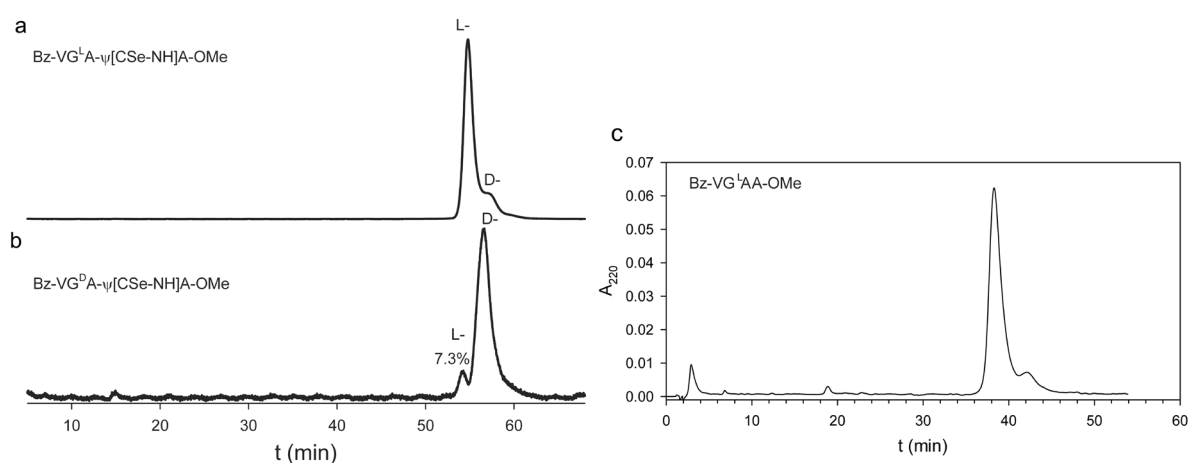
Figure 4.5 Enantiopurity analysis of Bz-Val-Gly-[L]Ala-ψ[CSe-NH]Ala-OMe (a), Bz-Val-Gly-[D]Ala-ψ[CSe-NH]Ala-OMe (b) and Bz-Val-Gly-[L]Ala-Ala-OMe (c). Analyses were performed on a SYKAM HPLC system equipped with a GRACE Vydac® 208TP54, C8 (5 μm), 4.6 × 250 mm column. Isocratic elution of 22% ACN/H_2O was used for selenoxo peptides while 18% ACN/H_2O was used for oxo peptide. Detection was performed at 295 nm, and the solvent flow rate was set to 1 ml/min.

4.1.2.5 UV/Vis spectroscopy

The UV/Vis absorption spectra of the selenoxo peptides indicated a clear red shift compared to the oxo and thioxo peptides (Figure 4.6). In Bz-Val-Gly-Ala-ψ[CSe–NH]Ala-OMe, the strong absorption band centered at 294 nm was assigned to the π−π* transition with an extinction coefficient (ε) of 11280 $M^{-1}cm^{-1}$, and the weak band around 367 nm (ε = 177 $M^{-1}cm^{-1}$) was assigned to the n−π* transition, based on the absorption pattern of thioxo peptides (85, 120, 154). Thus, the electronic excitation wavelengths of selenoxo peptides are approximately 30 nm longer than the corresponding thioxo peptides (Figure 4.6). When the selenoxo peptide bond was flanked by aromatic residues, the absorption maxima moved to slightly longer wavelengths. For instance, the Bz-Val-Gly-Ala-ψ[CSe–NH]Phe-OMe showed a π−π* transition at 296 nm and a n−π* transition at 372 nm. For imidic selenoxo peptide bonds, the absorption bands were further red-shifted, with the π−π* and n−π* transition bands appearing at 302 nm and 376 nm, respectively (Figure 4.6).
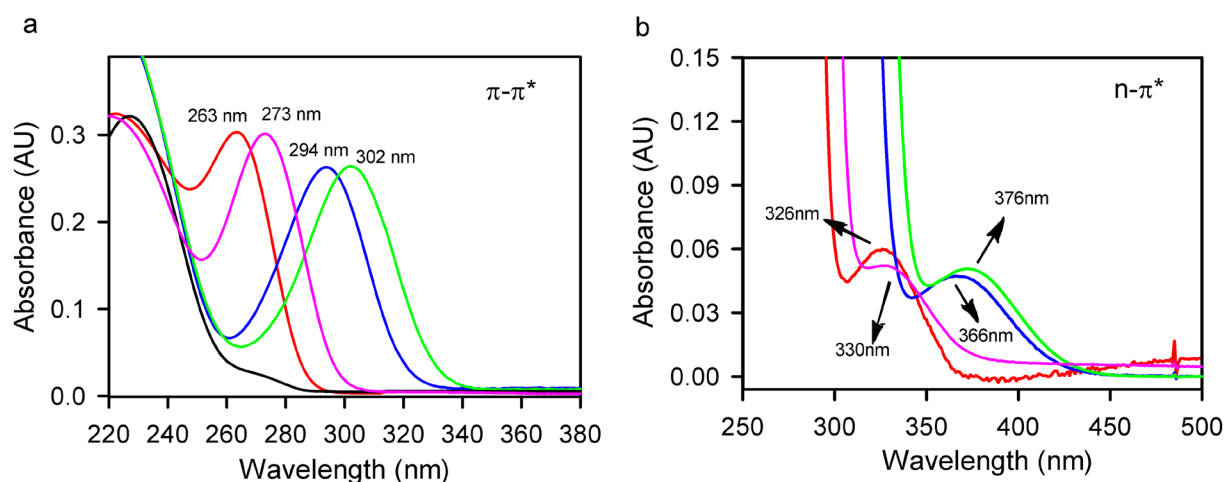
Figure 4.6 (a) π−π* transition bands in the UV/Vis spectra of Bz-VGAA-OMe (black line), Bz-VGA-ψ[CS–NH]A-OMe (red line), Bz-VGA-ψ[CS–N]P-OMe (pink line), Bz-VGA-ψ[CSe–NH]A-OMe (blue line) and Bz-VGA-ψ[CSe–N]P-OMe (green line). (b) n−π* transition bands of Bz-VGA-ψ[CS–NH]A-OMe (red line), Bz-VGA-ψ[CS–N]P-OMe (pink line), Bz-VGA-ψ[CSe–NH]A-OMe (blue line) and Bz-VGA-ψ[CSe–N]P-OMe (green line). Absorption intensity was normalized by concentration and all spectra were recorded in 33 mM phosphate buffer (pH 6.5), at 10 °C.

4.1.2.6 NMR spectroscopy

^{1}H-NMR

The ^{1}H-NMR spectra of selenoxo peptides indicated a strong downfield shift of the selenoxo amide proton resonance frequency as well as a much faster exchange with water compared to the oxo and thioxo congeners. For example, in the Bz-Val-Gly-Ala-ψ[C**X**–NH]Phe-OMe peptides series, the $\delta_{NH\,(Phe)}$ was shifted downfield from 8.45 ppm to 10.6 ppm and to 10.74 ppm in the order of **X** = O, S, Se (Figure 4.7a). Surprisingly, the peak broadening of the selenoxo amide proton was so intense that it needed to be confirmed by a two-dimensional ^{1}H-^{1}H correlation spectrum (Figure 4.7b). Moreover, H_α adjacent to the selenoxo group were also shifted downfield (discussed in **4.6**). The selenoxo peptides did not show any *cis* conformation related signals in aqueous buffer, while the imidic selenoxo group in Bz-Val-Gly-Ala-ψ[C**X**–N]Pro-OMe showed a *cis* content of 7.1% in the equilibrated state, which is slightly higher than 6.6% found in the corresponding oxo and thioxo congeners.
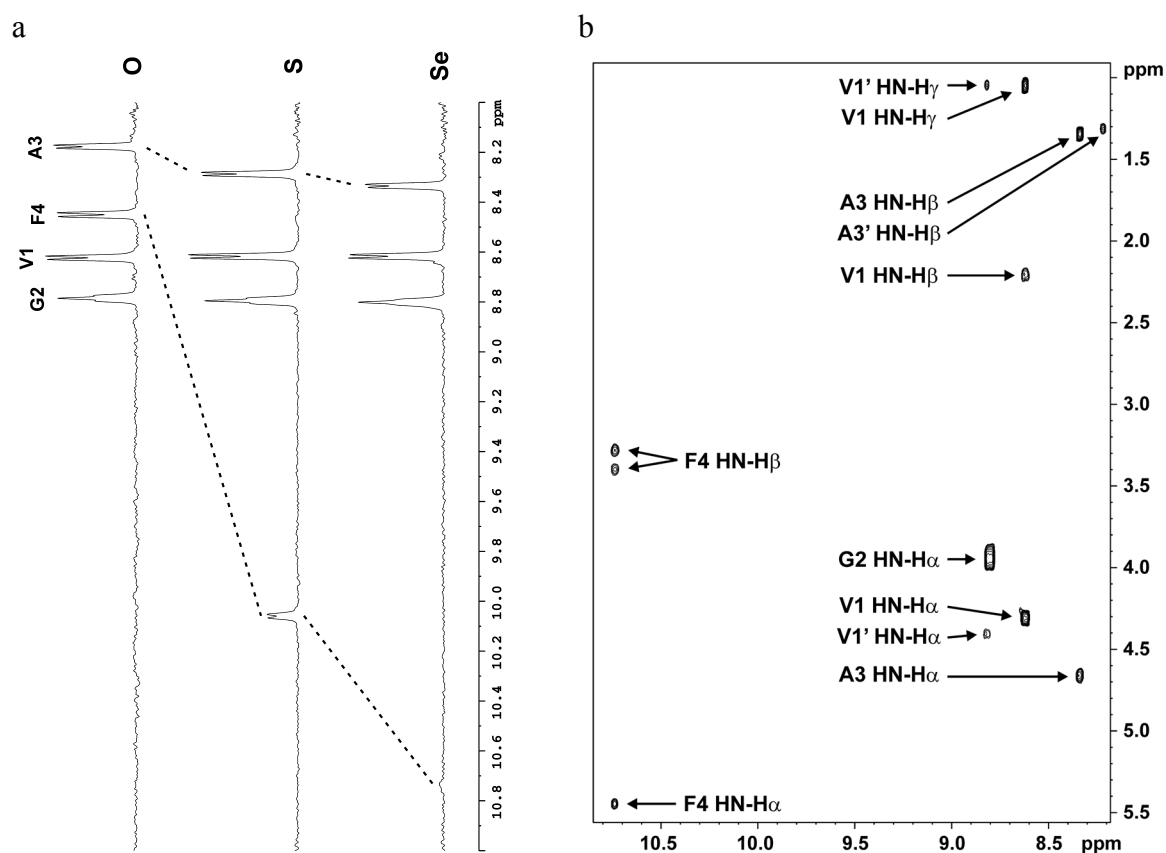


Figure 4.7 (a) Amide proton signals of Bz-VGA-ψ[C**X**–NH]F-OMe (**X** = O, S, Se). (b) Amide proton region from the ^{1}H-^{1}H TOCSY spectrum of the selenoxo congener. Spectra were recorded in 50 mM sodium acetate buffer (pH 6.0) at 10 °C.

^{13}C-NMR

The ^{13}C resonance frequencies of the selenoxo carbonyl groups were ~215 ppm, which is about 40 ppm higher than in the oxo congener (~175 ppm). The alpha carbons adjacent to the selenoxo group were also obviously shifted downfield (discussed in **4.6**).

^{77}Se-NMR

The ^{77}Se resonance frequency of the selenoxo carbonyl was about 390 ppm in the selenoxo peptide bonds and about 450 ppm in the imidic selenoxo peptide bonds (Table 4.4). Interestingly, the ^{77}Se chemical shift in the *cis* conformer of Bz-Val-Gly-Ala-ψ[CSe–N]Pro-OMe is 14 ppm higher than in the *trans* conformer (Figure 4.8).
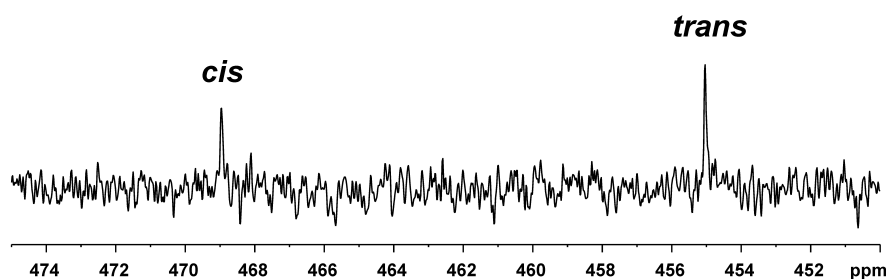
Figure 4.8 ^{77}Se-NMR spectrum of Bz-VGA-ψ[CSe–N]P-OMe. Spectrum was recorded with 0.8 mM peptide in 33 mM phosphate buffer (pH 6.5) at 10 °C after 10 min of irradiation at 296 nm.

Table 4.4 ^{77}Se chemical shifts in selenoxo amide bonds [a]

Peptides	δ_{Se} (ppm)
Bz-Val-Gly-Ala-ψ[CSe–NH]Ala-OMe	387.5
Bz-Val-Gly-Ala-ψ[CSe–NH]Phe-OMe	391.1
Bz-Val-Gly-Ala-ψ[CSe–NH]Ala-Ala-NH$_2$	423.5
Bz-Val-Gly-Ala-ψ[CSe–NH]Ala-OH	323.5 363.8 [b]
Bz-Val-Gly-Ala-ψ[CSe–N]Pro-OMe	*trans*: 455.0; *cis*: 469.0
Ac-Gly-Ala-ψ[CSe–NH]Ala-OMe	380.8
CH$_3$[CSe–NH]CH$_3$ [c]	*trans*: 523.5; *cis*: 566.9

[a] Spectra were collected in 33 mM phosphate buffer (pH 6.5) at 10 °C.
[b] Value measured at pH 3.0.
[c] Measured in CDCl$_3$, 20 °C.

4.1.2.7 Acidity of the selenoxo and thioxo amide protons

The UV/Vis spectra of selenoxo peptides were found to be highly sensitive to pH increase, especially when the pH was above eight, where the π–π* band showed a drastic decrease (Figure 4.9). Interestingly, the spectrum could be recovered after neutralization (Figure 4.9). The imidic selenoxo peptide, on the other hand, did not show such a behavior (Figure 4.10). Therefore, considering the fact that thioxo substitution lowered the pK_a of the amide proton from > 15 to ~12 (155), those observed spectroscopic changes should be due to dissociation of the selenoxo amide proton, i.e. a re-arrangement from selenoxo to selenoimidate anion (Scheme 4.2), as indicated by the disappearance of the characteristic absorption bands of the selenoxo carbonyl group. Instead, a new band appeared at ~260 nm might be assigned to the n-σ* transition of [C(Se$^-$)=N–]. In case of the imidic selenoxo group [CSe–N<], where no amide proton exists, this type of re-arrangement could not take place. Fitting the pH vs. absorbance plots according to the Henderson–Hasselbalch equation gave rise to pK_a values of 9 − 10 for selenoxo peptides (Table 4.5). For comparison, the pH-dependent absorbance of the thioxo peptides was also measured, featuring pK_a values around 11.5 (Figure 4.11, Table 4.5) which is about 2 units higher than the selenoxo peptides.
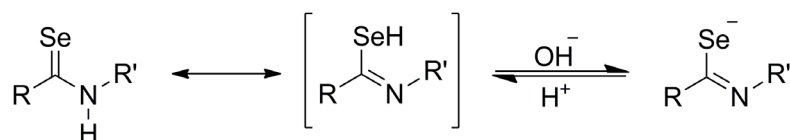
Scheme 4.2 Selenoxo amide proton dissociation
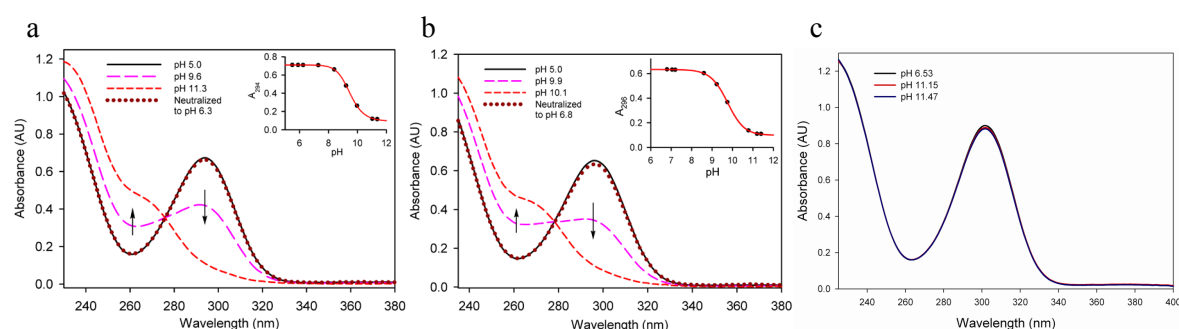
**Figure 4.9** pH-dependent UV/Vis spectra of selenoxo peptides. (a) 70 μM Bz-VGA-ψ[CSe-NH]A-OMe in water titrated with KOH or HCl solution. Inset: titration curve monitored at 294 nm. (b) 65 μM Bz-VGA-ψ[CSe-NH]F-OMe in water titrated with KOH or HCl solution. Inset: titration curve monitored at 296 nm. (c) 82 μM Bz-VGA-ψ[CSe-N]P-OMe in water titrated with KOH solution. All spectra were recorded at 20 °C.
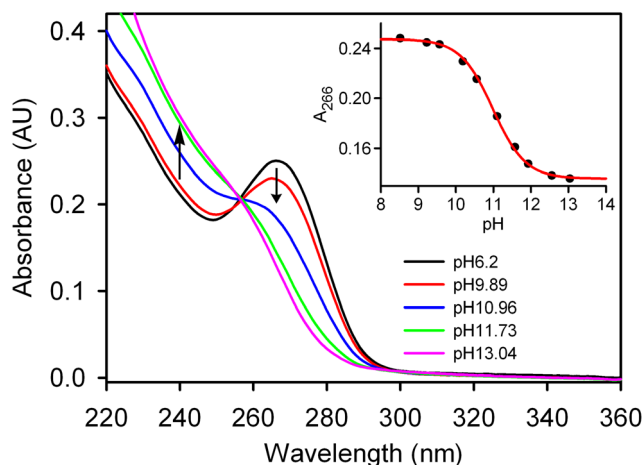
Figure 4.10 pH-dependent UV/Vis spectra of the thioxo peptide Bz-VGAψ[CS−NH]FA-NH$_2$ in aqueous solution titrated with KOH solution at 20 °C. Inset: the absorbance at 266 nm fitted to the Henderson-Hasselbalch equation, resulting in a pK$_a$ value of 11.0 for the thioxo amide group.

Table 4.5 pK$_a$'s of thioxo and selenoxo peptides in aqueous solution [a].

	Peptides	pK$_a$
1b	Bz-VGAψ[CS-NH]A-OMe	~12
2b	Bz-VGAψ[CS-NH]F-OMe	~12
4b	Bz-VGAψ[CS-NH]AA-NH$_2$	11.5
5b	Bz-VGAψ[CS-NH]FA-NH$_2$	11.0
8	Ac-VAψ[CS-NH]GG-OH	11.3
1c	Bz-VGAψ[CSe-NH]A-OMe	9.8
2c	Bz-VGAψ[CSe-NH]F-OMe	9.5
4c	Bz-VGAψ[CSe-NH]AA-NH$_2$	9.6
5c	Bz-VGAψ[CSe-NH]FA-NH$_2$	9.1

[a] Values were obtained by titrating the peptide solution in water with KOH at 20 °C. pH values were read from the pH meter except for pH > 12, which is calculated by the amount of KOH added and transformed to proton activity by Davies equation.

4.1.2.8 Alkylation on selenoxo group

Alkylation of selenoxo amides generally proceeds on the selenium atom but not on the nitrogen. The methylated derivatives have been shown to be very hygroscopic and easily hydrolyzed (156). To test the possibility of protecting the selenoxo group by alkylation, we conducted the methylation reaction of Boc-Alaψ[CSe-NH]Ala-OMe in DCM in the presence of 1 equiv. methyl iodide and 1 equiv. DBU, but no Se-methylated product formed. However the methylation in aqueous basic solution yielded selenoimidate Boc-Alaψ[C(SeCH₃)=N]Ala-OH successfully, which features an absorption maximum at 260 nm (Figure 4.11).
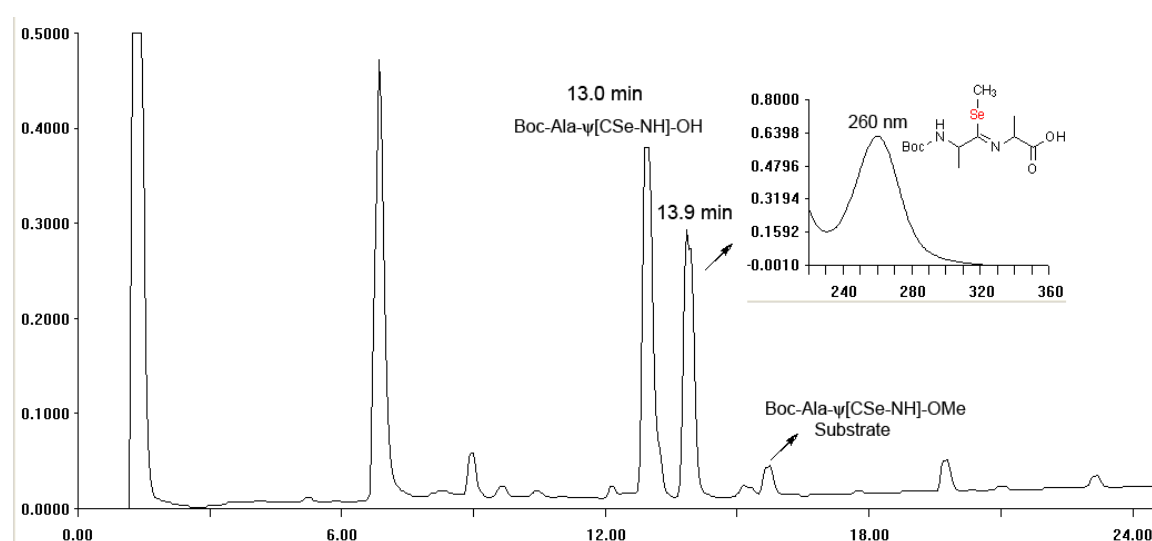

Figure 4.11 HPLC analysis of the reaction mixture of methylation. Reaction condition: 10 mg Boc-Alaψ[CSe-NH]Ala-OMe was dissolved in 0.1 M NaOH aqueous solution and cooled with ice-water bath, to which was added 1 equiv. methyl iodide. After 1 hour, the reaction flask was put into refrigerator (-20 °C) for 5 days and then sampled to HPLC analysis.

4.2 Photoisomerization

4.2.1 Characterization of photoisomerization by UV/Vis spectroscopy

The photoisomerization property of the selenoxo peptides was firstly characterized by UV/Vis spectroscopy. The UV/Vis spectrum of peptide Bz-VGA-ψ[CSe–NH]A-OMe was significantly red-shifted upon irradiation with 286 nm UV light, indicating an increase in the amount of *cis* conformer upon irradiation. After extensive equilibration in the dark, the original spectrum could be fully restored (Fig. 4.13a). This photoisomerization was reversible for at least 4 cycles. The difference spectrum shows that the absorbance at 286 nm was decreased most while that at 317 nm was increased most after irradiation, with an isosbestic point at 300 nm (Figure 4.12b). Similar photoswitching behavior was observed for other selenoxo peptides. By monitoring the absorbance at 317 nm after photoirradiation, a rate constant of 9.9×10^{-4} s^{-1} was obtained for Bz-VGA-ψ[CSe–NH]A-OMe at 10 °C. The peptide Bz-VGA-ψ[CSe–NH]F-OMe, where an aromatic side chain followed to the selenoxo group, showed a slower decay (k = 4.4×10^{-4} s^{-1}).

a

b
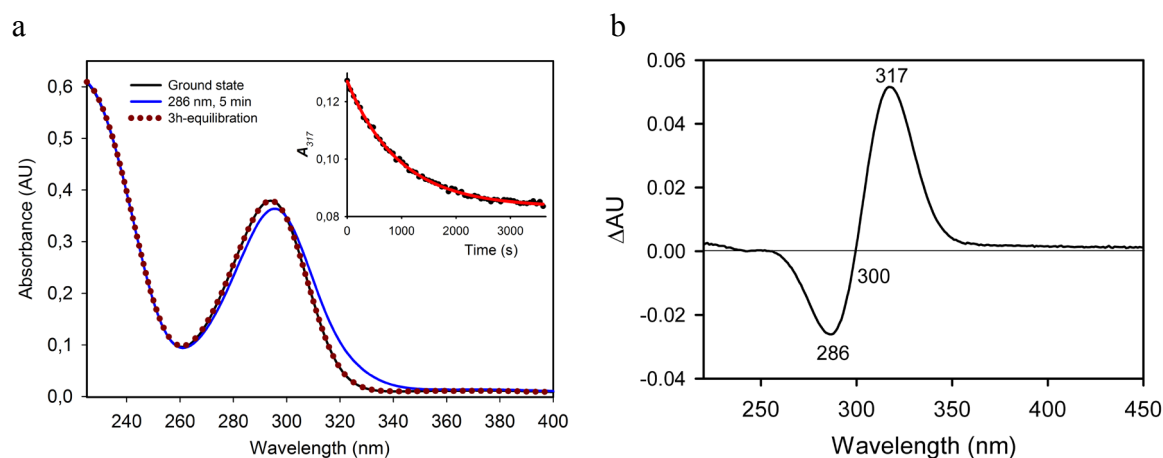
Figure 4.12 UV/Vis absorption spectra of 34 μM Bz-VGA-ψ[CSe-NH]A-OMe in 33 mM phosphate buffer (pH 6.5) at 10 °C. (a) Overlaid spectra in the ground state (black line), after 5 min of irradiation at 286 nm (blue line), and after four cycles of irradiation/equilibration (dotted line). Inset: time course of the thermal decay after irradiation. The red line represents the least squares fit with first order exponential equation, resulting in a rate constant of 9.9×10^{-4} s^{-1}. (b) Difference spectrum after photoirradiation.

The *cis* content in the ground state was so low that it was not detected in the NMR measurement, thus the UV/Vis spectrum represents the absorbance of the *trans* form. Using the UV/Vis spectra at ground state and PSS as well as the *cis*/*trans* ratio measured by NMR and extrapolated to PSS, the UV/Vis spectrum of the *cis* conformer was calculated based on Beer-Lambert's law (Figure 4.13).The *cis* conformer showed an absorption maximum at 310 nm (ε = 12620 M^{-1}cm^{-1}).
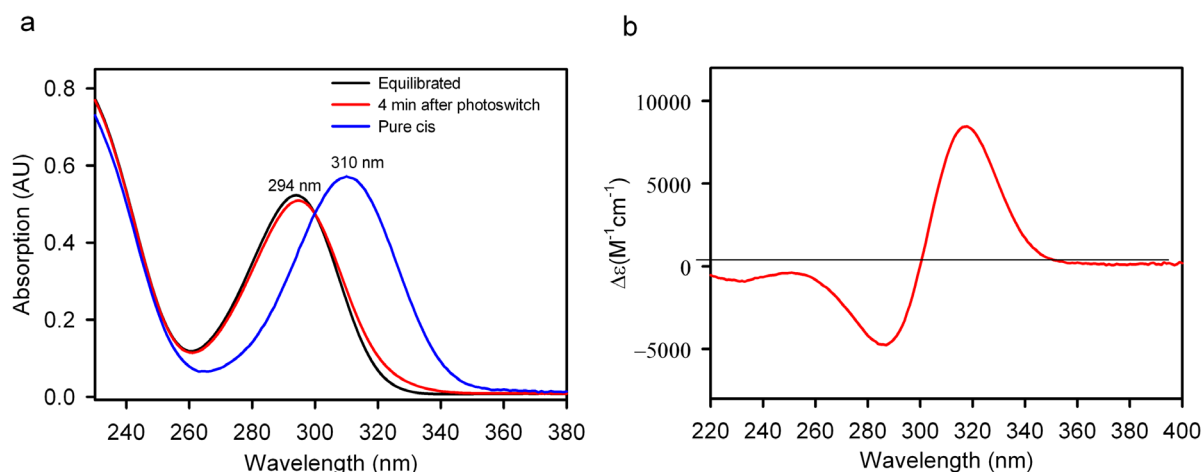
Figure 4.13 (a) UV/Vis spectra for *trans* (black line), PSS (red line), and *cis* states (blue line), respectively. Measurements were performed with 51 μM Bz-VGA-ψ[CSe-NH]A-OMe in 33 mM phosphate buffer, pH 6.5, 10 °C. (b) The difference of extinction between the *cis* and *trans* conformers.

Photoisomerization of the imidic selenoxo peptide bond in Bz-Val-Gly-Ala-ψ[CSe-N]Pro-OMe was also characterized. Unlike the case of [CSe-NH-], there was no obvious band shift for [CSe-N<] after irradiation by 296 nm UV light, rather, it only showed a slight but obvious increase in absorption intensity (Figure 4.14). Surprisingly, the *cis* to *trans* decay of [CSe-N<] in Bz-VGA-ψ[CSe–N]P-OMe was extremely slow, with a calculated rate constant of 1.3×10^{-5} s^{-1} (Table 4.6), that is, a half-life of 15 h.
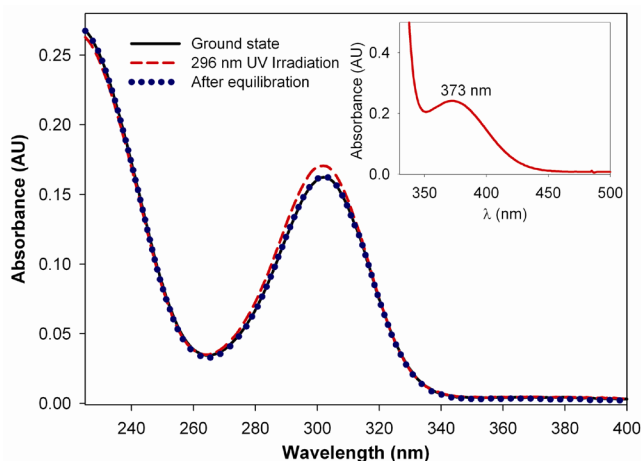
Figure 4.14 UV/Vis spectra of Bz-VGA-ψ[CSe-N]P-OMe in the ground state (black line), after 5 min irradiation (red line) and after extensive equilibration (dots). The spectra were recorded with 15 μM peptide in 33 mM phosphate buffer, pH 6.5, 40 °C. Inset: absorption band of n-π* transition (c = 40 mM).

Table 4.6 UV/Vis absorption bands and *cis→trans* isomerization rate constants in thioxo and selenoxo peptides.

| Peptide	λ_{max} (nm)		hv_{eff}	k_{ct} [b]
	π-π*	n-π*	(nm) [a]	(s-1)
Bz-Val-Gly-Ala-ψ[CS-NH]Ala-OMe	263	326	258	$(6.7 \pm 0.7) \times 10^{-3}$
Bz-Val-Gly-Ala-ψ[CS-NH]Phe-OMe	265	~330	259	$(2.6 \pm 0.2) \times 10^{-3}$
Bz-Val-Gly-Ala-ψ[CSe-NH]Ala-OMe	294	367	286	$(9.9 \pm 0.1) \times 10^{-4}$
Bz-Val-Gly-Ala-ψ[CSe-NH]Phe-OMe	296	374	288	$(4.4 \pm 0.1) \times 10^{-4}$
Bz-Val-Gly-Ala-ψ[CSe-N]Pro-OMe	302	373	296	1.28×10^{-5} [c]
H-Trp-ψ[CSe-NH]Leu-OH	288	~380	293	$(5.1 \pm 0.1) \times 10^{-4}$

[a] hv_{eff} is the most efficient photoswitching wavelength derived from difference spectrum
[b] Data were collected in 33 mM phosphate buffer (pH 6.5) at 10 °C.
[c] Value extrapolated from Eyring plot.

By measuring the temperature-dependent rate constants of *cis→trans* decay after photoisomerization, the Eyring plots were obtained (Figure 4.15). The thermodynamic parameters for the *cis→trans* isomerization in thioxo and selenoxo peptides could thus be derived from Eyring equation (Table 4.6). For the sake of comparison, the $\Delta G^{\ddagger}$ of an oxo peptide was also derived based on the literature data.
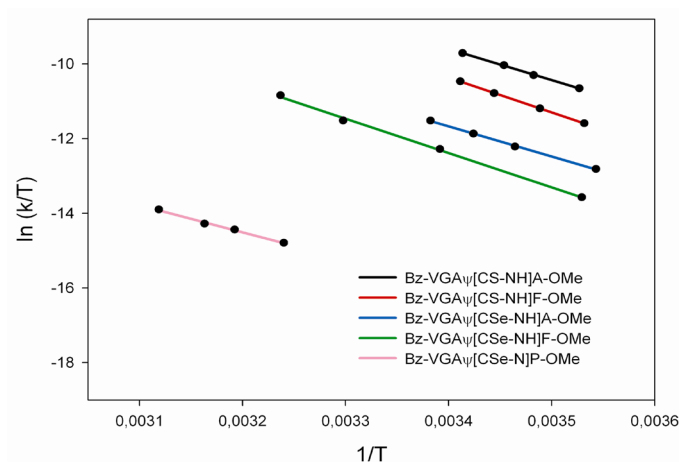

Figure 4.15 Eyring plots. The rate constants at different temperatures were measured in 33 mM phosphate buffer, pH 6.5. The rate constants were then fitted to the Erying equation:

$$\ln(k_{ct}/T) = (-\Delta H^{\ddagger}/R)/(1/T) + \ln(k_B/h) + \Delta S^{\ddagger}/R$$

where R is the universal gas constant; k_B is the Boltzmann constant and h is the Planck constant.

Table 4.7 Thermodynamic parameters for the *cis→trans* isomerization of oxo, thioxo and selenoxo peptides

Peptide	$\Delta H^{\ddagger}$ (kJ mol^{-1}) [a]	$\Delta S^{\ddagger}$ (J K^{-1} mol^{-1}) [a]	$\Delta G^{\ddagger}$ (kcal mol^{-1}) [b]
AAY[CO-NH]AA [c]	63.2 ± 2.8	-29 ± 8.6	17.1 ± 1.2
Bz-VGAψ[CS-NH]A-OMe	69.6 ± 1.2	-41 ± 4.1	19.4 ± 0.6
Bz-VGAψ[CS-NH]F-OMe	77.5 ± 0.7	-20 ± 2.4	19.9 ± 0.5
Bz-VGAψ[CSe-NH]A-OMe	67.1 ± 1.4	-67 ± 4.6	20.5 ± 0.6
Bz-VGAψ[CSe-NH]F-OMe	76.4 ± 2.4	-41 ± 8.0	21.0 ± 1.1
Bz-VGAψ[CSe-N]P-OMe	60.3 ± 2.9	-125 ± 9.3	22.9 ± 1.3

[a] from the Eyring plots
[b] based on Gibbs function $\Delta G^{\ddagger} = \Delta H^{\ddagger} - T\Delta S^{\ddagger}$ with T = 283 K
[c] from data in ref. (19)

4.2.2 Characterization of photoisomerization by NMR spectroscopy

To further confirm the photo-initiated *trans→cis* isomerization, ^{1}H-NMR spectra were collected before and after irradiation. Taking Bz-Val[1]-Gly[2]-Ala[3]-ψ[CSe–NH]Ala[4]-OMe as an example, a new signal appeared at an upfield position after 5 min irradiation at 286 nm, which disappeared after extensive relaxation (Figure 4.16a). Therefore, by comparing with the photoisomerization of thioxo peptides, which also showed an upfield-shifted *cis* signal after irradiation (120), this new peak was assigned to the *cis* form of the Ala[3] methyl group. Other selenoxo peptides showed similar behaviors (Table 4.8). In the ground state, the *cis* conformer of [CSe–NH] was not detected due to its extremely low population; upon irradiation, the amount of *cis* content (extrapolated to PSS) was increased to 11.2% in Bz-Val-Gly-Ala-ψ[CSe–NH]Ala-OMe, 20% in Bz-Val-Gly-Ala-ψ[CSe–NH]Phe-OMe and 23% in Bz-Val-Gly-Ala-ψ[CSe–NH]Pro-OMe (Figure 4.16). The rate of *cis→trans* decay was very slow for [CSe-NH<] (Figure 4.16c), which is consistent with the UV/Vis measurements (Table 4.6).
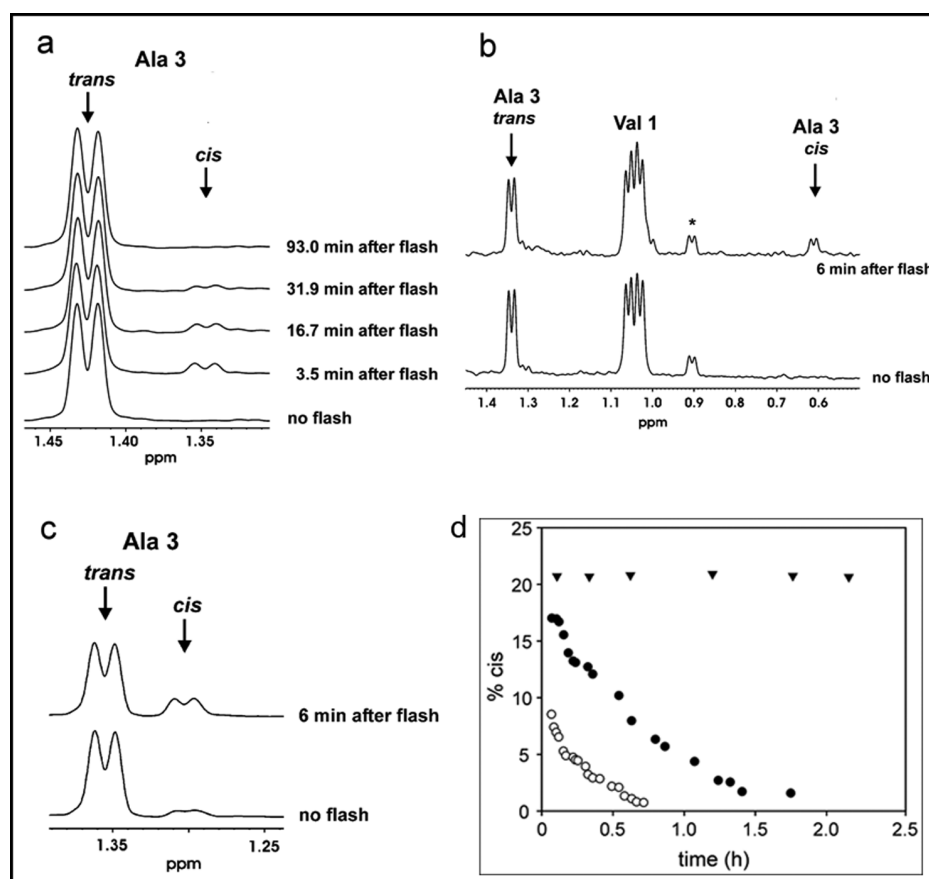
Figure 4.16 ^{1}H-NMR spectra of 0.51 mM Bz-Val-Gly-Ala-ψ[CSe-NH]Ala-OMe (a), 0.2 mM Bz-Val-Gly-Ala-ψ[CSe-NH]Phe-OMe (b), and 0.8 mM Bz-Val-Gly-Ala-ψ[CSe-N]Pro-OMe (c) in 33 mM phosphate buffer (pH 6.5) at 10 °C. Peptide samples were irradiated in a quartz cuvette at the appropriate wavelength for 5 min and then transferred immediately to the NMR spectrometer (Bruker DRX 500 MHz). The methyl group signals of Ala[3] were employed to determine the *cis*/*trans* ratio. The asterisk indicates an impurity. (d) NMR-monitored *cis*-to-*trans* back-relaxation curves of Bz-Val-Gly-Ala-ψ[CSe-NH]Ala-OMe (○), Bz-Val-Gly-Ala-ψ[CSe-NH]Phe-OMe (●) and Bz-Val-Gly-Ala-ψ[CSe-N]Pro-OMe (▼) following a 5 min UV irradiation. Back-conversion from the *cis* to *trans* conformer occurred with half-life times of 12.6 and 29.4 min for (○) and (●), respectively, whereas (▼) showed no significant decrease in the *cis* proline content over a period of two hours at the applied temperature (10 °C).

Table 4.8 Characteristic *cis* signals in ^{1}H-NMR spectra.

Entry	Peptides	-	*trans*	*cis*	Δppm
1	Bz-Val-Gly-Ala-ψ[CSe–NH]Ala-OMe	Ala[3]	1.43	1.35	0.08
		Ala[4]	1.57	1.54	0.03
2	Boc-Val-Gly-Ala-ψ[CSe–NH]Ala-OMe	Ala[3]	1.44	1.37	0.07
		Ala[4]	1.58	1.54	0.04
3	Bz-Val-Gly-Ala-ψ[CSe–N]Pro-OMe	Ala[3]	1.36	1.31	0.05
4	Bz-Val-Gly-Ala-ψ[CSe–NH]Phe-OMe	Ala[3]	1.34	0.61	0.73
5	Ac-Ala-ψ[CS–NH]Phe-NH₂ [a]	Ala[1]	1.33	0.63	0.70
6	Ac-Cys-Ala-ψ[CO–NH]Phe-Cys-His-	Ala[2]	1.27	0.79	0.48

[a] Values are from Ref.(120); [b] Values are from Ref.(20)

4.3 Selective photoswitching of thioxo and selenoxo peptide bonds

As described in 4.2.1, the efficient photoswitching wavelength of selenoxo peptides is around 290 nm, which is 30 nm red shifted compared to the corresponding thioxo peptides. Therefore, it might be possible to selective excite the selenoxo or thioxo chromophores in the same peptide chain. To test this hypothesis, a thioxo and selenoxo dual-labeled peptide Ac-Val-Ala-ψ[CS−NH]Phe-Gly-Gly-Ala-ψ[CSe−NH]Phe-OMe was synthesized.

4.3.1 UV/Vis spectroscopic characterization

The UV/Vis spectrum of peptide Ac-VA-ψ[CS−NH]FGGA-ψ[CSe−NH]F-OMe featured two bands at 270 nm and 298 nm, which are originated from the thioxo and the selenoxo chromophore, respectively (Figure 4.17). After irradiation at 254 nm (6 mm slit), the excitation of the thioxo group was accompanied by a partial switching of the selenoxo group, as indicated by a small increase at 320 nm in the difference spectrum (Figure 4.18a). Exciting the selenoxo group with UV light at 288 nm (6 mm slit) led to a partial excitation of the thioxo group (Figure 4.18b). Nevertheless, by carefully adjusting the wavelength and slit (reduces the bandpass of the light beam), a better selective photoswitching could be achieved. To selectively switch the thioxo chromophore, the light beam was set to 254 nm with 2 mm slit (Figure 4.19). From the difference spectrum, 6% *cis*-[CS−NH] conformer was estimated to be formed after 6 min irradiation. To selectively switch the selenoxo chromophore, the light beam was set to 300 nm with 4 mm slit (Figure 4.20). 11% *cis*-[CSe−NH] conformer was estimated to be formed after 5 min irradiation. Therefore, the selectivity is controlled by the light purity, while the switching efficiency (amount of *cis* isomer in PSS) is controlled by the light intensity.
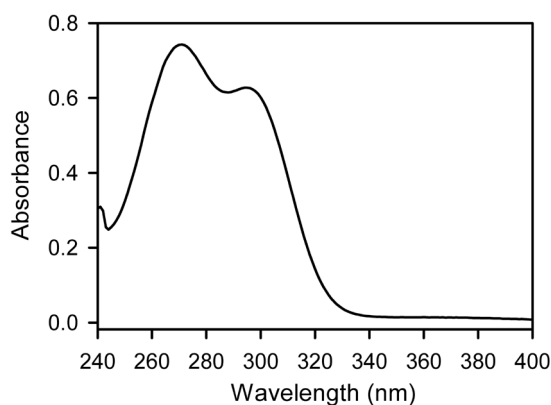
Figure 4.17 UV/Vis spectrum of Ac-VA-ψ[CS−NH]FGGA-ψ[CSe−NH]F-OMe in 33 mM phosphate buffer containing 5% DMF collected at 10 °C.

a

b
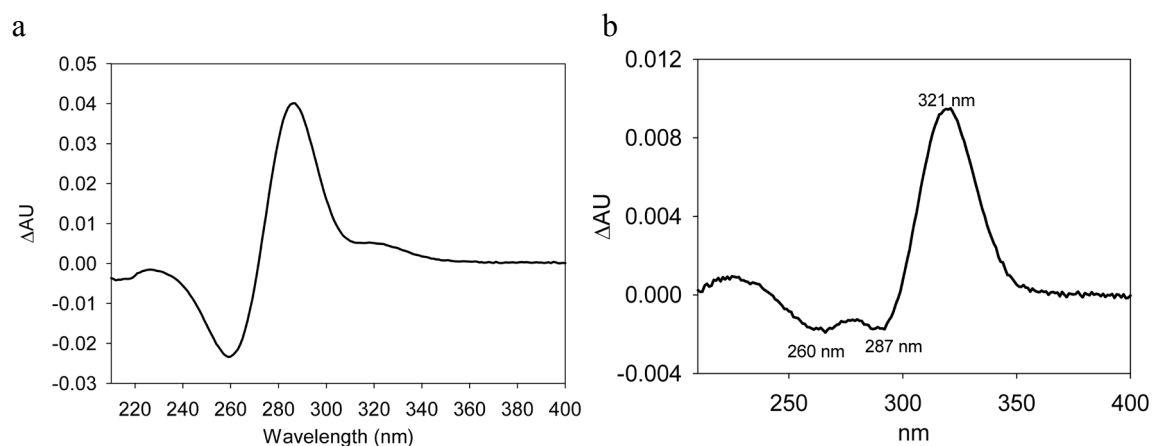
Figure 4.18 UV/Vis difference spectra of Ac-VA-ψ[CS−NH]FGGA-ψ[CSe−NH]F-OMe in 33 mM phosphate buffer containing 5% DMF collected at 10 °C. (a) Irradiation condition: 254 nm, 6 mm slit. (b) Irradiation condition: 288 nm, 6 mm slit.

a

b
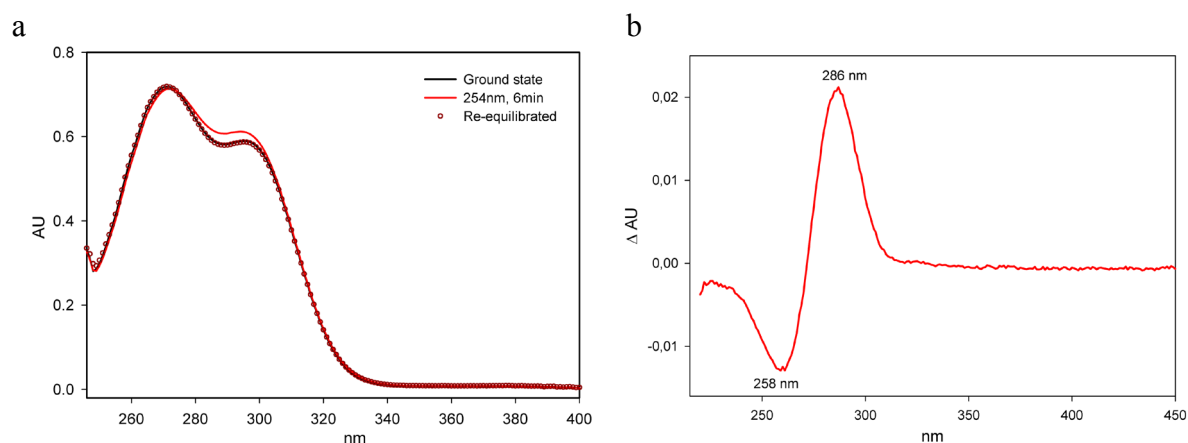
Figure 4.19 UV/Vis spectra of Ac-VA-ψ[CS−NH]FGGA-ψ[CSe−NH]F-OMe (52 μM) in 33 mM phosphate buffer containing 5% DMF collected at 10 °C. (a) Irradiation condition: 254 nm, 2 mm slit. (b) Difference spectrum.

a

b
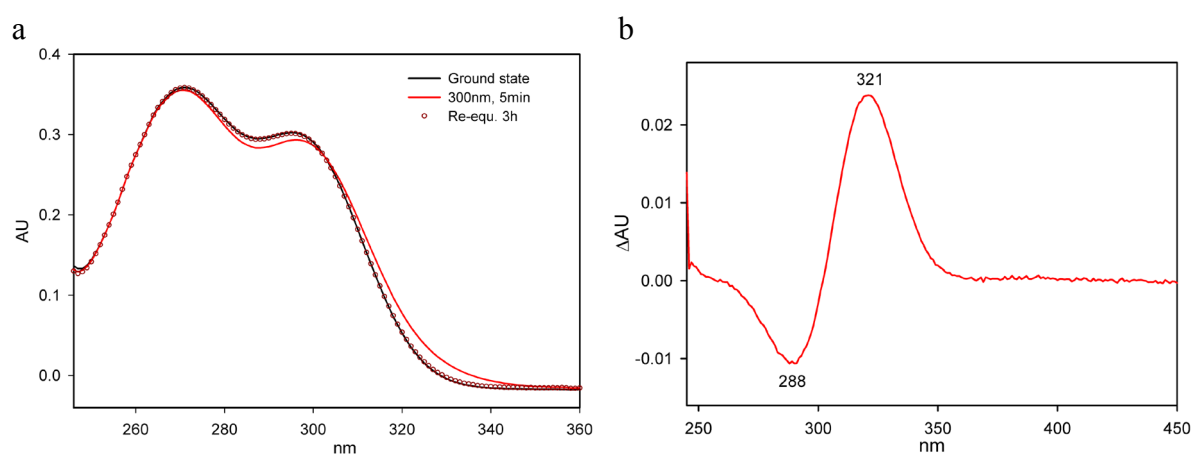
Figure 4.20 UV/Vis spectra of Ac-VA-ψ[CS−NH]FGGA-ψ[CSe−NH]F-OMe (27 μM) in 33 mM phosphate buffer containing 5% DMF collected at 10 °C. (a) Irradiation condition: 300 nm, 4 mm slit. (b) Difference spectrum.

4.3.2 NMR spectroscopic characterization

The photoswitching of Bz-VA-ψ[CS–NH]FGGA-ψ[CSe–NH]F-OMe was also confirmed by ^{1}H-NMR spectroscopy. Switching the thioxo chromophore by irradiation at 260 nm produced a new signal at 0.61 ppm, which was identified as the methyl group resonance of Ala[2] in the *cis* conformation (Figure 4.21b). Switching the selenoxo chromophore by irradiation at 288 nm produced a new signal appeared at 0.67 ppm, which was identified as the methyl group resonance of Ala[6] in the *cis* conformation (Figure 4.19c). Switching both chromophores by irradiation at 288 nm for 10 min followed by 260 nm for 4 min led to the appearance of both signals of 0.61 ppm and 0.67 ppm. Although the *cis* signals were very weak due to a high percentage of organic solvent (50% DMF) used to increase the peptide solubility, these results clearly indicated that two different conformations were produced upon irradiation at different wavelengths.
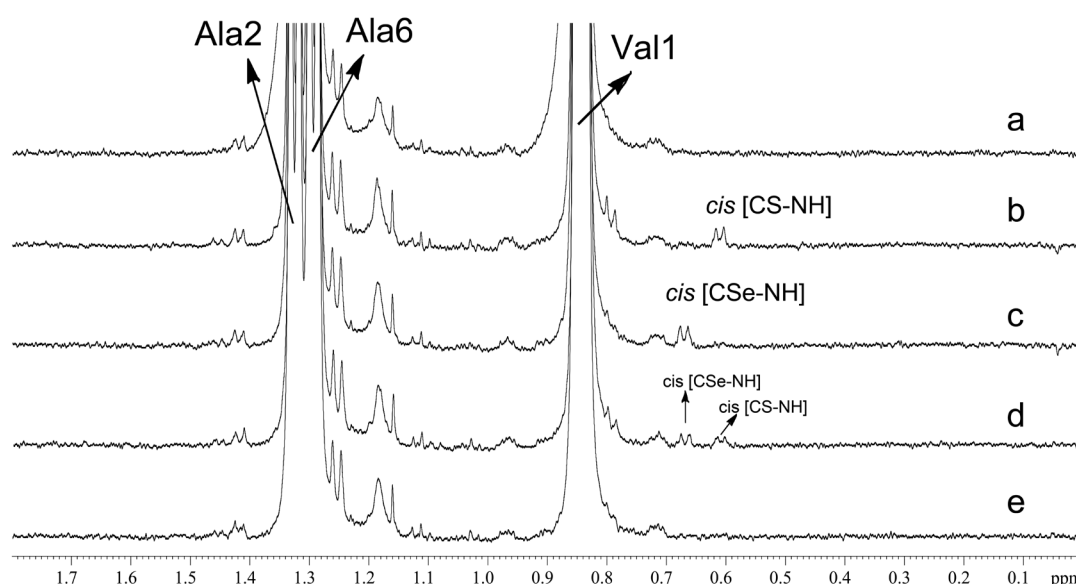
Figure 4.21 ^{1}H-NMR spectra of Ac-VA-ψ[CS–NH]FGGA-ψ[CSe–NH]F-OMe before and after UV irradiation. (a) ground state, (b) 10 min irradiation at 260 nm, (c) 10 min irradiation at 288 nm, (d) 10 min irradiation at 288 nm, followed by 4 min irradiation at 260 nm, (e) after equilibration. All spectra were collected with 1.7 mM peptide in 50% DMF/phosphate buffer (15 mM, pH 6.5) at 10 °C.

4.3.3 Influence of the conformation of the selenoxo group on the *cis→trans* isomerization of the thioxo group

By selectively switching the thioxo chromophore, the rate constant of the subsquent *cis→trans* decay was determined as $(4.6 \pm 0.1) \times 10^{-3}$ s^{-1}. To avoid the influence from the selenoxo chromophore, the monitoring wavelength for the *cis→trans* decay of ψ[CS−NH] was set to 258 nm. Since the *cis→trans* decay of the selenoxo peptide bond is considerably slower than the thioxo peptide bond, sequential excitation of the two chromophores could be achieved by 10 min irradiation at 288 nm followed by 260 nm irradiation for additional 4 min. In the dark reaction, the decay of *cis*-[CS−NH] finished while the [CSe−NH] is still in *cis* state. In this case, the rate constant of *cis*-[CS−NH] decay was determined as (4.0 ± 0.1) $\times 10^{-3}$ s^{-1}, which is slightly smaller than that in the single excitation experiments (Figure 4.22, Table 4.9). Therefore, the decay of the thioxo *cis* isomer was influenced by the conformation of the selenoxo group.
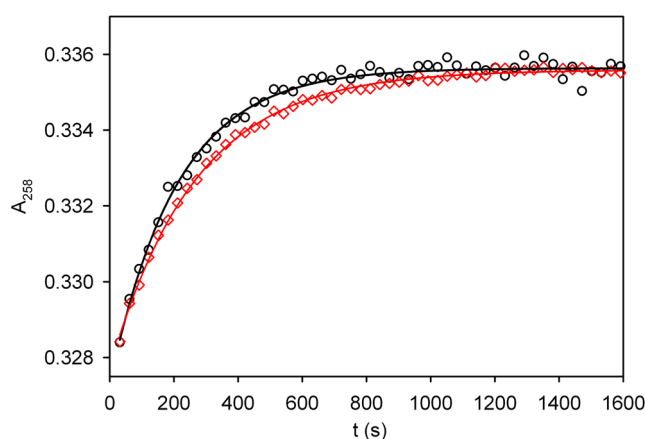
Figure 4.22 Time courses of the *cis*-[CS−NH] decay after selectively switching the thioxo group by 258 nm irradiation (circles) and after 10 min irradiation at 288 nm followed with 4 min irradiation at 260 nm (diamonds). Measurements were conducted at 10 °C with 20 μM Ac-VA-ψ[CS−NH]FGGA-ψ[CSe−NH]F-OMe in 30 mM phosphate buffer (pH 6.5) containing 5% DMF.

Table 4.9 Influence of different conformations of ψ[CSe−NH] on the ψ[CS−NH] *cis→trans* isomerization rate of Ac-VA-ψ[CS−NH]FGGA-ψ[CSe−NH]F-OMe

Peptide conformation	k_{ct} for [CS−NH] (s^{-1}) [a]
cis-ψ[CS−NH], *trans*-[CSe−NH]	$(4.6 \pm 0.1) \times 10^{-3}$
cis-[CS−NH], *cis*-[CSe−NH]	$(4.0 \pm 0.1) \times 10^{-3}$

[a] Time courses were recorded at 10 °C with 20 μM peptide in 30 mM phosphate buffer (pH 6.5) containing 5% DMF. Values represented an average of at least 3 times.

4.4 Enzymatic catalysis of *cis→trans* isomerization of selenoxo peptides

The peptidyl-prolyl *cis/trans* isomerization is well known to be catalyzed by human cyclophilin 18 (hCyp18). Herein, the ability of hCyp18 to catalyze selenoxo prolyl peptide bond *cis→trans* isomerization was tested. The *cis* content of Bz-VGA-ψ[CSe−N]P-OMe in the equilibrium was determined as 7.1%. After irradiation at 296 nm to achieve a higher *cis/trans* ratio, the *cis→trans* decay of [CSe−N] preceded slowly with a rate constant of $(1.5 \pm 0.2) \times 10^{-4}$ s^{-1}. Addition of 20 μl 100 mM hCyp18 to the photoswitched sample resulted in a rate constant of $(1.3 \pm 0.4) \times 10^{-4}$ s^{-1} which did not show any acceleration on the *cis→trans* decay (Figure 4.23).
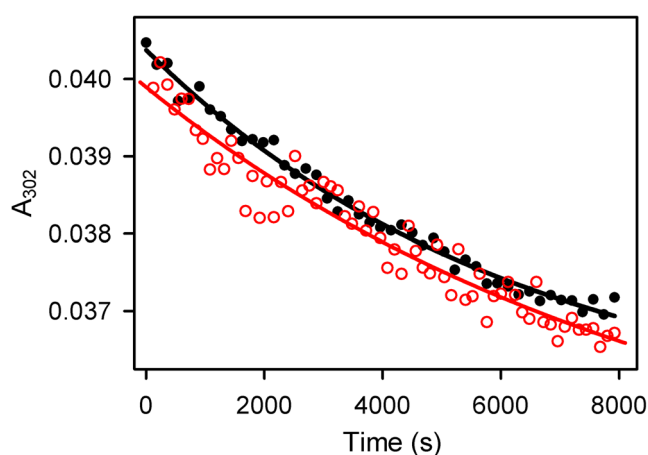
Figure 4.23 Time courses for the *cis→trans* decay of Bz-VGA-ψ[CSe−N]P-OMe in the presence (red circles) and absence of hCyp18 (black dots). Solid lines represent the least squares fits with exponential decay equation (first order), resulting in a rate constant of 1.12×10^{-4} s^{-1} and 1.58×10^{-4} s^{-1} in the presence and absence of hCyp18, respectively. Experimental condition: 2 ml 20 μM peptide solution in HEPES buffer (50 mM, pH 7.8) was irradiated for 5 min at 296 nm; then 20 μl hCyp18 (100 mM in HEPES buffer, pH 7.8) or buffer (as a control) was added to the cuvette and the *cis→trans* decay was monitored at 30 °C.

4.5 pH-dependent *cis→trans* isomerization of selenoxo peptides

4.5.1 *Cis→trans* isomerization of selenoxo peptides in alkaline aqueous solution

The *cis→trans* isomerization of the selenoxo peptides was found to be very sensitive to the pH conditions, especially above pH 8.0 (Figure 4.24, 4.26, 4.27). In contrast to a first-order exponential decay at neutral conditions, the decay at high pH showed a sigmoid curve (Figure 4.24b). Comparison of curve shapes did not reveal any dependence on peptide structure from Bz-VGAψ[CSe–NH]FA-NH$_2$ to Bz-VGAψ[CSe–NH]AA-NH$_2$ and Bz-VGAψ[CSe–NH]A-OMe (Figure 4.25, 4.27). Similar to the photoisomerization at neutral conditions (Figure 4.12a), the UV/Vis spectrum at alkaline conditions upon irradiation could also be restored after equilibration (Figure 4.27). In contrast, the *cis→trans* isomerization of the imidic selenoxo group [CSe–N<] in Bz-VGA-ψ[CSe–N]P-OMe was not accelerated by increasing the pH up to 10 (Figure 4.28); instead, a slight decrease of k_{ct} was observed, which might be resulted from the small amount of the ester-hydrolyzed peptide.
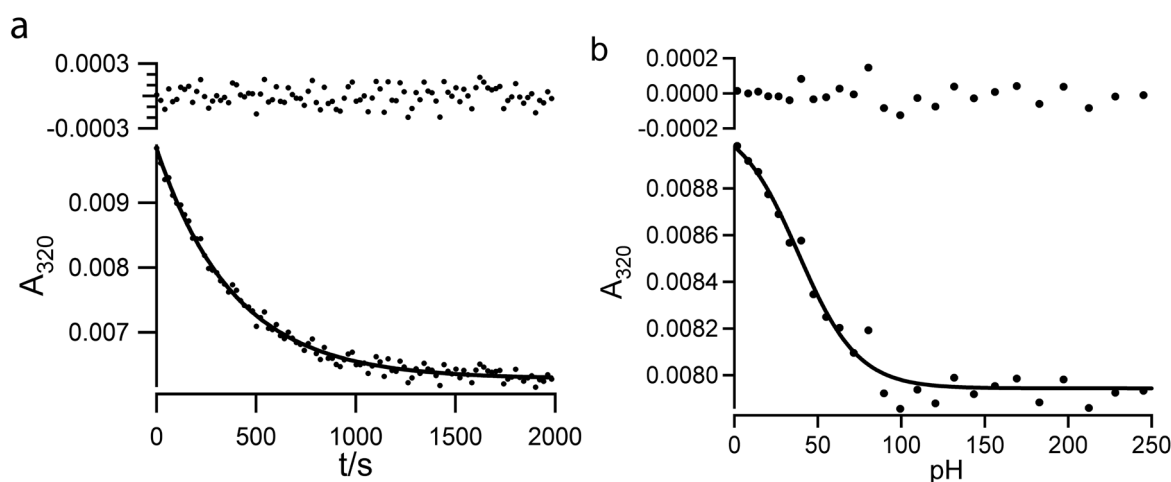
Figure 4.24 Time courses of the *cis* decay with peptide Bz-VGAψ[CSe–NH]FA-NH$_2$ (1 mM phosphate buffer) at pH 7.1 (a) and pH 9.9 (1 mM Gly-NaOH buffer) (b). Experiments were performed in 4.5 μM peptide solution at 20 °C. Excess of *cis* conformer was achieved by UV irradiation (288 nm, 4 min) and its decay was monitored at 320 nm. For the time course at pH 7.1, a first-order rate constant of 2.58×10^{-3} s^{-1} was calculated. The time course at pH 9.9 was fitted by equation (**I**) (see discussion in **5.4.2**), resulting in an apparent rate constant $k_{app} = 0.053$ s^{-1}. The solid lines represent least-squares fits. The plots of the residuals are given at the top of each graph.
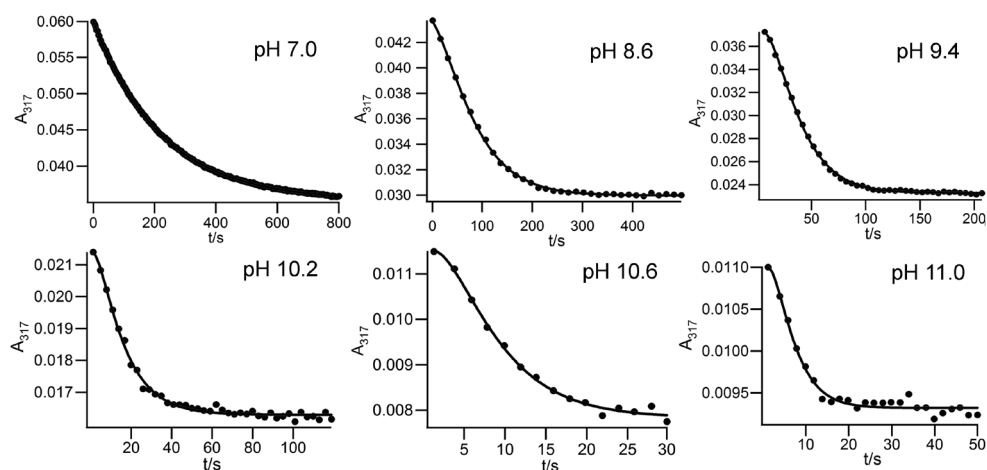
Figure 4.25 pH-dependence of *cis→trans* isomerization of Bz-VGAψ[CSe−NH]A-OMe at 20 °C. Measurements were performed with 10 μM peptide in 1 mM Gly-NaOH (for pH > 8) or 1 mM phosphate buffer (pH < 8). Time course recorded at pH < 8 was fitted by exponential equation (first order). Time courses recorded at alkaline conditions were fitted by equation (**I**) (see discussion in **5.4.2**). Irradiation condition: 286 nm, 4 min.
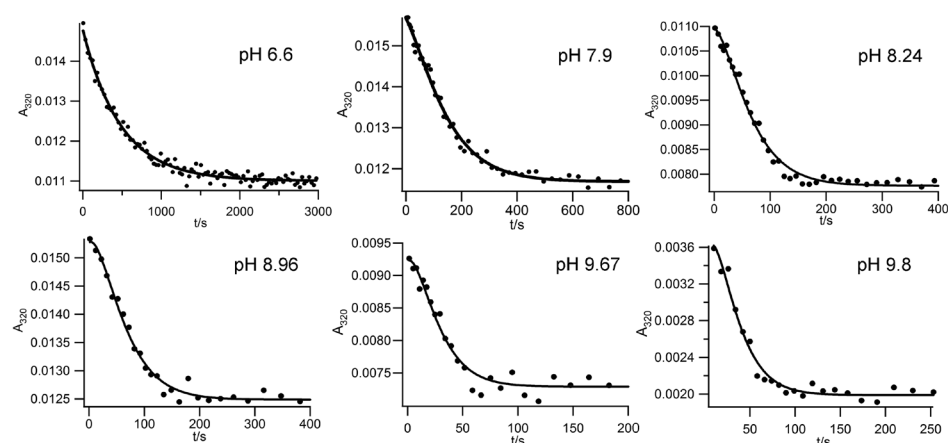
Figure 4.26 pH-dependence of *cis→trans* isomerization of Bz-VGAψ[CSe−NH]AA-NH$_2$ at 20 °C. Measurements were performed with 6 μM aqueous solution by adding NaOH solution to achieve an appropriate pH. Final pH was determined after photo-initiated *cis→trans* decay. Time course recorded at pH 6.6 was fitted by exponential equation (first order). Time courses recorded at alkaline conditions were fitted by equation (**I**) (See discussion in **5.4.2**). Irradiation condition: 288 nm, 4 min.
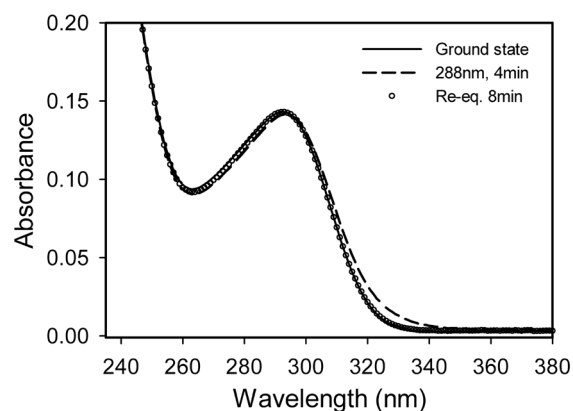
Figure 4.27 Reversible photoisomerization of 50 μM Bz-VGAψ[CSe−NH]FA-NH$_2$ in 1 mM Gly−NaOH buffer, pH 9.0, at 20 °C. Irradiation condition: 288 nm, 4 min.
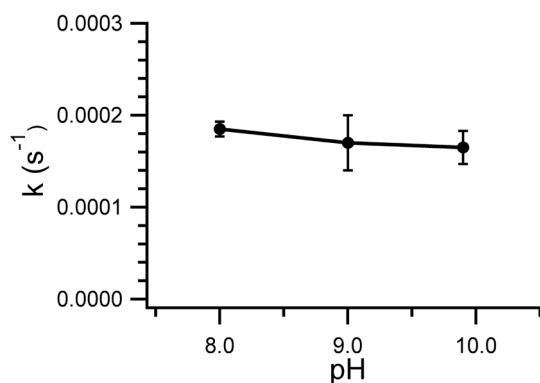
Figure 4.28 pH-dependence of k_{ct} determined for Bz-VGAψ[CSe–N]P-OMe at 30 °C. Measurements were performed in 1 mM phosphate buffer (pH 8.0) and 1 mM Gly-NaOH buffer (pH > 8). Irradiation condition: 296 nm, 4 min.

4.5.2 Peptide stability under photoswitching condition

To test the stability of the selenoxo peptide upon irradiation at alkaline conditions, NMR and HPLC analyses were performed before and after irradiation. HPLC analysis indicated that, although partial epimerization (Figure 4.29, green line) was observed after very long incubation period (1 week) at pH 9.8, the sample undergone a photo-initiated *cis→trans* decay did not show any degradation or epimerization (Figure 4.29, red line). ^{1}H-NMR experiments also confirmed that no new signal appeared after photoisomerization (Figure 4.30). Those results indicated that the observed kinetic behaviors are only resulted from conformational changes.
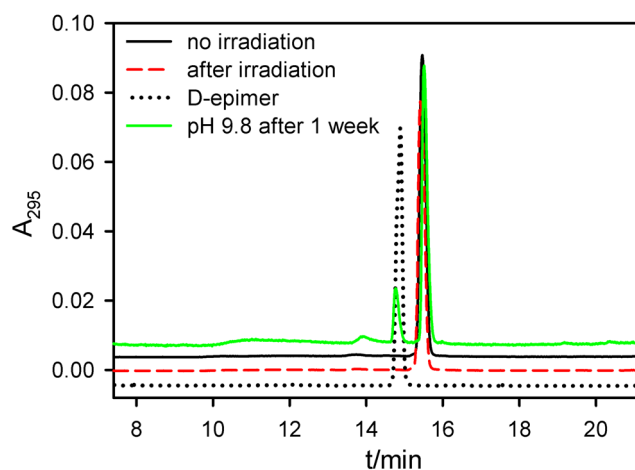
Figure 4.29 HPLC chromatograms of Bz-VGAψ[CSe–NH]FA-NH$_2$ before (black line) and after (red line) photoisomerization in 1 mM Gly-NaOH, pH 9.2. For comparison, the sample incubated at pH 9.8 for 1 week (green line), which showed partial epimerization, and the pure Bz-VGA^{D}ψ[CSe–NH]FA-NH$_2$ epimer (black dots) were also analyzed. Column: LiChrospher® 100, RP8 (5 μm) LiChroCART® 125-4; mobile phases: 0.05% TFA/H$_2$O (A); 0.05% TFA/ACN (B); gradient: 5-100% B, 30 min; flow rate: 1 ml/min.
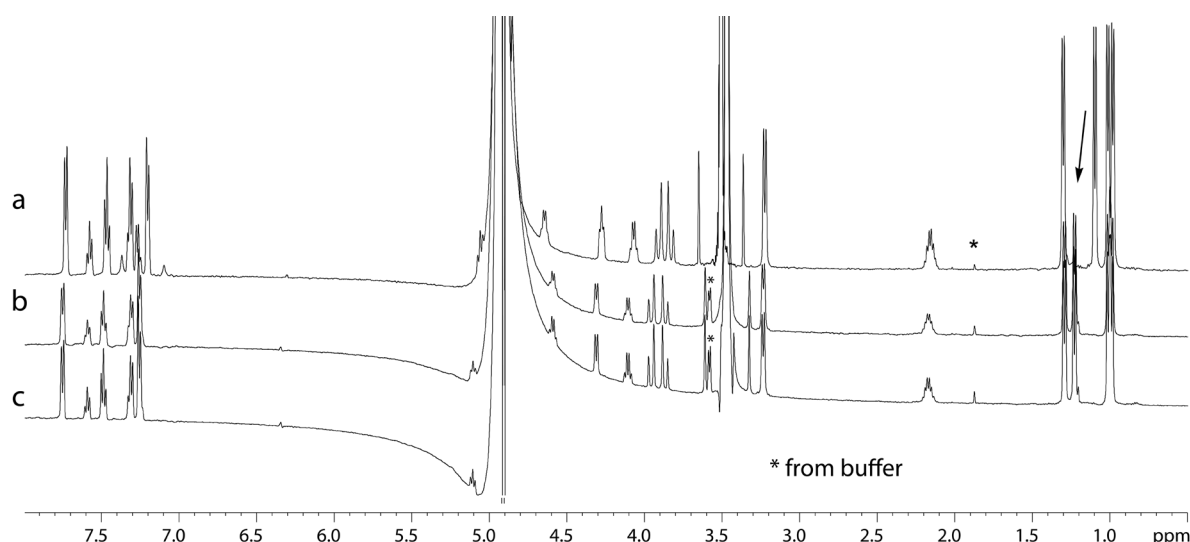
Figure 4.30 ^{1}H-NMR spectra of 0.4 mM Bz-VGAψ[CSe–NH]FA-NH$_2$ in 20 mM Gly-NaOH at pH 7.0 (a), pH 9.6 (b), and pH 9.6 after 5 min irradiation at 288 nm (c). The arrow indicates the shift of the Ala^5 methyl group signal upon pH jump from 7.0 to 9.6.

4.5.3 Concentration dependence of *cis→trans* isomerization rate at alkaline conditions

It was found that the rates for *cis→trans* isomerization of Bz-VGAψ[CSe–NH]A-OMe at alkaline conditions is concentration-dependent, with a faster rate at high sample concentration. The rate constants calculated based on the proposed mechanism (discussed in **5.4.2**) were linearly increased upon concentration increase (Figure 4.31). Extrapolating the concentration to zero resulted in a k_{EZ}^{obs} value of 0.1 s^{-1}.
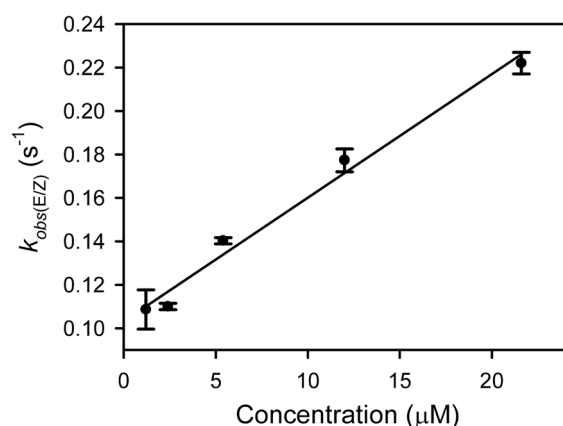
Figure 4.31 Concentration dependence of k_{EZ}^{obs} of Bz-VGAψ[CSe–NH]A-OMe in 1 mM Gly-NaOH buffer (pH 9.7) at 20 °C. k_{EZ}^{obs} values were derived from equation (**II**) with restrictions of k_{ct} = 0.003 s^{-1} pK^{trans} = 9.8, and pK^{cis} = 9.7 (in Discussion, Figure 5.6b). The linear fit resulted in a slope of 0.0057 and an intercept of 0.10 s^{-1}.

4.5.4 Solvent deuterium kinetic isotope effect on the selenoxo amide dissociation and *cis→trans* isomerization

Solvent deuterium kinetic isotope effect (SKIE) is very usful to evaluate the involvement of water molecules in a reaction since a hydrogen bond with deuterium is slightly stronger than that involved with ordinary hydrogen (157). It has long been known that the pK_a of weak acids are larger in deuterium oxide (D_2O) than in protium oxide (H_2O) (158). The pK_a of Bz-VGAψ[CSe−NH]FA-NH$_2$ was determined as 9.1 in water solution (Figure 4.32), whereas the pK_a in heavy water was 9.75, i.e. 0.65 units higher than in water. As the dissociation of selenoxo amide proton has strong influence on the rate of *cis→trans* decay, the SKIE was determined as a value of $k_{EZ}^{obs}(H_2O)/k_{EZ}^{obs}(D_2O) = 1.13 \pm 0.04$ at the same level of dissociation, i.e. pH 9.2 in H_2O and at pD 9.85 in D_2O (Figure 4.32b). At pH 6.6, the selenoxo group is overwhelmingly in the protonated form with the SKIE value of $k_{ct}(H_2O)/k_{ct}(D_2O) = 1.004 \pm 0.008$.
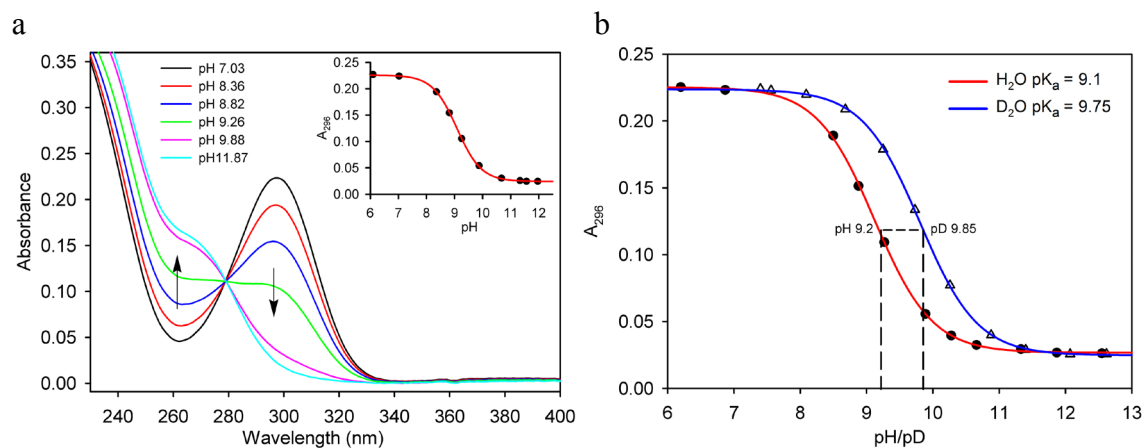
Figure 4.32 (a) pH-dependent UV/Vis spectra of Bz-VGAψ[CSe−NH]FA-NH$_2$ in aqueous solution. (b) pH-dependent dissociation of the selenoxo amide proton in H_2O and D_2O monitored at 296 nm. The solid curves represented the least squares fit to Henderson-Hasselbalch equation, resulting in a pK_a value of 9.1 in H_2O and 9.75 in D_2O, respectively. All spectra were collected at 20 °C.

4.5.5 C−N rotational barrier and nitrogen inversion barrier

The rotational barrier of Bz-VGA-ψ[CSe−NH]A-OMe at pH 6.5 was determined as 20.7 kcal/mol at 20 °C (Table 4.7), whereas both C−N rotation and nitrogen inversion contributed to the *cis→trans* isomerization in alkaline conditions (discussed in **5.4**). The apparent rate constants for *cis→trans* isomerization could be obtained using equation (**I**) (see discussion **5.4.2**). Presuming that k_{ct} is not pH dependent within the actual pH range, the k_{EZ}^{obs} was calculated using equation (**II**). Based on the concentration vs. k_{EZ}^{obs} relation in

Figure 4.31, the uncatalyzed inversion rate constant k_{EZ}^{uncat} was derived as $k_{EZ}^{uncat} = k_{EZ}^{obs} -$ 0.0057c (where c is the peptide concentration). Thus, the Eyring plot for the uncatalyzed nitrogen inversion in selenoimidate anion of Bz-VGAψ[CSe–NH]A-OMe at pH 9.7 was obtained (Figure 4.33), which showed a linear trend. A barrier of 18.4 kcal/mol was calculated for the $E{\rightarrow}Z$ inversion in the selenoimidate anion (Table 4.10).
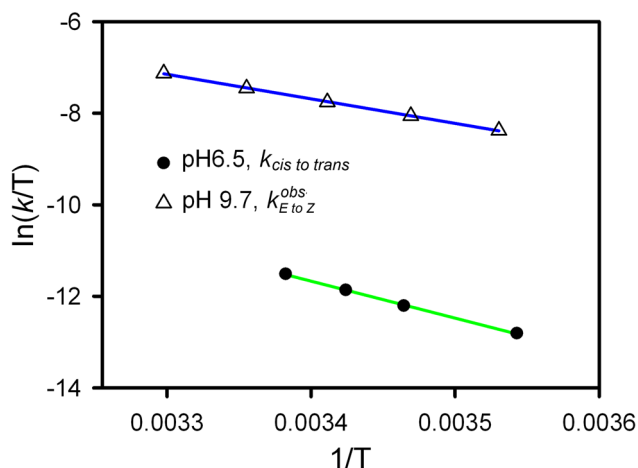
Figure 4.33 Eyring plots of *cis→trans* isomerization and $E{\rightarrow}Z$ inversion of Bz-VGAψ[CSe–NH]A-OMe. Data at pH 6.5 (dots) and pH 9.7 (triangles) were measured in 33 mM phosphate buffer and 1 mM Gly-NaOH buffer, respectively.

Table 4.10 Kinetic and thermodynamic parameters of *cis→trans* isomerization and $E{\rightarrow}Z$ inversion in Bz-VGAψ[CSe–NH]A-OMe.

	k (s^{-1}) [a]	$\Delta H^{\ddagger}$ [b] (kJ mol^{-1})	$\Delta S^{\ddagger}$ [b] (J K^{-1} mol^{-1})	$\Delta G^{\ddagger}$ [c] (kcal mol^{-1})
[CSe–NH-] pH 6.5, *cis→trans*	$(2.9 \pm 0.45) \times 10^{-3}$	67.1 ± 1.4	-67 ± 1.3	20.7 ± 0.4
[C(Se$^-$)=N-] pH 9.7, $E{\rightarrow}Z$	0.125 ± 0.01 [d]	44.5 ± 1.5	-110 ± 5.1	18.4 ± 0.7

[a] values at 293 K.
[b] from the Eyring plots.
[c] based on Gibbs function $\Delta G^{\ddagger} = \Delta H^{\ddagger} - T\Delta S^{\ddagger}$ with T = 293 K.
[d] k_{EZ}^{uncat} calculated based on $k_{EZ}^{uncat} = k_{EZ}^{obs} - 0.0057c$ (c = 10 μM).

4.5.6 pH-dependence of the *cis→trans* isomerization of thioxo peptides

For the sake of comparison, the pH dependence of k_{ct} was also studied for thioxo peptides. As shown in Figure 4.34a, in contrast to the selenoxo peptides that showed a remarkable acceleration upon pH increase, the *cis→trans* isomerization rate of Bz-VGA-ψ[CS−NH]FA-NH$_2$ revealed a decreasing trend at high pH conditions. Moreover, no sigmoid decay behavior was observed (Figure 4.34b). Bz-VGA-ψ[CS−NH]AA-NH$_2$ showed a similar behavior.

a   b
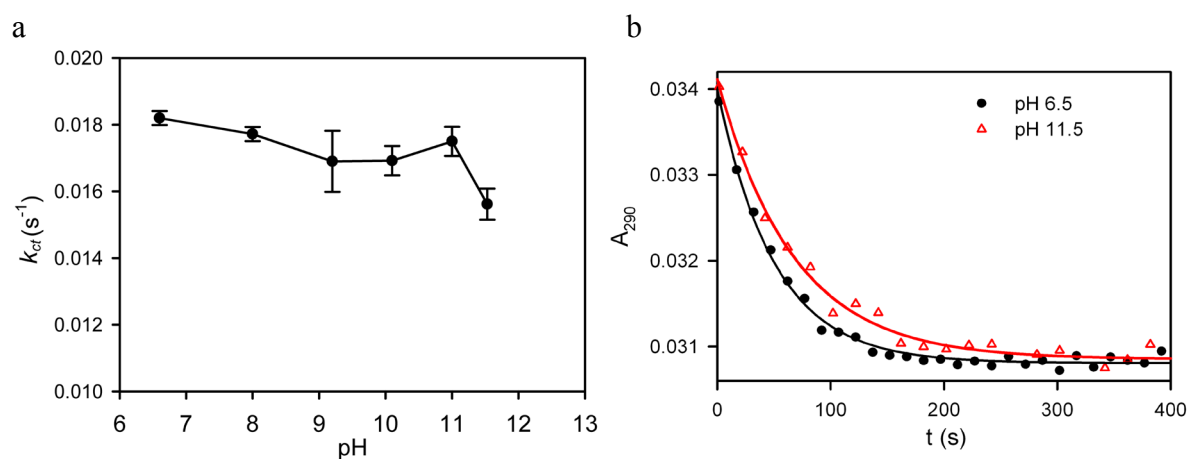
Figure 4.34 (a) pH-dependent *cis→trans* isomerization of Bz-VGAψ[CS−NH]FA-NH$_2$ (20 μM) at 20 °C. An excess of *cis* isomer was achieved by irradiation with 260 nm UV light for 4 min and the *cis* decay was then monitored at 290 nm. (b) Superposition of time courses of pH 6.5 and pH 11.5. Solid lines represent the least-squares fits with exponential decay equation (first-order). Data for pH < 8 and pH > 10.8 were measured in 1 mM phosphate buffer; data for 8 ≤ pH ≤ 10.8 were measured in 1 mM Gly-NaOH buffer.

4.5.7 Irreversibility of the photoisomerization under high pH conditions

When we investigated the pH-dependent *cis→trans* isomerization, we found that at high pH conditions photoisomerization was not reproducible by re-irradiation. Namely, after one cycle of photoisomerization-relaxation, a re-irradiation led to only a weak absorbance increase at 320 nm, and the decay was apparently faster than after the first irradiation process (Figure 4.35). Even adding some fresh peptide solution into the irradiated peptide solution, an efficient photoisomerization of the mixture could not be observed (Figure 4.36). Surprisingly, by neutralizing to pH 7.3, the photoswitching efficiency could be restored (Figure 4.35) and showed a *cis→trans* decay rate constant of 3.2×10^{-3} s^{-1}, which is close to the value of 2.58×10^{-3} s^{-1} measured at the normal conditions (1 mM phosphate buffer, pH 7.1).
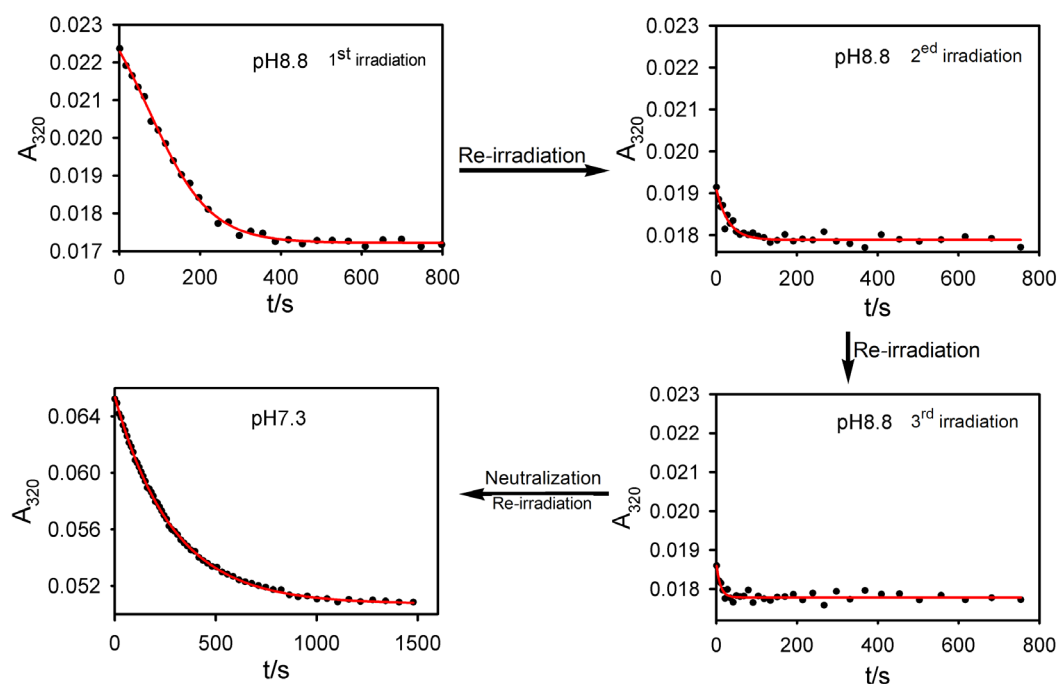
Figure 4.35 Repetitive irradiation of 15 μM Bz-VGAψ[CSe−NH]FA-NH$_2$ in 5 mM Gly-NaOH, pH 8.8. After three irradiation-relaxation steps, the peptide solution was neutralized with HCl to pH 7.3 and irradiated again. The time interval among each irradiation (288 nm, 4 min) is 15 min.
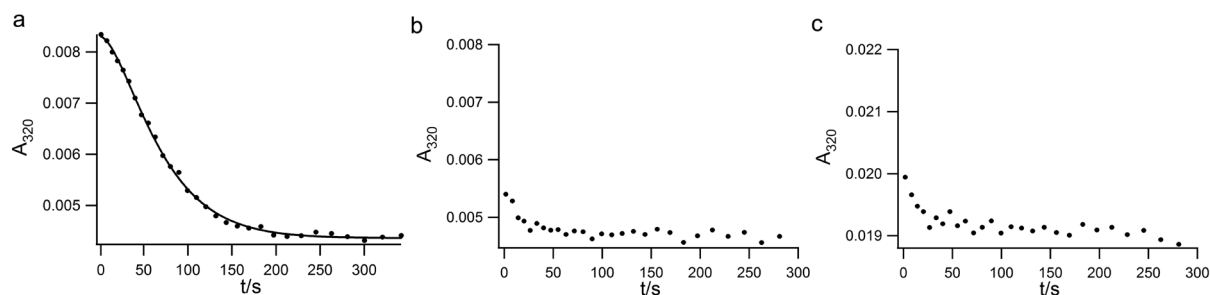
Figure 4.36 The time course of *cis→trans* decay irradiation of 5 μM Bz-VGAψ[CSe−NH]FA-NH$_2$ in 5 mM Gly-NaOH (pH 9.2) monitored after the first irradiation (a). After 10 min decay the same sample was re-irradiated and the time course was monitored for 5 min (b). To the same cuvette was added 10 μM new peptide stock solution and irradiated again, and the time course was then monitored (c).

4.6 Comparative analysis of the physicochemical properties of peptides upon chalcogen substitutions

The physicochemical properties of oxo, thioxo and selenoxo peptide bonds always follows the same general trend. For example the $\Delta G^{\ddagger}$ increases in the order of Se > S > O. However, the widely used electronegativity of the chalcogen atoms is apparently not applicable to explain such substitution effect, thus a further analysis is required. For this purpose, the following peptides (Table 4.11) as well as some literature data were employed to investigate the influences of thioxo and selenoxo modulation on the backbone structure of peptides and proteins.

Table 4.11 Peptides used for evaluating the effects of chalcogen substitution on peptide backbones.

Name	Sequence
1a	Bz-Val-Gly-Ala-Ala-OMe
1b	Bz-Val-Gly-Ala-ψ[CS−NH]Ala-OMe
1c	Bz-Val-Gly-Ala-ψ[CSe−NH]Ala-OMe
2a	Bz-Val-Gly-Ala-Phe-OMe
2b	Bz-Val-Gly-Ala-ψ[CS−NH]Phe-OMe
2c	Bz-Val-Gly-Ala-ψ[CSe−NH]Phe-OMe
3a	Bz-Val-Gly-Ala-Pro-OMe
3b	Bz-Val-Gly-Ala-ψ[CS−N]Pro-OMe
3c	Bz-Val-Gly-Ala-ψ[CSe−N]Pro-OMe

4.6.1 Absorption bands in UV/Vis spectra

The electronic absorption of amide bonds in peptides and simple amides has been studied extensively to date. In secondary amide bonds, the $\pi-\pi^*$ transition generally is found at 185-190 nm and the $n-\pi^*$ transition at 210-220 nm (159). Upon oxygen to sulfur substitution in Bz-VGAψ[C**X**−NH]A-OMe (**1**), the resulting thioxo group of peptide **1b** showed characteristic electronic absorption bands at 263 nm ($\pi-\pi^*$ transition) and at 326 nm ($n-\pi^*$ transition). These bands were further red-shifted to 294 nm and 366 nm, respectively, in the corresponding selenoxo peptide **1c** (Figure 4.6).
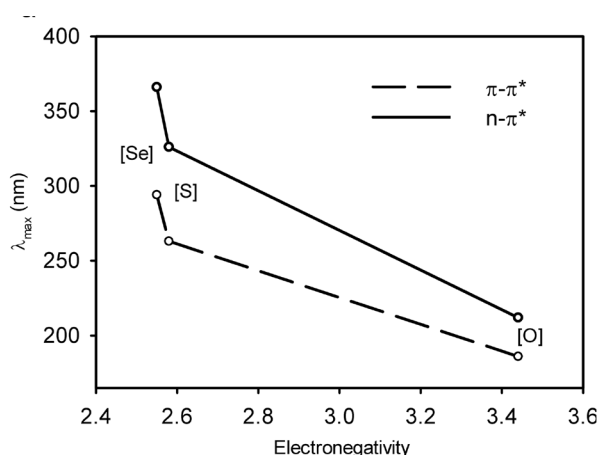
Figure 4.37. Correlation of λ_{max} versus electronegativity for the Bz-VGAψ[C**X**–NH]A-OMe (**X** = O, S, Se) peptide series.

When the electronic absorption data of the chalcogen-substituted peptides were plotted against the corresponding chalcogen atomic electronegativities (Table 1.1, pp11), no simple correlation could be obtained (Figure 4.37). The atomic polarizability, on the other hand, revealed perfect linear trends (Figure 4.38a). Moreover, the same linear correlation is also observed in the case of imidic peptide bond (Figure 4.38b).
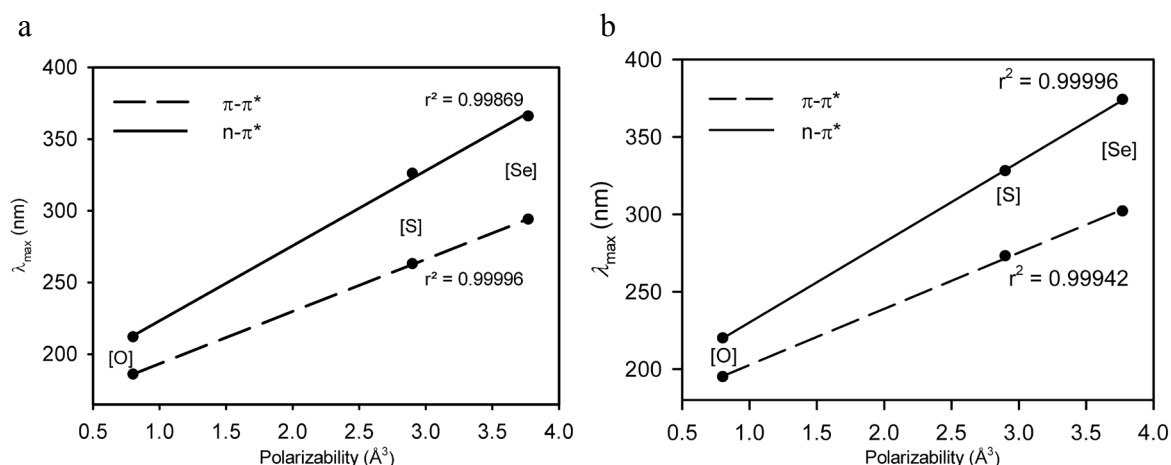
Figure 4.38 Correlation of λ_{max} versus polarizability for the Bz-VGAψ[C**X**–NH]A-OMe and Bz-VGAψ[C**X**–N]P-OMe (**X** = O, S, Se) peptide series. For the oxo peptide bond, wavelength values of 185 nm and 214 nm were chosen as representative for the π–π^* and n–π^* transitions, respectively (159).

4.6.2 Infrared spectroscopy

The infrared spectra of the oxo, thioxo and selenoxo forms of Bz-VGAψ[C**X**–NH]A-OMe peptide series were collected in tetrahydrofuran. The NH stretching band in oxo peptide was centered at 3287 cm^{-1}. In case of **X** = S or Se, a new peak appeared at lower frequency (Figure 4.39a), which may be due to the lower bond strength of N–H upon chalcogen substitution. Interestingly, the NH stretching frequencies were also linearly shifted with the increasing chalcogen atomic polarizabilities (Figure 4.39b).
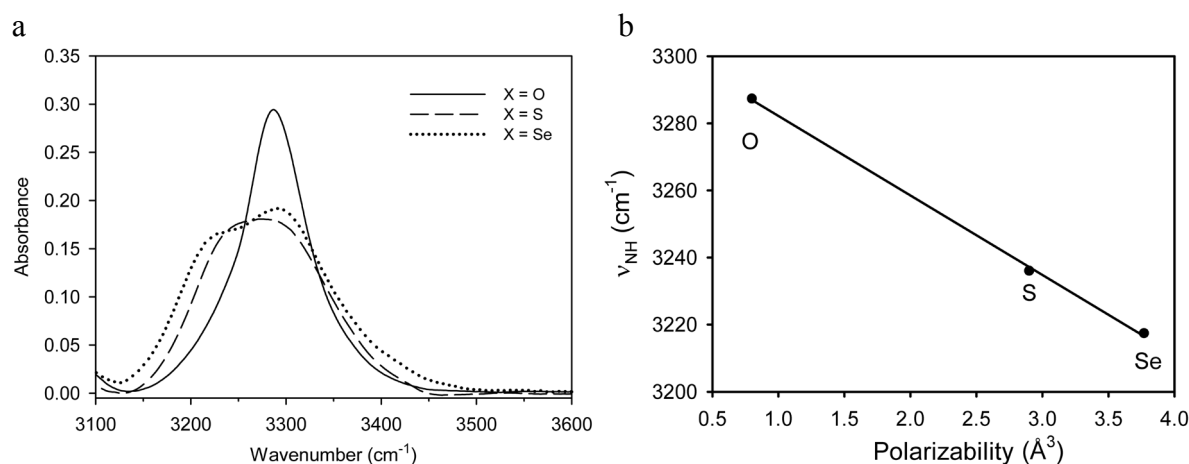
Figure 4.39 (a) The NH stretching region of Bz-VGAψ[CX–NH]A-OMe in infrared spectra collected in THF at rt. (b) ν_{NH} plots against chalcogen atomic polarizability.

4.6.3 NMR spectroscopic analysis of oxo, thioxo, and selenoxo peptides

In order to better understand the electronic properties of peptide bonds upon chalcogen-substitution, the ^{1}H, ^{13}C and ^{77}Se (natural abundance) resonances of a series of model peptides (Table 4.11) were assigned using multidimensional NMR (Appendix Tables App1-App9). The ^{1}H-NMR spectra of the Bz-VGAψ[CX–NH]F-OMe peptide series showed that the ^{1}H resonances of both Ala^3 and Phe^4 amide protons were continuously downfield shifted in the order O < S < Se (Figure 4.7a), thus indicating that, although the heavier chalcogen atoms are less electronegative than oxygen, the heavier chalcogen substitution resulted in an increasing "electron-withdrawing" effect on the peptide amide protons.
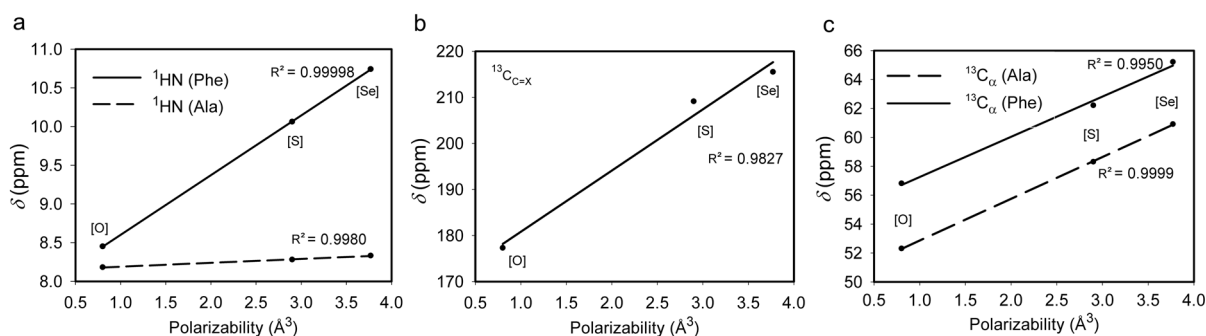
Figure 4.40 (a) Plot of chemical shift values of the Ala^3 and Phe^4 amide protons versus chalcogen atomic polarizability. Spectra were recorded in 50 mM sodium acetate buffer, pH 6.0, 10 °C. (b) Plots of ^{13}C=X (X = O, S, Se) and (c) the adjacent two alpha carbons chemical shift values versus chalcogen polarizability for the Bz-VGAψ[CX–NH]F-OMe peptide series. Spectra were recorded in 33 mM phosphate buffer, pH 6.5, 10 °C.

Analogous to the above-described linear relationships, the chemical shifts of the amide proton in Ala^3 and Phe^4 also linearly varies against the chalcogen polarizabilities (Figure 4.40a). Furthermore, linear correlations to the chalcogen polarizability were found for the

^{13}C chemical shift values of the chalcogen-substituted carbonyl carbon (i.e., ^{13}C=**X**) as well as the two adjacent C$_\alpha$ atoms (Figure 4.40b, 4.41c). A slight deviation of the ^{13}C=**X** vs. polarizability plot may be due to the anisotropic effect of the large S and Se atoms.

Similar chalcogen-dependent electronic effects were observed also for the Bz-VGAψ[C**X**–NH]A-OMe and Bz-VGAψ[C**X**–N]P-OMe peptide series. In the latter case, the chemical shifts of both *trans* and *cis* prolyl conformers were assigned (Figure 4.41, Tables in Appendix).
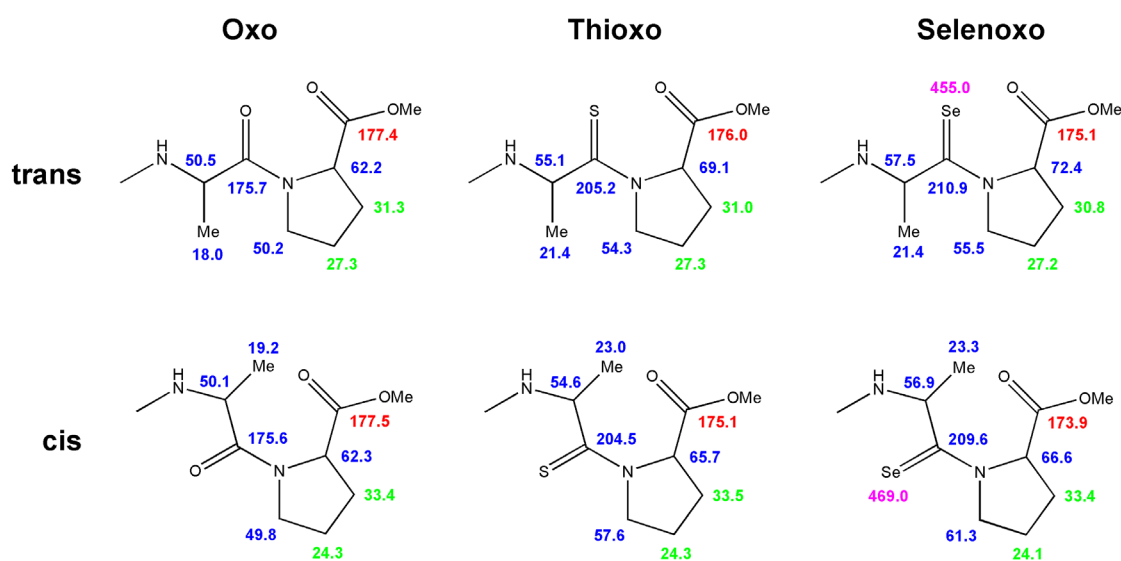
Figure 4.41. ^{13}C and ^{77}Se NMR resonance assignments of Ala^3 and Pro^4 in the *trans* and *cis* prolyl conformers of Bz-VGAψ[C**X**–N]P-OMe peptide series. Chemical shift values in blue and red color highlights ^{13}C nuclei showing significant downfield or upfield shifts, respectively, in the order O → S → Se. ^{77}Se chemical shifts are indicated in pink. Spectra were recorded in 33 mM phosphate buffer, pH 6.5, 10 °C.

The chemical shift values of all ^{13}C nuclei within a three-bond distance to the chalcogen atoms again displayed linear correlations to the polarizability (Figures 4.43). Moreover, comparison of the observed frequency shifts in the C$_\alpha$ and C$_\delta$ resonances of Pro^4 revealed a stereochemical influence on the electron-withdrawing effects exerted by the chalcogen atoms, depending on the relative conformation of the peptide bond. While the C$_\alpha$ resonance of Pro^4 showed a stronger downfield shift in the *trans* prolyl conformer (slope = 3.41) than in the *cis* prolyl conformer (slope = 1.48), the opposite trend was observed for the C$_\delta$ resonance of Pro^4, where the downfield shift is stronger in the *cis* conformer (slope = 3.85) than in the *trans* conformer (slope = 1.82) (Figure 4.42c). These data suggested that the electron-withdrawing effect due to the chalcogen atom is dependent not only on the through-bond distance but also on the spatial arrangement of those bonds. Considering the pronounced double bond character between carbonyl carbon and amide nitrogen, the

aliphatic carbon nucleus in **Z** position to the chalcogen atom is always more strongly deshielded than the aliphatic carbon in **E** position. This stereochemical influence on nuclear shielding, which is due to the stronger ^3J coupling between the substitutents positioned in **E** conformation across a double bond, apparently becomes more pronounced in case of **X** = S, Se than **X** = O, probably due to the enhanced double bond character of C–N in the heavier chalcogen-substituted peptide bonds.
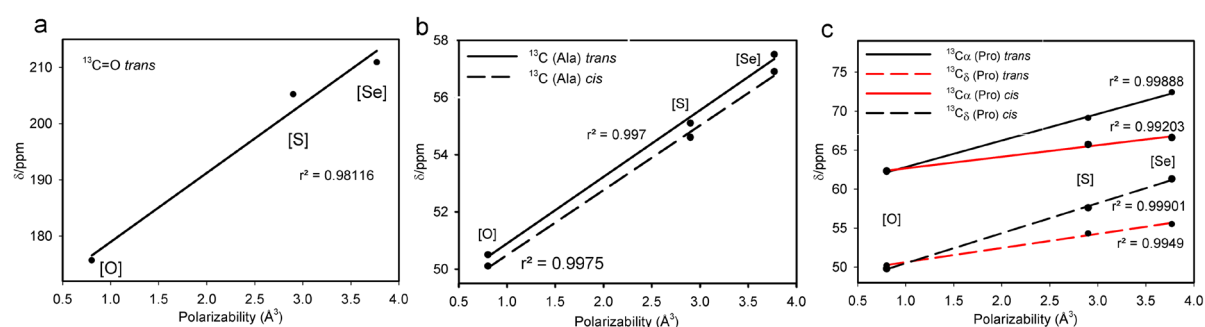
Figure 4.42 Correlation plots showing ^{13}C chemical shift values versus chalcogen polarizability in the Bz-VGAψ[C**X**–N]P-OMe peptide series.

Interestingly, the carbonyl ^{13}C resonances of the C-terminal amino acid in the oxo, thioxo and selenoxo forms of the same peptide sequence are considerable shielded in the order of Se > S > O. In other words, while heteronuclei within a three-bond distance to the chalcogen are generally increasingly deshielded with higher chalcogen order, the C-terminal carbonyl carbon at a four-bond distance to the chalcogen in contrast are increasingly shielded. Analogous shielding trends for the C-terminal carbonyl carbon atom were also found in the Bz-VGAψ[C**X**–NH]A-OMe and Bz-VGAψ[C**X**–NH]F-OMe peptide series (Figure 4.43). It must be noted, however, that the shielding trend in the *cis* conformer of the Bz-VGAψ[C**X**–N]P-OMe peptide series showed a larger magnitude than in the *trans* conformers, which coincides with the reduced electron depletion of the Pro[4] C_α in the *cis* conformer due to the different stereochemical arrangement.
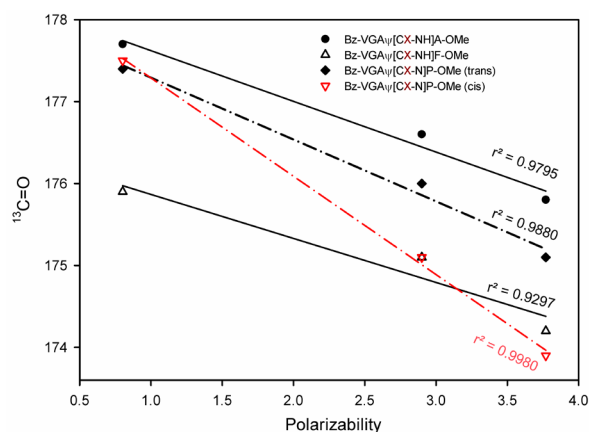
Figure 4.43 Comparison of carbonyl ^{13}C shift values (in ppm) at the C-terminal end of the oxo, thioxo and selenoxo peptides at pH 6.5. All slopes are similar except for the *cis* form of Bz-VGAψ[C**X**–N]P-OMe shown in red.

4.6.4 Influence of chalcogen substitutions on the C–N rotational barrier and other chemical properties

The above described relationships of the chalcogen atomic polarizabilities with the UV/Vis absorption wavelengths, NH vibration frequencies and nuclei shielding intrigued us to analyze whether other physicochemical parameters of the chalcogen-substituted peptide bonds also show a linear relation to the chalcogen atomic polarizabilities. Therefore, the chalcogen atomic polarizabilities were plotted against C–N rotation barriers, dipole moments and pK_a values in oxo, thioxo and selenoxo peptides or amides.

The rotational barrier values of peptides **2b** and **2c** were listed in Table 4.7. For the corresponding oxo peptide bonds, a value reported for the peptide Ala-Ala-ψ[CO–NH]Tyr-Ala-Ala was employed (19), since the rotation barriers of peptide bonds preceding aromatic residues feature similar amplitudes. The dipole moments were all taken from a model study of $CH_3[C\mathbf{X}–N](CH_3)_2$ (**X** = O, S, Se) in benzene (160). For the pK_a values of the oxo, thioxo and selenoxo peptide bonds, we applied 17.5 (obtained from Gly-Gly (161)), 11.6 (obtained from **1b**), and 9.8 (obtained from **1c**), respectively. Remarkably, all plots in Figure 4.44 delineate nearly perfect linear correlations. Moreover, the decreasing pK_a values of the heavier chalcogen-substituted peptides coincide with the above-mentioned line broadening of the amide proton signals due to faster solvent exchange (Figure 4.7a).
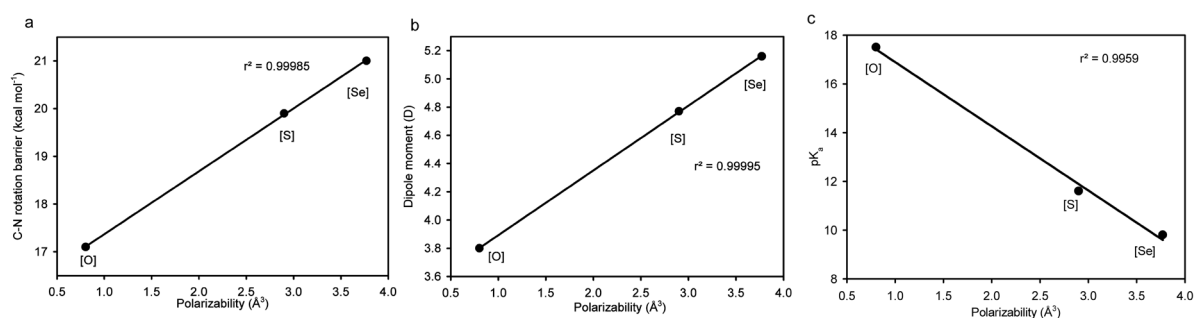
Figure 4.44. Correlation plots of chalcogen polarizability versus rotational barrier (a), dipole moment (b) and pK_a value (c) of the chalcogen-substituted peptides or amides. The origin of the data is described in the text.

5. Discussion

5.1 Synthesis and characterization of selenoxo peptides

Modification of peptide backbones by thioxo substitution has been well developed during the last two decades. Especially, the thioxylation method that uses a highly reactive thioxylation building block has been widely used to synthesize endo-thioxo peptides with site-specificity and high enantiopurity. Importantly, this method has proven compatible with Fmoc-based solid phase peptide synthesis (162, 163). Up to date, three types of building blocks have been developed that no racemization observed in the thioxylation reaction (Figure 5.1): (**I**) Benzimidazolinone (164), (**II**) Benzotriazole (165) and (**III**) Phthalimide (166). The benzotriazole derivatives are most widely used.

I   **II**   **III**
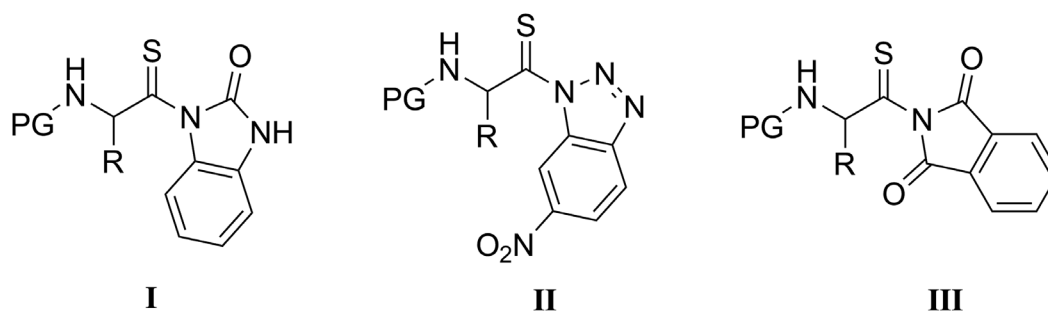
Figure 5.1 Thioxylation building blocks. PG = protecting group.

However, attempts to synthesize the selenium-substituted surrogates of those three types of derivatives were not successful (167). Therefore, we turned our attention to the selenation strategy where Woollins' reagent (2,4-diphenyl-1,3-diselenadiphosphetane 2,4-diselenide) is used to selenate a protected dipeptide as shown in Scheme 4.1. Most peptide bonds were selenated with a moderate to high yield, except for the imidic peptide bond (Table 4.1). Replacing the Boc protecting group with Fmoc led to an apparent improvement in yield, although the selenation reaction was much slower due to the steric hindrance by the Fmoc group.

Despite the high reactivity of the selenoxo carbonyl, deprotection of the Boc protecting group succeeded by using $ZnCl_2 \cdot Et_2O$ solution or 50% TFA/DCM. The coupling of the free amino dipeptide ester with the C-terminal fragment was carried out by the mixed anhydride method, resulting in selenoxo peptides with a moderate yield. The present method provides a possibility to synthesize selenoxo peptides for the first time.

By deprotecting the C-terminal ester group of the selenoxo peptides, elongation at the C-terminal carboxyl was also possible. However, as in thioxo peptide synthesis (97, 168-171), a partial epimerization was also encountered (Figure 5.2). Nevertheless, the epimers could be separated by HPLC in some cases.
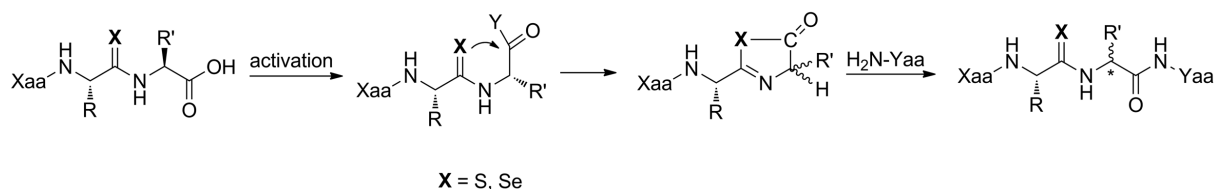
Figure 5.2 Epimerization during activation of the C-terminal carboxyl of thioxo and selenoxo peptides via the thiazolone and selenazolone intermediates.

On the other hand, alkylation of the selenoxo group is shown to take place on the selenium and form a selenoimidate (Figure 4.11, pp34), thus this reaction might be used to protect the selenoxo group. Therefore, by carefully choosing the protection group, the elongation at the C-terminus might be conducted in an epimerization-free manner by preventing the formation of the selenazolone intermediate (Scheme 5.1). However, further studies are needed to prove this strategy.
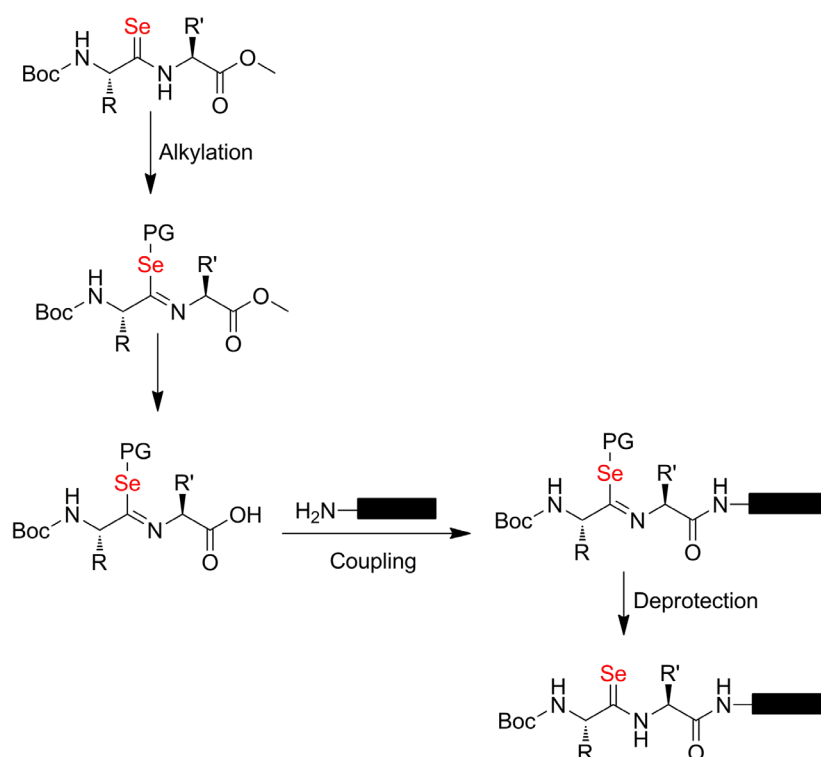
Scheme 5.1 A possible epimerization-free pathway to elongate the selenoxo peptide at the C-terminal end.

The selenoxo peptides are stable in aqueous solution at neutral or near-neutral conditions. At alkaline conditions, an accelerated selenium to oxygen exchange was observed (Figure 4.4, pp27). Moreover, like in thioxo peptides (172), the peptide bond or the ester bond next to the selenoxo group is prone to break under certain conditions through an Edman degradation-like mechanism (Figure 5.3). Nevertheless, the selenoxo peptides showed much better stability than the small selenoxo amides, which have been reported to undergo decomposition in solution (134). The moderate stability in aqueous solution allows us to investigate the physicochemical properties under near-physiological conditions.
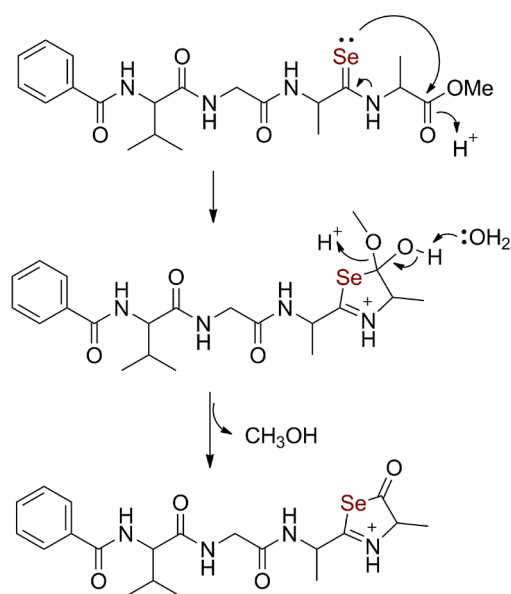
Figure 5.3 Fragmentation of selenoxo peptides.

The selenium atom is much larger and less electronegative than oxygen. Therefore, weaker hydrogen bonding ability and larger hydrophobic area of the selenoxo peptide bonds were expected, which is confirmed by a longer retention time than the oxo and thioxo congeners in the reverse-phase HPLC analysis (Figure 4.3, pp27). The observation that the solubility of selenoxo peptides was poorer in aqueous solution but better in organic solvent is consistent with those properties.

The element selenium has six natural isotopes. Only ^{77}Se (7.58%), having a nuclear spin quantum number of ½, is NMR-active, thus enabling us to collect high-resolution ^{77}Se-NMR spectra (173). ^{77}Se-NMR spectra acquired for selenoxo peptides (Table 4.4, pp31) showed ^{77}Se resonance values are in the range of 380-470 ppm. Those values were shifted markedly to higher field compared to the values reported for small selenoxo amides in organic solvents (~600 ppm) (151), probably due to a strong shielding by the water

molecules in aqueous solution. In the peptide bond, the nearly identical shielding of ^{17}O in the *trans* and *cis* conformations indicated a similar solvation model in the two conformational states (174, 175). In Bz-VGAψ[CSe–N]P-OMe, however, the ^{77}Se nucleus in the *trans* conformation is 14 ppm more shielded than in the *cis* state (Figure 4.41, pp56), which may result from an electronic influence by the C-terminal carbonyl.

5.2 Photoisomerization of selenoxo peptide bonds

Previous work by Frank *et al.* (85) and Zhao *et al.* (86) has revealed that the thioxo peptide bonds in aqueous solution have a strong absorption band around 260 nm (π-π*, ε: 12000 $M^{-1}cm^{-1}$) and a weak band around 330 nm (n-π*). Excitation of the π-π* band with UV light near 260 nm could selectively switch the thioxo peptide bond conformation from *trans* to *cis* with high quantum efficiency but without any effect on the regular peptide bonds.

Compared with the thioxo peptide bonds, the electronic absorptions of selenoxo peptide bonds are further shifted to ~295 nm and ~370 nm for π-π* transition and n-π* transition, respectively (Figure 4.6, pp29). This implies that the excitation energy for the photo-triggered *trans*→*cis* isomerization might be lower in selenoxo peptide bonds. In fact, the selenoxo peptide bonds can be efficiently photoswitched in phosphate buffer by using UV light with a wavelength of ~290 nm, which is ~30 nm longer than the thioxo congeners. The full recovery of the UV/Vis spectrum and the clear isosbestic point at 300 nm (Figure 4.12a, pp35) indicate that the photoisomerization of the selenoxo group is reversible. The *cis* content in the photostationary state ranges from 11% to 37% depending on residues flanking the selenoxo group. However, it should be noted that the *cis* content depends not only on the irradiation wavelength but also on light intensity, beam/sample area ratio, sample concentration, temperature and solvent. A further improvement of the *cis* content may thus be achieved by a careful optimization of those factors. The UV/Vis spectrum of the *cis* conformer constructed by using Beer-Lambert's law showed an absorption maximum at 310 nm, which is 16 nm longer than the value of 294 nm for the *trans* conformer. The maximal difference in UV absorbance between the *cis* and *trans* conformers is located at a wavelength of ~320 nm (Figure 4.12b, pp35). UV light at this wavelength may thus be used to trigger the *cis*→*trans* photoisomerization, as a similar case with thioxo peptide bonds was confirmed (86).

Photoswitching of the selenoxo imide bond in Bz-VGAψ[CSe–N]P-OMe was conducted by irradiation at a wavelength of 296 nm. In contrast to selenoxo amide bonds, a spectral redshift did not occur in the selenoxo imide bond upon irradiation and only a slight increase in absorption intensity was observed. The reason for this behavior is that the double alkyl substitutions at the nitrogen results in a similar intramolecular environment for the selenium atom in both *cis* and *trans* conformations (Figue 5.4), thus leading to a nearly identical influence on the electronic excitation energy of the C=Se group.
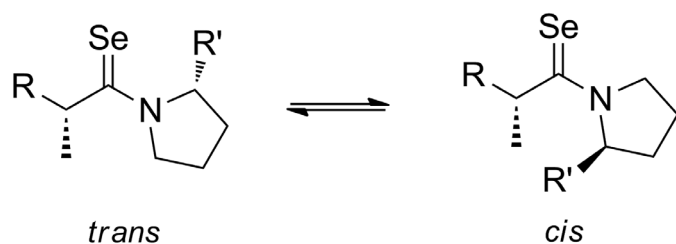
Figure 5.4 *cis* and *trans* conformations of imidic selenoxo peptide bond.

The *cis→trans* decay of selenoxo peptide bonds are considerably slower than in the corresponding thioxo peptide bonds. As shown in Table 4.7, the $\Delta G^{\ddagger}$ of selenoxo peptides is generally ~1 kcal/mol higher than that of thioxo peptides. This observation is consistent with the theoretical calculation that the nitrogen delocalizes more lone pair electron density to C=Se than to C=S (141, 146). The deceleration of *cis→trans* isomerization in selenoxo peptides is driven entirely by a large unfavorable activation entropy term (Table 4.7, pp38). The lower *trans→cis* excitation energy and the slower *cis* decay rate compared to the thioxo photoswitch enable the selenoxo peptide bond to serve as an efficient, structure-compatible photoswitch to trigger the conformational changes. Selenoxo photoswitch can thus be applied in a wider range of conformation-specific processes.

For the oxo and thioxo peptide bonds flanked with non-aromatic side chains, the *cis* conformer could not be detected due to rapid decay or signal overlap in NMR spectra. However, the *cis* signal of Ala^3-CH_3 in Bz-VGAψ[CSe–NH]A-OMe was observed in a slightly upfield shifted position (Figure 4.16a, pp39). This shielding effect might be caused by steric crowding of the two Ala-CH_3 groups but not by the Bz group (Figure 5.5), because substituting Bz with Boc showed a similar pattern of signals (Table 4.8, pp39). In the case of Bz-VGAψ[CSe–NH]F-OMe, the close proximity of the Ala^3-CH_3 group and Phe-phenyl ring in the *cis* conformation (Figure 5.5), which is stabilized by a CH··π interaction (9, 176, 177), led to a considerable shielding on Ala^3-CH_3. This shielding effect must be due to the

ring current rather than to the anisotropic effect of the selenium atom, as a strong shielding of the CH_3 group in *cis* conformation was also observed in oxo and thioxo peptide bonds flanked with Phe but not in selenoxo peptides lacking Phe residue (Table 4.8, pp39).
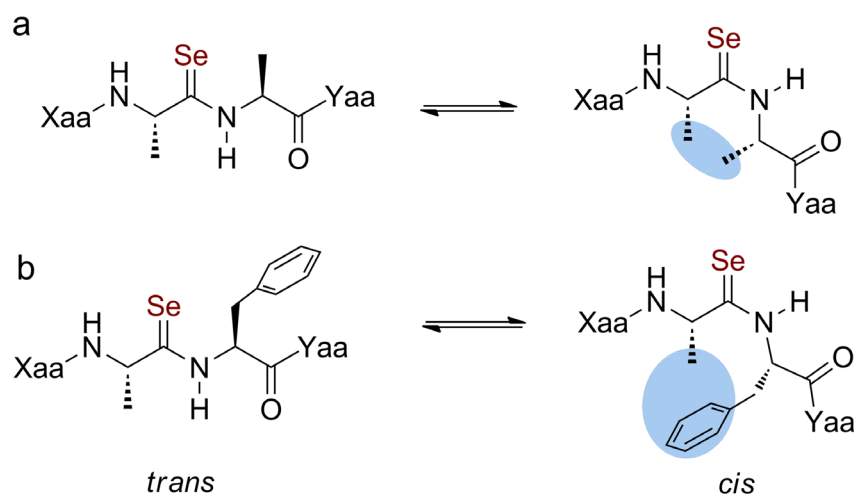
Figure 5.5 Side chain orientation in *trans* and *cis* conformations of the selenoxo peptide.

Cis/trans isomerization of the prolyl peptide bonds are catalyzed efficiently by cyclophilins. However, even though the thioxo substrate Ala-Xaa-ψ[CS-N]Pro-Phe-NH-Np (Xaa = Ala, Gly, Np = 4-nitroaniline) could bind the catalytic center of hCyp18 in a similar manner as the oxo form, Schutkowski *et al*. have shown that no accelerated *cis/trans* isomerization could be observed (178). In contrast, competitive inhibition did occur, with apparent K_i values ranging from 200 to 600 µM. In case of the selenoxo peptide Bz-VGAψ[CSe–N]P-OMe, the *cis→trans* isomerization was not catalyzed by hCyp18 either (Figure 4.23, pp43). Probably, the weaker hydrogen bond-accepting ability of thioxo and selenoxo groups and/or the large size of sulfur and selenium atoms impede the catalytic reaction. The increased hydrophobicity of the chalcogen-substituted peptides might be the reason for their stronger binding to hCyp18.

5.3 Multiple conformational photocontrol of the thioxo and selenoxo dual-labeled peptide

Although most peptide bonds overwhelmingly adopt a *trans* conformation (typically > 99.9% under unrestrained conditions) except for the imide bond preceding proline, the energetically less favored *cis* peptide bond is known to play an important role in protein folding and function. Nature chooses proline and the corresponding *cis*/*trans* isomerases to confer a *cis*/*trans* conformational control on proteins. Moreover, multiple *cis* peptide bonds are also often found in native protein structures (9, 179, 180). Biological organisms can use complicated enzymatic systems to regulate these conformational transitions with high spatial and temporal specificity. However, artificial control of multiple *cis*/*trans* isomerization processes is of great challenge because of the lack of tools to site-specifically manipulate the peptide bond conformations.

Nevertheless, in the last decade, site-selective replacement of the peptide bond oxygen with sulfur has provided the first tool to artificially manipulate the *cis* ↔ *trans* interconversion by using light, with minimal perturbation of the original peptide structure (120, 121). Now, the oxygen to selenium substitution provides another photo-controllable tool to manipulate the peptide bond conformation. Interestingly, the excitation wavelength difference (Δλ ~30 nm) between the thioxo and selenoxo photoswitches enabled us to selectively switch only one of those two chalcogen-based photoswitches (Figure 4.19, pp41; Figure 4.21, pp42). Additionally, switching of both chromophores allowed us to evaluate the intramolecular influence of one *cis* peptide bond on another. In Ac-VAψ[CS−NH]FGGAψ[CSe−NH]F-OMe, for example, a rate constant of 4.6×10^{-3} s^{-1} for the decay of the *cis*-ψ[CS−NH] bond was determined after selectively exciting the thioxo chromophore. By switching both ψ[CS−NH] and ψ[CSe−NH] bonds to *cis* conformations (Scheme 5.2), the *cis*-ψ[CS−NH] decay featured a rate constant of 4.0×10^{-3} s^{-1}, which is slightly slower than in case of ψ[CSe−NH] in *trans* conformation. Hence, this indicates that one *cis* peptide bond could influence the thermodynamics of *cis*→*trans* isomerization of another peptide bond, though the specific interaction for the influence cannot be determined based on the current data. Given the importance of *cis*/*trans* isomerization in protein folding, the multiple photocontrol of the *cis*/*trans* isomerization might provide a special tool to analyze the energy landscapes of protein folding. On the other hand, the thioxo and selenoxo dual labeling could also be applied for the multiple photocontrol of protein function.
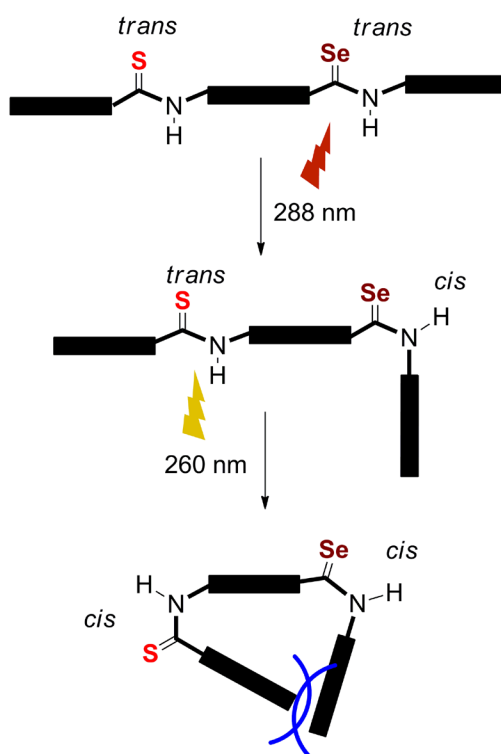
Scheme 5.2 Photocontrol of peptide backbone conformations in the thioxo and selenoxo dual-labeled peptide.

5.4 *Cis→trans* isomerization of selenoxo peptide bonds under alkaline conditions: C−N rotation versus nitrogen inversion

5.4.1 Effect of pH on peptide structure and *cis→trans* isomerization

The majority of experimental data for the spontaneous isomerization supported the assumption that the barrier of *cis/trans* isomerization in aqueous solution is from the C−N rotation rather than nitrogen inversion (3, 4, 181). Due to the extremely weak acidity of the peptide amide proton ($pK_a \approx 18$) (182), the presence of the deprotonated form, i.e. the imidate anion, is generally negligible in water. Nevertheless, the amide proton exchange is strongly accelerated at alkaline conditions via the imidate intermediate (183). Despite the strong effect of OH$^-$ on proton exchange, *cis→trans* isomerization appears insensitive to moderate pH variation (184). This is due to the extremely short lifetime of the imidate anion, which is too short to allow the C−N bond to rotate or the nitrogen lone pair to invert. On the other hand, Perrin *et al.* showed that, the imidate anions are constantly present under extremely basic conditions (in potassium hydride organic solution) and could interconvert between their **E** and **Z** conformations via the nitrogen inversion pathway but not via the C=N rotational pathway (185, 186).

In contrast to the oxo amide bonds, the *cis→trans* isomerization rate of selenoxo peptides was remarkably accelerated at high pH values (Figure 4.24, 4.25, 4.26, pp45-46). Intriguingly, the time-course for *cis→trans* decay varied depending on pH, with first-order exponential kinetics at neutral conditions (Figure 4.24a) yet with a sigmoid curve at alkaline conditions (Figure 4.24b). However, the *cis→trans* isomerization of the selenoxo imide bond [CSe−N<] in Bz-VGAψ[CSe−N]P-OMe was not accelerated at high pH up to 10 (Figure 4.28, pp47).

5.4.2 Mechanistic analysis of the pH-dependent *cis→trans* isomerization in selenoxo peptides

The fact that *cis→trans* decay of the selenoxo imide bond was not accelerated by OH$^-$ indicates that a nucleophilic attack on the selenoxo carbonyl carbon is unsuitable for explaining the high isomerization rates for the secondary selenoxo amide bonds. Deprotonation of the C_α atom attached to the C=Se can also be excluded, since this would lead to an epimerization that was not observed in the HPLC profiles and the NMR spectra

(Figure 4.29, pp47; Figure 4.30, pp48). Considering that the rate dependence on pH becomes sluggish after a sharp increase, the highest interconversion rate could be reached in a pH region corresponding to the complete formation of the selenoimidate anion (Figure 5.6). Given the structural features of this anionic species, which must make rotational movements at the C=N bond more energy-demanding, nitrogen inversion represents an alternative pathway for rapid *cis* isomer decay. Notably, it has been proposed that the *E/Z* interconversion of the N-Arylformimidate anion takes place via nitrogen inversion pathway in organic solvent (186). As the proton transfer steps are fairly fast and not rate-limiting for the slow conformational interconversions in aqueous solutions, the *trans* and *cis* conformers could rapidly equilibrate with the *Z* and *E* selenoimidate anions, respectively, in the photostationary state (Scheme 5.3). Furthermore, the sigmoidal decay curves at high pH values (Figures 4.24b, 4.25, 4.26, pp46), and the linear concentration dependence of isomerization rates (Figure 4.31, pp48) indicate the possibility of an autocatalytic term in the *cis* isomer decay. This term is most likely due to the transient presence of the *Z* selenoimidate anion for nucleophilic attack on the imine carbon atom of the *E* conformer, thus increasing the apparent rate of *cis*→*trans* decay (Scheme 5.3). The resulting tetrahedral adduct (discussed in 5.4.6) disrupts the amide resonance and would have a very low energy barrier for isomerization. This type of catalysis is consistent with the very high nucleophilicity of anionic selenium compounds (187).

In addition, the *cis* content is negligible for secondary selenoxo amide peptide bonds in equilibrium (Figure 4.16, pp42). For the selenoimidate anion, the *E* content should also be very low at equilibrium due to the strong lone pair repulsion in the *E* configuration. Hence, we can assume that $k_{ct} \gg k_{tc}$ and $k_{EZ} \gg k_{ZE}$, thus allowing us to ignore the reverse reactions in Scheme 5.3.
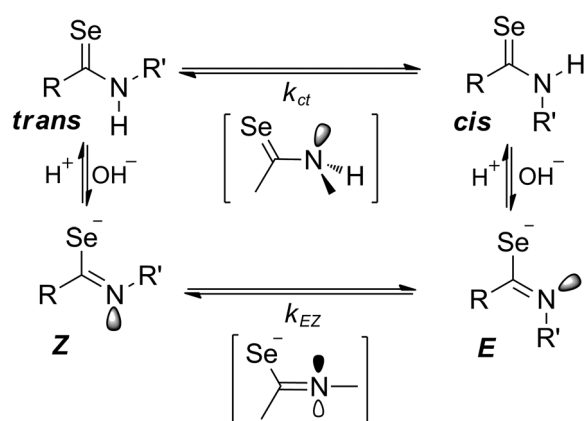
Scheme 5.3 *Cis/trans* isomerization, nitrogen inversion and proton dissociation in selenoxo peptides at alkaline conditions. The conventional *cis, trans* notation is used to define the conformation of the peptide bonds, whereas the configuration of the selenoimidate anions is defined by the *Z*, *E* notation.

As a consequence, the rate equations for the *cis* isomer decay based on the mechanism depicted in Scheme 5.3 can be derived as follow:

$$trans \xleftarrow{\quad k_{ct} \quad} cis$$

$$H^+ \Updownarrow K^{trans} \qquad H^+ \Updownarrow K^{cis}$$

$$2\,Z \xleftarrow[\quad k_{EZ} \quad]{} E + Z$$
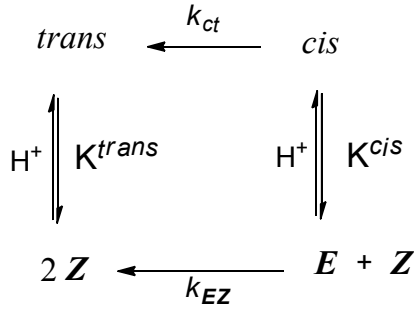
The rate for *cis*→*trans* isomerization is: $\dfrac{d[cis]}{dt} = -k_{ct}[cis]$ (1)

The rate for **Z**→**E** inversion is: $\dfrac{d[E]}{dt} = -k_{EZ}[E][Z]$ (2)

Considering that **E** is in fast equilibrium with *cis*, the overall decay rate of *cis* is defined as:

$$\frac{d[cis]}{dt} + \frac{d[E]}{dt} = -k_{ct}[cis] - k_{EZ}[E][Z] \quad (3)$$

$$\therefore \; K^{cis} = \frac{[E][H^+]}{[cis]} \; ; \quad K^{trans} = \frac{[Z][H^+]}{[trans]}$$

$$\Rightarrow \; [E] = 10^{(pH - pK^{cis})}[cis]\,; \quad [Z] = 10^{(pH - pK^{trans})}[trans]$$

The whole peptide concentration:

$$C_0 = [trans] + [Z] + [cis] + [E] = 10^{(pK^{trans} - pH)}[Z] + [Z] + [cis] + 10^{(pH - pK^{cis})}[cis]$$

$$\Rightarrow \; [Z] = \frac{C_0}{1 + 10^{(pK^{trans} - pH)}} - \frac{1 + 10^{(pH - pK^{cis})}}{1 + 10^{(pK^{trans} - pH)}}[cis]$$

By substituting $[E] = 10^{(pH - pK^{cis})}[cis]$ and $[Z] = \dfrac{C_0}{1 + 10^{(pK^{trans} - pH)}} - \dfrac{1 + 10^{(pH - pK^{cis})}}{1 + 10^{(pK^{trans} - pH)}}[cis]$ into (3), we get:

$$(1 + 10^{(pH - pK^{cis})})\frac{d[cis]}{dt} = -k_{ct}[cis] - k_{EZ}10^{(pH - pK^{cis})}[cis]\left(\frac{C_0}{1 + 10^{(pK^{trans} - pH)}} - \frac{1 + 10^{(pH - pK^{cis})}}{1 + 10^{(pK^{trans} - pH)}}[cis]\right) - k_{non}10^{(pH - pK^{cis})}[cis]$$

$$\Rightarrow \; \frac{d[cis]}{[cis]\left(\dfrac{10^{(pH - pK^{cis})}}{1 + 10^{(pK^{trans} - pH)}}k_{EZ}[cis] - \left(\dfrac{1}{1 + 10^{(pK^{trans} - pH)}}C_0 k_{EZ} + \dfrac{1}{1 + 10^{(pH - pK^{cis})}}k_{ct}\right)\right)} = dt \qquad (4)$$

Set: $a = \dfrac{10^{(pH - pK^{cis})}}{1 + 10^{(pK^{trans} - pH)}}k_{EZ}$; $k_{app} = \dfrac{1}{1 + 10^{(pK^{trans} - pH)}}C_0 k_{EZ} + \dfrac{1}{1 + 10^{(pH - pK^{cis})}}k_{ct}$

Formula (4) $\Rightarrow \dfrac{d[cis]}{[cis]\left(a[cis]-k_{app}\right)}=dt$ (5)

Integrating formula (5) at both sides: $\displaystyle\int_{[cis]_0}^{[cis]}\dfrac{d[cis]}{[cis]\left(a[cis]-k_{app}\right)}=\int_0^t t$

$\Rightarrow\ [cis]=\dfrac{k_{app}}{a+(\dfrac{k_{app}}{[cis]_0}-a)e^{k_{app}t}}$ (6)

Considering $A_{320}=[cis]\varepsilon_{320}$, equation (6) can be rewritten as:

$$A_{320}=\dfrac{k_{app}}{b+(\dfrac{k_{app}}{\Delta A}-b)e^{k_{app}t}}+A_{00} \qquad \textbf{(I)},$$

where

ΔA is the absorbance increase after irradiation,

A_{00} is the absorbance at infinite time,

k_{app} is the apparent rate constant of $cis{\rightarrow}trans$ isomerization:

$$k_{app}=\dfrac{1}{1+10^{(pK^{trans}-pH)}}C_0 k_{EZ}+\dfrac{1}{1+10^{(pH-pK^{cis})}}k_{ct} \quad \textbf{(II)},$$

b is a constant at given pH: $b=\dfrac{10^{(pH-pK^{cis})}}{(1+10^{(pK^{trans}-pH)})}\dfrac{k_{EZ}}{\varepsilon_{320}}$,

and k_{EZ}^{obs} is the observed rate constant of $\textbf{\textit{Z}}{\rightarrow}\textbf{\textit{E}}$ isomerization: $k_{EZ}^{obs}=C_0 k_{EZ}$ $\textbf{(III)}$.

5.4.3 Kinetic data analysis

The sigmoid kinetic curves were fitted perfectly using equation (**I**), and the resulting apparent rate constants k_{app} for $cis{\rightarrow}trans$ isomerization were pH-dependent. The pH vs. k_{app} plot for Bz-VGAψ[CSe–NH]FA-NH$_2$ was well fitted by equation (**II**) (Figure 5.6a), resulting in a pK$_a$ of 9.3 for the *cis* form and an observed rate constant (k_{EZ}^{obs}) of 0.077 s^{-1} for $\textbf{\textit{E}}{\rightarrow}\textbf{\textit{Z}}$ inversion, which is 35-fold fast than the rate of the C–N rotational pathway (0.0022 s^{-1}). Peptide Bz-VGAψ[CSe–NH]A-OMe shows similar pH dependence of k_{app} (Figure 5.6b), where fitting by equation (**II**) gave rise to a pK$_a$ of 9.7 for the *cis* form and an k_{EZ}^{obs} of 0.17 s^{-1}, which is 59-fold fast than the rate of the C–N rotational pathway (0.0029 s^{-1}).

According to equation (**III**), k_{EZ}^{obs} should be concentration-dependent. This was verified by a linear increase of k_{EZ}^{obs} with peptide concentration (Figure 4.31, pp48). By extrapolating the concentration to zero, the non-autocatalytic $E{\rightarrow}Z$ inversion rate constant in Bz-VGAψ[C(Se$^-$)=N]A-OMe was found as 0.1 s^{-1}, which is still 32 times faster than the rate of C–N rotation in [CSe–NH].
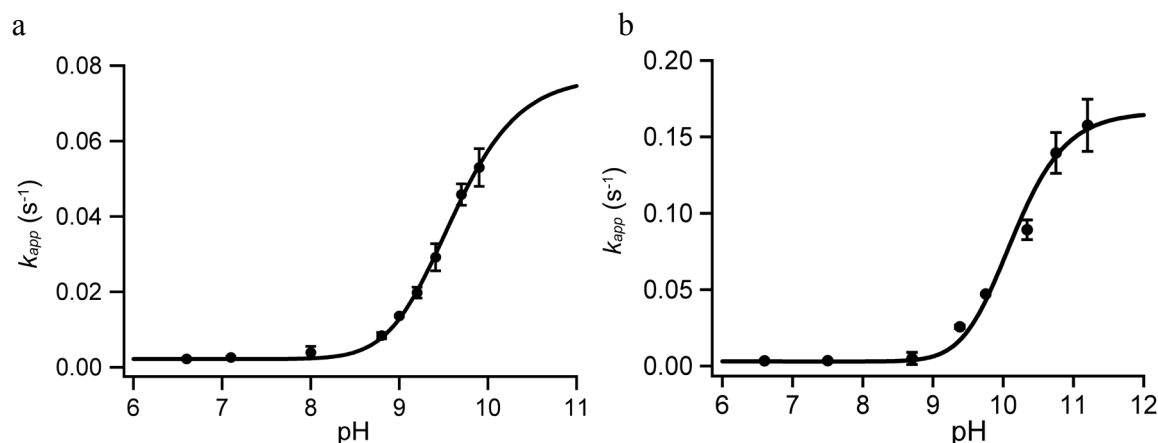
Figure 5.6 pH-dependent *cis*→*trans* isomerization (k_{app}) for 4.5 μM Bz-VGAψ[CSe–NH]FA-NH$_2$ (a) and 10 μM Bz-VGAψ[CSe–NH]A-OMe (b). Fitting the pH vs. k_{app} plot in (a) by equation (**II**), with experiment-determined restrictions of k_{ct} = 0.0022 s^{-1} and pK^{trans} = 9.1, resulted in k_{EZ}^{obs} = 0.077 s^{-1} and pK^{cis} = 9.3. Fitting the pH vs. k_{app} plot in (b) by equation (**II**), with experimentally determined restrictions of k_{ct} = 0.0029 s^{-1} and pK^{trans} = 9.8, resulted in k_{EZ}^{obs} = 0.17 s^{-1} and pK^{cis} = 9.7. Phosphate buffer (1 mM) was used at pH < 8 and Gly-NaOH buffer (1 mM) at pH ≥ 8. Data were collected at 20 °C.

The amide C–N rotation is generally known to be insensitive to solvent deuteration (188), whereas in the selenoimidate anion, since the hydrogen bond between the nitrogen lone pair of C=N and solvent water should be broken before the lone pair inversion, a slower inversion rate is expected in deuterated water. The solvent deuterium kinetic isotope effect (SKIE), defined as k_{EZ}^{obs} (H$_2$O) / k_{EZ}^{obs} (D$_2$O), was measured with Bz-VGAψ[CSe–NH]FA-NH$_2$ using the same ratio of the ionized and unionized species in H$_2$O (pH 9.2) and D$_2$O (pD 9.85) (Figure 4.32b, pp49). The SKIE value of 1.13 ± 0.04 indicated that solvent reorganization occurs in the transition state of nitrogen inversion to a much higher extent than in case of the rotational pathway, where the value of k_{ct} (H$_2$O) / k_{ct} (D$_2$O) = 1.004 ± 0.008 is consistent with the SKIE obtained for *cis*/*trans* isomerization via the rotational pathway in regular amide bonds (189, 190).

5.4.4 Nitrogen inversion barrier in the selenoimidate anion

The Eyring function was used to evaluate the thermodynamic properties of the nitrogen inversion. As Figure 4.33 shows, the Eyring plot displayed a very good linearity, indicating that the activation enthalpy ($\Delta H^{\ddagger}$) is constant in the current experimental temperature range. The activation energy for the non-catalyzed $E \rightarrow Z$ inversion was determined as 18.4 kcal/mol from the Eyring plot and Gibbs equation, which is 2.3 kcal/mol lower than the C–N rotational barrier of 20.7 kcal/mol (Table 4.10, pp50). The large negative entropy (-110 J K^{-1} mol^{-1}) indicates a significant solvent participation and reorganization.

The $E \rightarrow Z$ inversion barrier in the N-benzylformimidate anion has been determined as 23.3 kcal/mol in DMSO-d_6 (191) and for the N-benzylthioformimidate anion in MeOD a value of 19.6 kcal/mol was reported (192). The presently determined inversion barrier in selenoimidate anion in basic aqueous solution (18.4 kcal/mol) is lower than in the former two cases. Even though the polarity of the used solvents is not exactly the same, a linearly decreasing trend is clearly observed in the $\Delta G_{EZ}^{\ddagger}$ vs. chalcogen polarizability plot (Figure 5.7), which is in agreement with the hypothesis (discussed in **5.5**) that the chalcogen atomic polarizability dominates the physicochemical properties of [C**X**–NR–] (X = O, S, Se; R = H, alkyl).
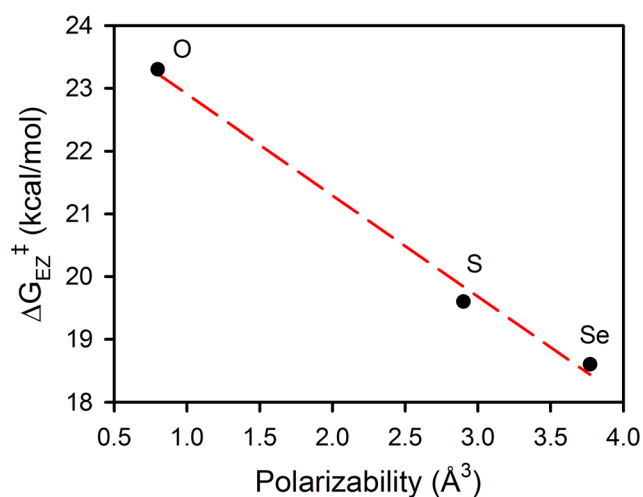
Figure 5.7 $E \rightarrow Z$ inversion barrier versus chalcogen atomic polarizability in [C($\mathbf{X}^{-}$)=N–] (X = O, S, Se). The value of 23.3 kcal/mol for imidate anion was taken from the N-benzylformimidate anion in DMSO-d_6 (191). The value of 19.6 kcal/mol for thioimidate anion was taken from the N-benzylthioformimidate anion in MeOD (192). The value of 18.4 kcal/mol for selenoimidate anion was determined with Bz-VGAψ[C(Se^{-})=N–]A-OMe in 1 mM Gly-NaOH buffer (pH 9.7).

The pH-dependence of the thioxo peptide Bz-VGAψ[CS–NH]FA-NH$_2$ indicated that the *cis→trans* isomerization is slower at high pH conditions than at neutral conditions (Figure 4.34, pp51). This is reasonable to be rationalized by a slower or similar nitrogen inversion barrier in the thioimidate anion compared to the normal *cis→trans* rotation. Hence, only the selenoimidate anions are able to invert rapidly and accelerate *cis→trans* isomerization.

Consequently, the selenoxo peptide bond, due to its low pK$_a$ and rapid *E/Z* inversion under mild basic conditions, provides a non-enzymatic pathway to accelerate the dynamics of peptide backbone conformation in a site-specific manner. Chalcogen substitutions may also be helpful to study other anionic peptide bond involved biochemical processes.

5.4.5 Autocatalysis of conformational interconversion of the selenoimidate anion

The selenolate anion RSe$^-$ (R = alkyl or aryl) is strongly nucleophilic and has widely been used as organoselenium catalyst (187, 193). Taking into account that: (i) the k_{ct} in [CSe–N<] is not sensitive to pH variation, (ii) the rate acceleration only occurs in selenoxo peptides but not in thioxo peptides, (iii) no loss of selenium and no loss of C$_\alpha$ chirality take place, (iv) the catalysis features steric specificity, (v) a weak electrophilicity of the carbon in C=Se, and (vi) the nucleophilic attack on the carbon of C=N is well established (194-197), the catalytic pathway might be a nucleophilic attack by the negatively charged selenium in the *Z* form to the imine bond carbon in the *E* form of the selenoimidate anion, forming a tetrahedral intermediate that allows rotation around a C–N single bond (Scheme 5.4).
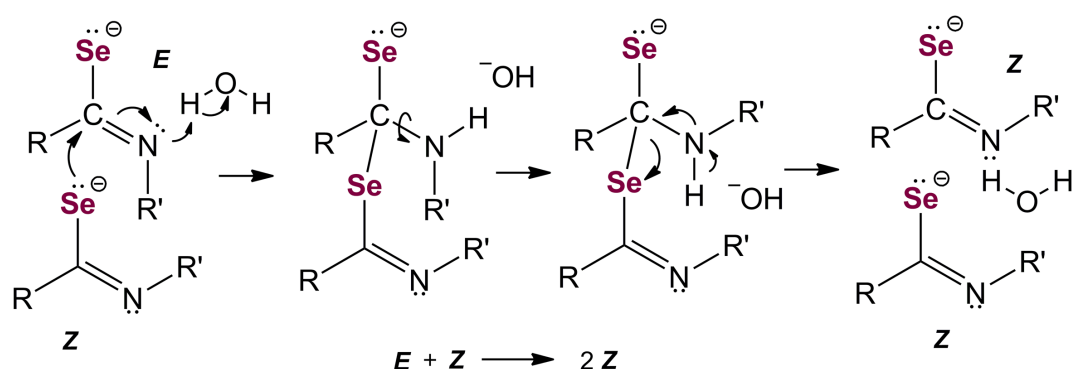
Scheme 5.4 Possible autocatalytic mechanism of the *E→Z* inversion of selenoimidate anion

The first order exponential decay of the thioxo peptide at high pH conditions (Figure 4.34b) indicated that no autocatalysis takes place in the thioimidate anion, probably due to the weaker nucleophilicity of anionic sulfur than anionic selenium.

Although the autocatalysis can explain the sigmoid decay curves, the reason for the irreversible photoswitching at alkaline conditions (Figure 4.35) is still not clear. UV/Vis and NMR spectra showed no degradation during the photoswitching. We, therefore, propose that a photo bleaching might occur upon photo-irradiation. However, a detailed explanation of this effect is not possible based on the current data.

5.5 Electronic effects of chalcogen substitution in peptide bonds

5.5.1 Electronegativity and polarizability

The concept of electronegativity, symbol χ, first proposed by L. Pauling (198), is a chemical property that describes the tendency of an atom or a functional group to attract electrons (or electron density) towards itself. It has become an indispensible tool for chemists. Unfortunately, electronegativity is not a directly measurable experimental property of an isolated atom. On the other hand, atomic polarizability, symbol α, a basic physical entity that reflects how readily the electron cloud of an atom can be distorted, has been tabulated quite comprehensively and with high precision by theoretical calculations as well as experimental measurements (129, 199). The atomic polarizability proved to be linearly related to the charge capacity (200), symbol κ, which plays an important role in the determination of charge density redistribution in molecule formation. Sanderson (201-203) stated that, when atoms interact to form a molecule, their electronegativities change until they achieve an equilibrium. This principle of electronegativity equalization has been rationalized based on a firm theoretical foundation (204-206), which implies that the electron-attracting tendency of an atom in a molecule depends not only on its initial intrinsic affinity for electronic charge but also on its ability to accommodate this additional charge, i.e. its charge capacity, as formulated by Politzer (200). The magnitude of the charge capacity depends upon the repulsion between the electrons already present on the atom and the approaching charge; therefore, there is no doubt for a close relation between charge capacity and atomic size. For example, while fluorine exerts a strong initial attraction on the electrons in a molecule, its small size leads to the formation of a highly concentrated electron distribution, thus permitting relatively little additional electronic charge to be accommodated around the fluorine atom. In fact, an increase in polarizability and decrease in electronegativity from the first to subsequent rows of the periodic table are well documented (207).

In contrast to the electronegativity, the atomic polarizability has been greatly under-appreciated in chemistry (208), although it proved very useful in explaining a number of puzzling observations such as (i) the gas phase acidities of halogen-substituted acetic acid molecules (209) and (ii) the higher partial negative charge of sulfur compared to oxygen in thiocyanate versus cyanate ions (210).

5.5.2 The role of chalcogen atomic polarizability in amide bonds

Glendening and Hrabal (146) suggested that chalcogen polarizability may be responsible for the higher rotational barriers observed for thioxo and selenoxo analogues of formamide. In good agreement with this theoretical study, the results presented here for sulfur- and selenium-substituted peptide bonds provide experimental proof that several physicochemical properties of [C**X**–NR] (**X** = O, S, Se) the peptide bond are in fact dominated by the polarizability rather than the electronegativity of these chalcogen atoms. Aside from the observed deshielding effects, the electron movements furthermore resulted in (i) lower electronic excitation energies, (ii) lower NH stretching frequencies, (iii) higher C–N rotation barriers, (iv) larger dipole moments, and (v) higher acidity of the amide proton as reflected by the decreasing pK$_a$ values as well as increasing NH line-broadening effects in the NMR spectra.

In regular amide bonds, the strong electronegativity of oxygen is generally considered as the main driving force for electron delocalization from nitrogen to oxygen. Interestingly, since the ^{13}C chemical shift typically reflects the electron density at the carbon atom (152), the NMR-derived resonance assignments of carbon nuclei within a three-bond distance of the chalcogen atom demonstrate that an increasing amount of electron density is withdrawn in the order O < S < Se (Figures 4.39b,c. pp55). At first glance, it certainly seems puzzling that the less electronegative sulfur and selenium atoms withdraw more electron density than oxygen. Nevertheless, previous ^{15}N-NMR studies also have reported that, despite its high electronegativity (χ= 3.04), the chemical shift of the nitrogen in thioamides experiences a pronounced downfield shift relative to the corresponding amides (211, 212), which suggests that the electron density in fact is drawn from nitrogen to sulfur. These observations can be explained by Wiberg's theoretical calculations (5, 213), which indicate that there are two components, σ and π electrons, involved in the movement of electron density. The nitrogen attracts nearby σ electrons, while its own π electrons are disengaged and move toward the chalcogen. The lower electronic excitation energies of the thioxo and selenoxo peptides are in accordance with such an increased π-electron contribution to the resonance structure.

Moreover, the more π electrons are delocalized from the nitrogen in such a manner with increasing atomic polarizability in the order O < S < Se, the more σ electrons need to be attracted from the adjacent nuclei to compensate the π-electron deficiency, thus leading to a

reduction of the electron density at the neighboring atoms. The delocalization of the π-electron component shrinks the 2p orbitals and causes a significant increase of the paramagnetic term (211), resulting in a drastic ^{15}N downfield shift in thioamides. The withdrawal of the σ component is reflected by the corresponding downfield shifts we observed in the adjacent $^{13}C_\alpha$, ^1H_N and $^{13}C_\delta$ (Pro^4) resonances (Figures 4.41, pp56; Figure 4.43, pp57). As a consequence, our present NMR data as well as previous ^{15}N-NMR data on thioamides (211, 212) and twisted amides (214, 215) thus support the significance of resonance form **II** (Scheme 1.1,).

Politzer *et al*. (216) suggested that the intrinsic electronegativity determines the electron distribution when only a limited amount of polarizable electronic charge is present in the system, whereas the charge capacities, which are directly related to the polarizability, may become the dominant factor when considerable polarizable charge is available. Consistent with this hypothesis, our data suggest that the oxygen in the peptide bond apparently is quickly saturated and achieve an equilibrium despite its initially strong attraction for charge, whereas sulfur and selenium, with lower electronegativity values but considerably higher polarizabilities (Table 1.1, pp11), are much more effective in accommodating a larger amount of electronic charge.

5.5.3 n−π* interaction in selenoxo peptides

Recently, Raines *et al*. (217-222) reported a new weak non-covalent interaction, n-π* interaction, which is expected (i) to occur in polypeptide chains between one lone pair (n) of a backbone chalcogen and the antibonding orbital (π*) of the carbonyl carbon in the subsequent peptide bond and (ii) to contribute to the stability of helical structure elements such as α-, 3_{10}- and PPII-helix. It has been furthermore reported that replacement of oxygen by sulfur strengthens the n-π* interaction because sulfur is a better electron-pair donor (217). As a consequence, the n-π* interaction should be further enhanced in selenoxo peptides. Since this through-space interaction is possible only in the *trans* conformation, we now compared the nuclear shielding in *trans* and *cis* conformers of the selenoxo peptide Bz-VGAψ[CSe−N]P-OMe (Figure 4.41, pp56). However, the shielding of ^{77}Se and deshielding of ^{13}C=O in the *trans* conformation relative to the *cis*, are unlikely to reflect the electron delocalization of n-π* interaction. Linear-like relationships between the chalcogen

atomic polarizability and the chemical shift value of the C-terminal carbonyl carbon are found independent of the stereochemical arrangement (Figure 4.43, pp57), which suggests that these shielding trends are dominated by the substantial through-bond effect, possibly masking an additional contribution due to the n-π* interaction. However, the slight but apparent deviation from the linearity of nuclear shielding in the *trans* conformers, might hint at additional geometry-related factors that could derive from through-space effects such as the n-π* interaction (Figure 5.8b).
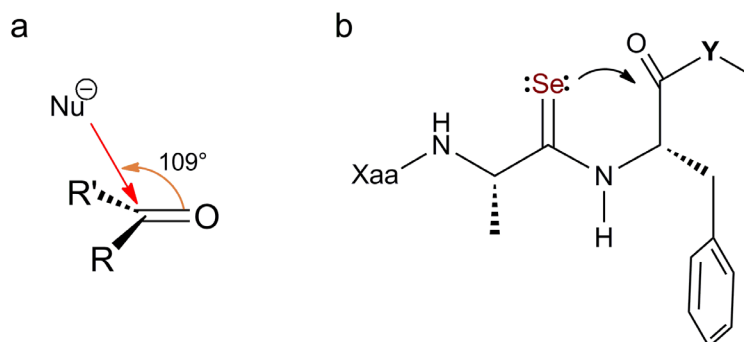
Figure 5.8 (a) Bürgi−Dunitz trajectory. (b) Possible n-π* interaction in selenoxo peptides.

In oxo peptides, a meaningful n−π* interaction is expected at an O···C distance ≤ 3.2 Å and an O···C=O angle of 109° ± 10° (222), i.e. similar to the Bürgi−Dunitz trajectory (Figure 5.8a) (223) that is crucial for nucleophilic attack on a carbonyl group. A survey of a recently published crystal structure of the selenoxo compound $C_6H_5\psi$[CSe−NH]Val-OMe (224) found out that the Se···C=O distance is 3.4 Å, i.e. shorter than the theoretical van der Waals distance 3.6 Å, and the Se···C=O angle is 110.9° (Figure 5.9), i.e. similar to the perfect Bürgi−Dunitz trajectory. These values, therefore, strongly suggest a n-π* interaction between Se and C=O. Although the nuclear shielding in the NMR spectra provided no direct evidence for a n-π* interaction in the selenoxo peptides, the currently available crystal structure does support an interaction between the C=Se and the following C=O.
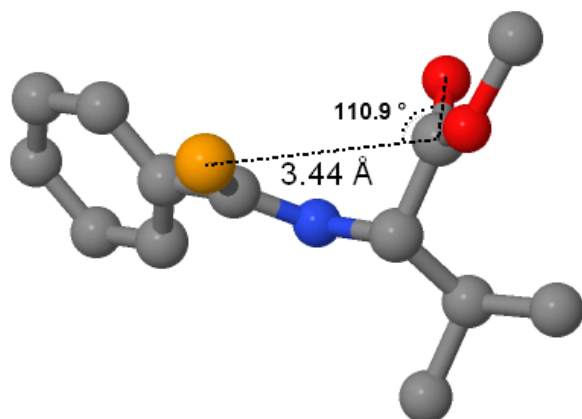
Figure 5.9 n-π* interaction in the crystal of $C_6H_5\psi$[CSeNH]Val-OMe. The structure was drawn based on the atomic coordinates reported in Ref. (224).

The enhanced alkaline hydrolysis of the C-terminal ester in selenoxo peptides compared to their oxo and thioxo congeners (Table 4.3) probably is due to the stronger n-π* interaction as well as the stronger nucleophilicity of the selenium anion, which functions as an intramolecular catalyst (Figure 5.10).
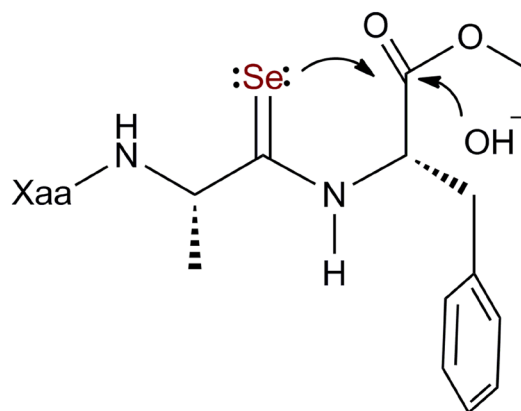
Figure 5.10 n-π* interaction and ester hydrolysis

On the other hand, in the case of C-terminal carboxylic acid at pH 6.5, the negatively charged COO⁻ strongly repulses with the Se via n)(π Pauli repulsion (Figure 5.11), thus forcing the COO⁻ to re-orientate to other direction and leading to an upfield shift of the ^{77}Se resonance. However, lowering the pH to 3, where part of the COO⁻ is protonated, the ^{77}Se resonance shifted back downfield again (Table 4.4), probably due to a recovery of the n-π* interaction between the Se and the carboxyl group.
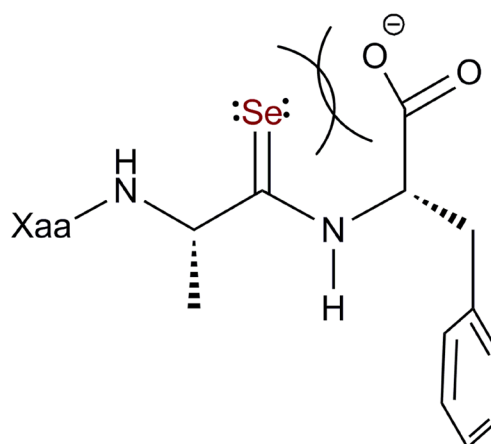
Figure 5.11 Repulsion between the Se atom and the negatively charged carboxyl.

5.5.4 NH···π interaction in selenoxo and thioxo peptides

Recently, more and more attention has been given to the local interactions in intrinsically unstructured proteins and folding intermediates (225-228). The NH···π interaction has been found to play a role in stabilizing both the local and 3D protein structure (177, 229, 230). Due to the partial positive charge of amide proton, the NH···π interaction is weaker than the cation···π interaction (231-233) but stronger than the CH···π interaction (229, 234-237). In spite that the NH···π interaction has been shown to exist between the aromatic ring and the amide proton of the same residue in the *trans* conformation of -Pro-Xaa- peptides (Xaa is an aromatic residue) (229), most of the NH···π interactions have been discussed in the context of protein tertiary structures (238), and a general occurrence of the NH···π interaction in oligopeptides is lacking.

The UV/Vis absorption spectrum (π–π*: 296 nm; n–π*: 372 nm) of Bz-VGAψ[CSe–NH]F-OMe is slightly red-shifted compared to Bz-VGAψ[CSe–NH]A-OMe (π–π*: 294 nm; n–π*: 364 nm). This difference may be resulted from the interaction between NH and the phenyl ring (Figure 5.12a). Due to the considerably enhanced acidity of the selenoxo amide proton, the NH···π interaction should be stronger than in case of the regular amide. Such a steric arrangement is also supported by the shielding of the NH resonance in the presence of Phe[4] (Table 5.1), which shows a 0.1 – 0.15 upfield shift compared to the Ala[4] congeners, where the NH···π interaction is missing. Interestingly, the $\Delta\delta_{NH(4)}$ values are also linear with the chalcogen atomic polarizability (Figure 5.12b).

a

b
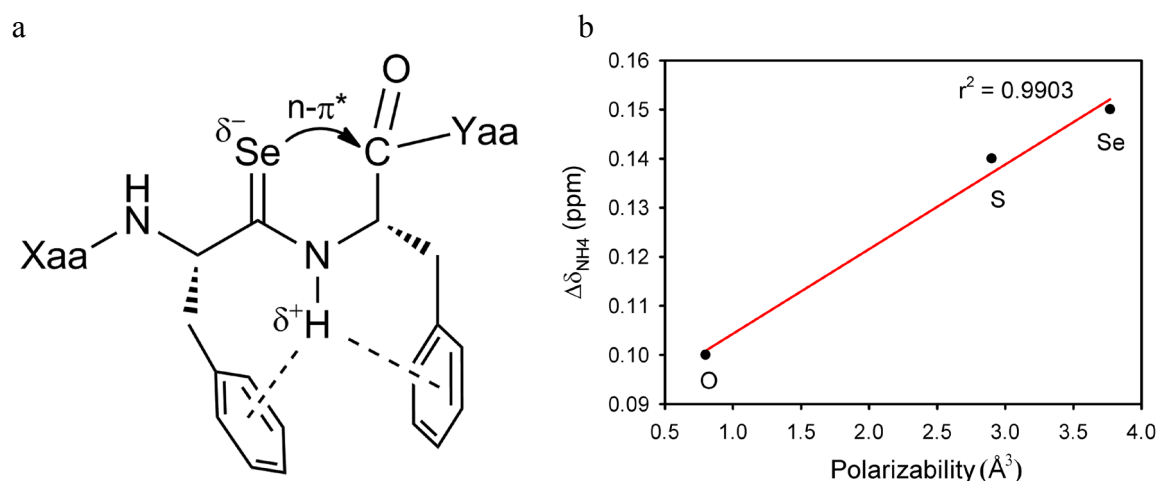
Figure 5.12 (a) NH···π interaction between the peptide backbone and aromatic side chains. (b) The $\Delta\delta_{NH(4)}$ values plot against chalcogen atomic polarizability.

Table 5.1 Chemical shift values of the amide proton in the C-terminal residue of Bz-VGAψ[C**X**–NH]A-OMe and Bz-VGAψ[C**X**–NH]F-OMe peptide series [a]

X	δ_{NH} Ala (4) (ppm)	δ_{NH} Phe (4) (ppm)	$\Delta\delta_{NH(4)}$ (ppm)
O	8.55	8.45	-0.10
S	10.20	10.06	-0.14
Se	10.89	10.74	-0.15

[a] Data were collected in 50 mM sodium acetate buffer (pH 6.0) at 10 °C.

As the UV absorption of the peptide bond is usually around 220 nm, the weak effect due to a NH···π interaction is most likely masked by the solvent absorbance. The selenoxo peptide bond, which is characterized by a strong red-shift in the UV spectrum, might provide an easy yet sensitive probe to evaluate the role of NH···π interactions in stabilizing local peptide structure.

6. Summary and outlook

– Protected dipeptides were successfully selenated in an epimerization-free manner by using Woollins' reagent. The desired selenoxo peptides could then be synthesized by elongation at the N- and C-terminal ends. An unexpected stability of the selenoxo peptides allowed us to investigate their photochemical and physicochemical properties in aqueous solution.

– The selenoxo peptide bonds can be photoswitched from *trans* to *cis* conformation by UV irradiation at ~290 nm, which is ~30 nm longer than the efficient photoswitching wavelength (~260 nm) of thioxo peptide bonds. The *cis*→*trans* thermal decay was quite slow, with the lifetime ranging from 17 min to 21 h depending on the residues adjacent to the selenoxo group. The corresponding *cis*→*trans* rotational barrier for the selenoxo peptide bonds ranged from 20.5 to 22.9 kcal/mol, which is about 1 kcal/mol higher than for the thioxo analogues. The reduced photo-excitation energy and enhanced thermal stability of the *cis* conformation makes the selenoxo peptide bond applicable to study a wider range of conformation-specific processes than their thioxo congeners.

– For the thioxo and selenoxo dual-labeled peptide, the selective photoswitching of either the thioxo or the selenoxo chromophore could be achieved by carefully adjusting the irradiation wavelength. The switching orthogonality enabled us to selectively photocontrol the peptide backbone conformation and to study the intramolecular influence of one peptide bond conformation on the conformational dynamics of another one. For the peptide Ac-VAψ[CS–NH]FGGAψ[CSe–NH]F-OMe, the *cis* state of [CSe–NH] retarded the *cis*→*trans* decay of [CS–NH] from a k_{ct} value of 4.6×10^{-3} s^{-1} (in case of [CSe–NH] in the *trans* state) to 4.0×10^{-3} s^{-1}.

– The [CSe–NH-] bond can undergo a rapid *cis*→*trans* decay via a selenoimidate nitrogen inversion pathway under alkaline conditions. The inversion rate is about 30 times faster than the C–N rotation rate.

– The inversion process in the selenoimidate anion was autocatalyzed, i.e. the **Z** conformer was able to catalyze the **E**→**Z** inversion. This remarkably faster *cis/trans* isomerization at alkaline conditions, which occurs via a nitrogen inversion pathway, provides a nonenzymatic way to enhance the backbone flexibility.

– The *cis→trans* isomerization of the selenoxo imidic prolyl bond in Bz-Val-Gly-Ala-ψ[CSe–N]Pro-OMe could not be catalyzed by the peptidyl prolyl *cis/trans* isomerase hCyp18.

– Chalcogen substitutions are able to exert some structural and electronic effects on the peptide chain, for example, an increased *cis/trans* rotational barrier and a remarkably enhanced amide proton acidity in the selenoxo group. Chalcogen electronegativity, which was generally thought to be the source of these changes, cannot explain these chalcogen substitution effects. Instead, atomic polarizability of chalcogen atoms provides a reasonable interpretation. i.e. many structural and physicochemical properties in [C**X**–NR-] (**X** = O, S, Se; R = H, alkyl) such as UV/Vis absorption wavelength, C–N rotational barrier, pK_a and stretching frequency of NH, chemical shift of ^{1}H and ^{13}C in NMR, dipole moment, and nitrogen inversion barrier in the imidate anions are linearly correlated with the chalcogen atomic polarizability. These linear correlations emphasize that not only the chalcogen electronegativity but also the polarizability, the capacity of an atom to adopt additional electron density, plays an important role in the structure of chalcogen-substituted peptide bonds. The linearity also provides a predictable way of estimating the impact of a certain selenoxo substitution on the peptide backbone structure and dynamics.

– Two non-covalent intramolecular interactions, NH···π and n−π*, have been discussed for the selenoxo peptides. The selenoxo peptide, due to the stronger electron-donating ability of Se, may adopt a conformation featuring a significant n−π*. The enhanced acidity of selenoxo amide proton strengthens its interaction with the aromatic side chain flanked to the selenoxo group, resulting in a slight redshift of the UV/Vis spectra and an upfield shift of the HN resonance in the ^{1}H-NMR spectra compared with the selenoxo peptide bond flanked with nonaromatic side chain. Interestingly, the NH···π interaction in the Bz-Val-Gly-Ala-ψ[C**X**–NH]Phe-OMe peptide series also showed a linear relationship with the chalcogen atomic polarizability. Therefore, the selenoxo substitution may provide a valuable way to evaluate these non-bonding local interactions in peptides.

– The work depicted in this PhD thesis represents only the beginning of selenoxo peptide chemistry. Future work might be focused on the following aspects: (i) improving the synthesis to yield more complicated selenoxo peptides; (ii) applying the selenoxo

substitution to model peptides of significant biological importance to study the conformation-specific and electronic effects; (iii) expanding the selenoxo substitution to protein systems via chemical ligation strategy.

7. References

1. Pauling L (1960) *The Nature of the Chemical Bond* (Connell University Press, Ithaca, New York).
2. Robin MB, Bovey FA, & Basch H (2010) Molecular and electronic structure of the amide group. *Amides (1970)*, (John Wiley & Sons, Ltd.), pp 1-72.
3. Wiberg KB (1999) The interaction of carbonyl groups with substituents. *Acc. Chem. Res.* 32(11):922-929.
4. Schnur DM, Yuh YH, & Dalton DR (1989) A molecular mechanics study of amide conformations. *J. Org. Chem* 54(16):3779-3785.
5. Wiberg KB & Breneman CM (1992) Resonance interactions in acyclic systems. 3. Formamide internal rotation revisited. Charge and energy redistribution along the C-N bond rotational pathway. *J. Am. Chem. Soc.* 114(3):831-840.
6. Ramachandran GN & Sasisekharan V (1968) Conformation of polypeptides and proteins. *Adv. Protein Chem.*, eds C.B. Anfinsen MLAJTE & Frederic MR (Academic Press), Vol 23, pp 283-437.
7. Stewart DE, Sarkar A, & Wampler JE (1990) Occurrence and role of *cis* peptide bonds in protein structures. *J. Mol. Biol.* 214(1):253-260.
8. MacArthur MW & Thornton JM (1991) Influence of proline residues on protein conformation. *J. Mol. Biol.* 218(2):397-412.
9. Jabs A, Weiss MS, & Hilgenfeld R (1999) Non-proline *cis* peptide bonds in proteins. *J. Mol. Biol.* 286(1):291-304.
10. Weiss MS, Jabs A, & Hilgenfeld R (1998) Peptide bonds revisited. *Nat. Struct. Mol. Biol.* 5(8):676-676.
11. Reimer U*, et al.* (1998) Side-chain effects on peptidyl-prolyl *cis/trans* isomerisation. *J. Mol. Biol.* 279(2):449-460.
12. Taylor CM, Hardré R, Edwards PJB, & Park JH (2003) Factors affecting conformation in proline-containing peptides. *Org. Lett.* 5(23):4413-4416.
13. Yao J*, et al.* (1994) Stabilization of a type-VI turn in a family of linear peptides in water solution. *J. Mol. Biol.* 243(4):736-753.
14. Bhattacharyya R & Chakrabarti P (2003) Stereospecific interactions of proline residues in protein structures and complexes. *J. Mol. Biol.* 331(4):925-940.
15. Meng HY, Thomas KM, Lee AE, & Zondlo NJ (2006) Effects of i and i+3 residue identity on *cis-trans* isomerism of the aromatic(i+1)-prolyl(i+2) amide bond: Implications for type VI beta-turn formation. *Biopolymers* 84(2):192-204.
16. Fischer G (2000) Chemical aspects of peptide bond isomerisation. *Chem. Soc. Rev.* 29(2):119-127.
17. Kern D, Schutkowski M, & Drakenberg T (1997) Rotational barriers of *cis/trans* isomerization of proline analogues and their catalysis by cyclophilin. *J. Am. Chem. Soc.* 119(36):8403-8408.
18. Schiene-Fischer C, Aumüller T, & Fischer G (2012) Peptide bond *cis/trans* isomerases: a biocatalysis perspective of conformational dynamics in proteins. Topics in Current Chemistry, (Springer Berlin / Heidelberg), pp 1-33.
19. Scherer G, Kramer ML, Schutkowski M, Reimer U, & Fischer G (1998) Barriers to rotation of secondary amide peptide bonds. *J. Am. Chem. Soc.* 120(22):5568-5574.
20. Nguyen K, Iskandar M, & Rabenstein DL (2010) Kinetics and equilibria of *cis/trans* isomerization of secondary amide peptide bonds in linear and cyclic peptides. *J. Phys. Chem. B* 114(9):3387-3392.
21. Ramachandran GN & Mitra AK (1976) An explanation for the rare occurrence of *cis* peptide units in proteins and polypeptides. *J. Mol. Biol.* 107(1):85-92.
22. Radzicka A, Pedersen L, & Wolfenden R (1988) Influences of solvent water on protein folding: free energies of solvation of *cis* and *trans* peptides are nearly identical. *Biochemistry* 27(12):4538-4541.

23.   Drakenberg T, Dahlqvist KI, & Forsen S (1972) Barrier to internal rotation in amides. IV. N,N-Dimethylamides. Substituent and solvent effects. *J. Phys. Chem.* 76(15):2178-2183.

24.   Martin RB & Hutton WC (1973) Predominant nitrogen-bound hydrogen exchange via Oxygen-protonated amide. *J. Am. Chem. Soc.* 95(14):4752-4754.

25.   Martin RB (1972) O-protonation of amides in dilute acids. *J. Chem. Soc., Chem. Commun.* (13):793-794.

26.   Texter FL, Spencer DB, Rosenstein R, & Matthews CR (1992) Intramolecular catalysis of a proline isomerization reaction in the folding of dihydrofolate reductase. *Biochemistry* 31(25):5687-5691.

27.   Cox C, Wack H, & Lectka T (1999) Nucleophilic catalysis of amide isomerization. *J. Am. Chem. Soc.* 121(34):7963-7964.

28.   Fanghanel J & Fischer G (2004) Insights into the catalytic mechanism of peptidyl prolyl *cis/trans* isomerases. *Front. Biosci.* 9:3453-3478.

29.   Cox C & Lectka T (2000) Synthetic catalysis of amide isomerization. *Acc. Chem. Res.* 33(12):849-858.

30.   Cox C, Ferraris D, Murthy NN, & Lectka T (1996) Copper(II)-catalyzed amide isomerization: evidence for N-coordination. *J. Am. Chem. Soc.* 118(22):5332-5333.

31.   Fischer G, Bang H, & Mech C (1984) Determination of enzymatic catalysis for the *cis-trans*-isomerization of peptide binding in proline-containing peptides. *Biomed. Biochim. Acta* 43(10):1101-1111.

32.   Fischer G, Wittmann-Liebold B, Lang K, Kiefhaber T, & Schmid FX (1989) Cyclophilin and peptidyl-prolyl *cis-trans* isomerase are probably identical proteins. *Nature* 337(6206):476-478.

33.   Fischer G & Aumüller T (2003) Regulation of Peptide Bond *cis/trans* Isomerization by Enzyme Catalysis and its Implications in Physiological Processes. *Rev. Physiol. Biochem. Pharmacol.* (Springer Berlin Heidelberg), Vol 148, pp 105-150.

34.   Schiene-Fischer C, Habazettl J, Schmid FX, & Fischer G (2002) The Hsp70 chaperone DnaK is a secondary amide peptide bond *cis-trans* isomerase. *Nat. Struct. Mol. Biol.* 9(6):419-424.

35.   Bang H*, et al.* (2000) Prolyl isomerases in a minimal cell. Catalysis of protein folding by trigger factor from Mycoplasma genitalium. *Eur. J. Biochem.* 267(11):3270-3280.

36.   Brandts JF, Halvorson HR, & Brennan M (1975) Consideration of the possibility that the slow step in protein denaturation reactions is due to *cis-trans* isomerism of proline residues. *Biochemistry* 14(22):4953-4963.

37.   Creighton TE (1978) Possible implications of many proline residues for the kinetics of protein unfolding and refolding. *J. Mol. Biol.* 125(3):401-406.

38.   Schmid FX & Baldwin RL (1978) Acid catalysis of the formation of the slow-folding species of RNase A: evidence that the reaction is proline isomerization. *Proc. Natl. Acad. Sci. U. S. A.* 75(10):4764-4768.

39.   Lin LN & Brandts JF (1984) Involvement of prolines-114 and -117 in the slow refolding phase of ribonuclease A as determined by isomer-specific proteolysis. *Biochemistry* 23(24):5713-5723.

40.   Kim PS & Baldwin RL (1990) Intermediates in the folding reactions of small proteins. *Annu. Rev. Biochem.* 59:631-660.

41.   Lang K, Schmid FX, & Fischer G (1987) Catalysis of protein folding by prolyl isomerase. *Nature* 329(6136):268-270.

42.   Schmid FX (1993) Prolyl isomerase: enzymatic catalysis of slow protein-folding reactions. *Annu. Rev. Biophys. Biomol. Struct.* 22(1):123-143.

43.   Fischer G & Bang H (1985) The refolding of urea-denatured ribonuclease A is catalyzed by peptidyl-prolyl *cis-trans* isomerase. *Biochim. Biophys. Acta* 828(1):39-42.

44.   Fischer G (1994) Peptidyl-prolyl *cis/trans* isomerases and their effectors. *Angew. Chem. Int. Ed.* 33(14):1415-1436.

45.   Tweedy NB, Nair SK, Paterno SA, Fierke CA, & Christianson DW (1993) Structure and energetics of a non-proline *cis*-peptidyl linkage in a proline-202→alanine carbonic anhydrase II variant. *Biochemistry* 32(41):10944-10949.

46. Schultz DA & Baldwin RL (1992) *Cis* proline mutants of ribonuclease A. I. Thermal stability. *Protein Sci.* 1(7):910-916.

47. Mayr LM & Schmid FX (1993) Kinetic models for unfolding and refolding of ribonuclease T1 with substitution of *cis*-proline 39 by alanine. *J. Mol. Biol.* 231(3):913-926.

48. Osvath S & Gruebele M (2003) Proline can have opposite effects on fast and slow protein folding phases. *Biophys. J.* 85(2):1215-1222.

49. Odefey C, Mayr LM, & Schmid FX (1995) Non-prolyl *cis-trans* peptide bond isomerization as a rate-determining step in protein unfolding and refolding. *J. Mol. Biol.* 245(1):69-78.

50. Reimer U & Fischer G (2002) Local structural changes caused by peptidyl-prolyl *cis/trans* isomerization in the native state of proteins. *Biophys. Chem.* 96(2-3):203-212.

51. Lu KP, Finn G, Lee TH, & Nicholson LK (2007) Prolyl *cis-trans* isomerization as a molecular timer. *Nat. Chem. Biol.* 3(10):619-629.

52. Breheny PJ, Laederach A, Fulton DB, & Andreotti AH (2003) Ligand specificity modulated by prolyl imide bond *cis/trans* isomerization in the Itk SH2 domain: a quantitative NMR study. *J. Am. Chem. Soc.* 125(51):15706-15707.

53. Mallis RJ, Brazin KN, Fulton DB, & Andreotti AH (2002) Structural characterization of a proline-driven conformational switch within the Itk SH2 domain. *Nat. Struct. Mol. Biol.* 9(12):900-905.

54. Pastorino L*, et al.* (2006) The prolyl isomerase Pin1 regulates amyloid precursor protein processing and amyloid-[beta] production. *Nature* 440(7083):528-534.

55. Eakin CM, Berman AJ, & Miranker AD (2006) A native to amyloidogenic transition regulated by a backbone trigger. *Nat. Struct. Mol. Biol.* 13(3):202-208.

56. Lummis SCR*, et al.* (2005) *Cis-trans* isomerization at a proline opens the pore of a neurotransmitter-gated ion channel. *Nature* 438(7065):248-252.

57. Eckert B, Martin A, Balbach J, & Schmid FX (2005) Prolyl isomerization as a molecular timer in phage infection. *Nat. Struct. Mol. Biol.* 12(7):619-623.

58. Tchaicheeyan O (2004) Is peptide bond *cis/trans* isomerization a key stage in the chemo-mechanical cycle of motor proteins? *FASEB J.* 18(7):783-789.

59. Henzler-Wildman K & Kern D (2007) Dynamic personalities of proteins. *Nature* 450(7172):964-972.

60. Goh CS, Milburn D, & Gerstein M (2004) Conformational changes associated with protein-protein interactions. *Curr. Opin. Struct. Biol.* 14(1):104-109.

61. Perutz MF (1989) Mechanisms of cooperativity and allosteric regulation in proteins. *Q. Rev. Biophys.* 22(2):139-237.

62. Gerstein M, Lesk AM, & Chothia C (1994) Structural mechanisms for domain movements in proteins. *Biochemistry* 33(22):6739-6749.

63. Steven OS (2010) Structure and activation of the visual pigment rhodopsin. *Annu. Rev. Biophys.* 39:309-328.

64. Rockwell NC, Su Y-S, & Lagarias JC (2006) Phytochrome structure and signaling mechanisms. *Annu. Rev. Plant Biol.* 57:837-858.

65. Gorostiza P & Isacoff EY (2008) Optical switches for remote and noninvasive Control of Cell Signaling. *Science* 322(5900):395-399.

66. Renner C & Moroder L (2006) Azobenzene as conformational switch in model peptides. *ChemBioChem* 7(6):868-878.

67. Erdmann F & Zhang Y (2010) Reversible photoswitching of protein function. *Mol. BioSyst.* 6(11):2103-2109.

68. Fehrentz T, Schonberger M, & Trauner D (2011) Optochemical genetics. *Angew. Chem. Int. Ed.* 50(51):12156-12182.

69. Kumita JR, Smart OS, & Woolley GA (2000) Photo-control of helix content in a short peptide. *Proc. Natl. Acad. Sci. U. S. A.* 97(8):3803-3808.

70. Burns DC, Zhang FZ, & Woolley GA (2007) Synthesis of 3,3'-bis(sulfonato)-4,4'-bis(chloroacetamido)azobenzene and cysteine cross-linking for photo-control of protein conformation and activity. *Nat. Protoc.* 2(2):251-258.

71. Beharry AA & Woolley GA (2011) Azobenzene photoswitches for biomolecules. *Chem. Soc. Rev.* 40(8):4422-4437.

72.   Zhang Y, Erdmann F, & Fischer G (2009) Augmented photoswitching modulates immune signaling. *Nat. Chem. Biol.* 5(10):724-726.

73.   Fissi A*, et al.* (1993) Photoresponsive polypeptides: Photochromism and conformation of poly (L-glutamic acid) containing spiropyran units. *Biopolymers* 33(10):1505-1517.

74.   Behrendt R*, et al.* (1999) Photomodulation of the Conformation of Cyclic Peptides with Azobenzene Moieties in the Peptide Backbone. *Angew. Chem. Int. Ed.* 38(18):2771-2774.

75.   Erdélyi M, Karlén A, & Gogoll A (2006) A new tool in peptide engineering: a photoswitchable stilbene-type β-hairpin mimetic. *Chem. Eur. J.* 12(2):403-412.

76.   Dong SL*, et al.* (2006) A photocontrolled beta-hairpin peptide. *Chem. Eur. J.* 12(4):1114-1120.

77.   Schrader TE*, et al.* (2007) Light-triggered beta-hairpin folding and unfolding. *Proc. Natl. Acad. Sci. U. S. A.* 104:15729-15734.

78.   Doran TM, Anderson EA, Latchney SE, Opanashuk LA, & Nilsson BL (2012) An azobenzene photoswitch sheds light on turn nucleation in amyloid-beta self-assembly. *ACS Chem Neurosci* 3(3):211-220.

79.   Deeg AA*, et al.* (2011) Light-triggered aggregation and disassembly of amyloid-like structures. *ChemPhysChem* 12(3):559-562.

80.   Sinicropi A, Bernini C, Basosi R, & Olivucci M (2009) A novel biomimetic photochemical switch at work: design of a photomodulable peptide. *Photochem. Photobiol. Sci.* 8(12):1639-1649.

81.   Regner N*, et al.* (2012) Light-switchable hemithioindigo–hemistilbene-containing peptides: ultrafast spectroscopy of the ***Z→E*** isomerization of the chromophore and the structural dynamics of the peptide moiety. *J. Phys. Chem. B* 116(14):4181-4191.

82.   Cordes T*, et al.* (2006) Hemithioindigo-based photoswitches as ultrafast light trigger in chromopeptides. *Chem. Phys. Lett.* 428(1–3):167-173.

83.   Wang Y, Purrello R, & Spiro TG (1989) UV photoisomerization of N-methylacetamide and resonance Raman enhancement of a new conformation-sensitive amide mode. *J. Am. Chem. Soc.* 111(21):8274-8276.

84.   Li PS, Chen XG, Shulin E, & Asher SA (1997) UV resonance Raman ground and excited state studies of amide and peptide isomerization dynamics. *J. Am. Chem. Soc.* 119(5):1116-1120.

85.   Frank R, Jakob M, Thunecke F, Fischer G, & Schutkowski M (2000) Thioxylation as one-atom-substitution generates a photoswitchable element within the peptide backbone. *Angew. Chem. Int. Ed.* 39(6):1120-1122.

86.   Zhao J, Wildemann D, Jakob M, Vargas C, & Schiene-Fischer C (2003) Direct photomodulation of peptide backbone conformations. *Chem Commun (Camb)* (22):2810-2811.

87.   Stewart WE & Siddall TH (1970) Nuclear magnetic resonance studies of amides. *Chem. Rev.* 70(5):517-551.

88.   Shaw RA, Kollát E, Hollósi M, & Mantsch HH (1995) Hydrogen bonding and isomerization in thioamide peptide derivatives. *Spectrochimica Acta Part A: Molecular and Biomolecular Spectroscopy* 51(8):1399-1412.

89.   Min BK*, et al.* (1998) A comparative study on the hydrogen bonding ability of amide and thioamide using near IR spectroscopy. *J. Mol. Struct.* 471(1-3):283-288.

90.   Lee HJ, Choi YS, Lee KB, Park J, & Yoon CJ (2002) Hydrogen bonding abilities of thioamide. *J. Phys. Chem. A* 106(30):7010-7017.

91.   Bachmann A, Wildemann D, Praetorius F, Fischer G, & Kiefhaber T (2011) Mapping backbone and side-chain interactions in the transition state of a coupled protein folding and binding reaction. *Proc. Natl. Acad. Sci. U. S. A.*

92.   Sifferlen T, Rueping M, Gademann K, Jaun B, & Seebach D (1999) beta-Thiopeptides: Synthesis, NMR solution structure, CD spectra, and photochemistry. *Helv. Chim. Acta* 82(12):2067-2093.

93.   Wu YD & Zhao YL (2001) A theoretical study on the origin of cooperativity in the formation of 3(10)- and alpha-helices. *J. Am. Chem. Soc.* 123(22):5313-5319.

94.   Miwa JH, Pallivathucal L, Gowda S, & Lee KE (2002) Conformational stability of helical peptides containing a thioamide linkage. *Org. Lett.* 4(26):4655-4657.
95.   De Zotti M*, et al.* (2012) Partial thioamide scan on the lipopeptaibiotic trichogin GA IV. Effects on folding and bioactivity. *Beilstein J. Org. Chem.* 8:1161-1171.
96.   Hollosi M, Kollat E, Kajtar J, Kajtar M, & Fasman GD (1990) Chiroptical labeling of folded polypeptide conformations: The thioamide probe. *Biopolymers* 30(11-12):1061-1072.
97.   Sherman DB & Spatola AF (1990) Compatibility of thioamides with reverse turn features - synthesis and conformational-analysis of 2 model cyclic pseudopeptides containing thioamides as backbone modifications. *J. Am. Chem. Soc.* 112(1):433-441.
98.   Czugler M*, et al.* (1993) Reverse turn conformation of N-thioacetyl thioprolyl glycine N'-methylamide in the crystal and in solution. *Tetrahedron* 49(30):6661-6668.
99.   Chen P & Qu J (2011) Backbone Modification of beta-Hairpin-Forming Tetrapeptides in Asymmetric Acyl Transfer Reactions. *J. Org. Chem.* 76(9):2994-3004.
100.   Miwa JH, Patel AK, Vivatrat N, Popek SM, & Meyer AM (2001) Compatibility of the thioamide functional group with beta-sheet secondary structure: Incorporation of a thioamide linkage into a beta-hairpin peptide. *Org. Lett.* 3(21):3373-3375.
101.   Reiner A, Wildemann D, Fischer G, & Kiefhaber T (2008) Effect of thioxopeptide bonds on alpha-helix structure and stability. *J. Am. Chem. Soc.* 130(25):8079-8084.
102.   Bartlett PA, Spear KL, & Jacobsen NE (1982) A thioamide substrate of carboxypeptidase A. *Biochemistry* 21(7):1608-1611.
103.   Campbell P & Nashed NT (1982) Carboxypeptidase A catalyzed hydrolysis of thiopeptide and thionester analogues of specific substrates. An effect on k_{cat} for peptide, but not ester, substrates. *J. Am. Chem. Soc.* 104(19):5221-5226.
104.   Beattie RE, Elmore DT, Williams CH, & Guthrie DJ (1987) The behaviour of leucine aminopeptidase towards thionopeptides. *Biochem. J.* 245(1):285-288.
105.   Song J*, et al.* (2011) Cellular uptake of transportan 10 and its analogs in live cells: Selectivity and structure–activity relationship studies. *Peptides* 32(9):1934-1941.
106.   Sherman DB*, et al.* (1989) Biological activities of cyclic enkephalin pseudopeptides containing thioamides as amide bond replacements. *Biochem. Biophys. Res. Commun.* 162(3):1126-1132.
107.   Clausen K, Spatola AF, Lemieux C, Schiller PW, & Lawesson S-O (1984) Evidence of a peptide backbone contribution toward selective receptor recognition for leucine enkephalin thioamide analogs. *Biochem. Biophys. Res. Commun.* 120(1):305-310.
108.   Lajoie G*, et al.* (1984) Synthesis and biological-activity of monothionated analogs of leucine-enkephalin. *Int. J. Pept. Protein Res.* 24(4):316-327.
109.   Hitotsuyanagi Y, Suzuki J, Matsumoto Y, Takeya K, & Itokawa H (1994) Studies on Rubia akane(RA) derivatives. Part 7. Thioamide analogues of RAs: antitumour cyclic hexapeptides. *J. Chem. Soc., Perkin Trans. 1* (14):1887-1889.
110.   Majer Z*, et al.* (1988) Solid phase synthesis of a GHRP analog containing C-terminal thioamide group. *Biochem. Biophys. Res. Commun.* 150(3):1017-1020.
111.   Tran TT, Burgess AW, Treutlein H, & Zeng J (2001) Conformational analysis of thiopeptides: free energy calculations on the effects of thio-substitutions on the conformational distributions of alanine dipeptides. *J. Mol. Graphics Modell.* 20(3):245-256.
112.   Artis DR & Lipton MA (1998) Conformations of thioamide-containing dipeptides: A computational study. *J. Am. Chem. Soc.* 120(47):12200-12206.
113.   Cervetto V, Bregy H, Hamm P, & Helbing J (2006) Time-resolved IR spectroscopy of N-methylthioacetamide: *Trans→cis* isomerization upon n-pi* and pi-pi* excitation and *cis→trans* photoreaction. *J. Phys. Chem. A* 110(40):11473-11478.
114.   Zhao JZ, Wildemann D, Jakob M, Vargas C, & Schiene-Fischer C (2003) Direct photomodulation of peptide backbone conformations. *Chem. Commun. (Cambridge, U. K.)* (22):2810-2811.
115.   Satzger H*, et al.* (2005) Photoswitchable elements within a peptide backbone-ultrafast spectroscopy of thioxylated amides. *J. Phys. Chem. B* 109(10):4770-4775.

116. Helbing J*, et al.* (2004) A fast photoswitch for minimally perturbed peptides: Investigation of the trans→cis photoisomerization of N-methylthioacetamide. *J. Am. Chem. Soc.* 126(28):8823-8834.
117. Cervetto V, Pfister R, & Helbing J (2008) Time-resolved infrared spectroscopy of thiopeptide isomerization and hydrogen-bond breaking. *J. Phys. Chem. B* 112(11):3540-3544.
118. Bregy H, Heimgartner H, & Helbing J (2009) A Time-resolved Spectroscopic Comparison of the Photoisomerization of Small beta-Turn-forming Thioxopeptides. *J. Phys. Chem. B* 113(6):1756-1762.
119. Cervetto V, Hamm P, & Helbing J (2008) Transient 2D-IR spectroscopy of thiopeptide isomerization. *J. Phys. Chem. B* 112(28):8398-8405.
120. Wildemann D*, et al.* (2007) A nearly isosteric photosensitive amide-backbone substitution allows enzyme activity switching in ribonuclease S. *J. Am. Chem. Soc.* 129(16):4910-4918.
121. Huang Y, Cong ZY, Yang LF, & Dong SL (2008) A photoswitchable thioxopeptide bond facilitates the conformation-activity correlation study of insect kinin. *J. Pept. Sci.* 14(9):1062-1068.
122. Atkins JF & Gesteland RF (2000) Translation: The twenty-first amino acid. *Nature* 407(6803):463-464.
123. Böck A*, et al.* (1991) Selenocysteine: the 21st amino acid. *Mol. Microbiol.* 5(3):515-520.
124. Stadtman TC (1996) Selenocysteine. *Annu. Rev. Biochem.* 65(1):83-100.
125. Johansson L, Gafvelin G, & Arnér ESJ (2005) Selenocysteine in proteins—properties and biotechnological use. *Biochim. Biophys. Acta.* 1726(1):1-13.
126. Flohe L, Gunzler WA, & Schock HH (1973) Glutathione peroxidase: a selenoenzyme. *FEBS Lett.* 32(1):132-134.
127. Behne D & Kyriakopoulos A (2001) Mammalian selenium-containing proteins. *Annu. Rev. Nutr.* 21:453-473.
128. Ursini F*, et al.* (1995) Diversity of glutathione peroxidases. *Methods Enzymol.* 252:38-53.
129. W. M. Haynes e (*Handbook of Chemistry and Physics. 91st Edition (Internet Version 2011)* (CRC Press/Taylor and Francis, Boca Raton, FL.) 91st Edition (Internet Version 2011) Ed.
130. Jacob C, Giles GI, Giles NM, & Sies H (2003) Sulfur and selenium: the role of oxidation state in protein structure and function. *Angew. Chem. Int. Ed.* 42(39):4742-4758.
131. Huber RE & Criddle RS (1967) Comparison of the chemical properties of selenocysteine and selenocystine with their sulfur analogs. *Arch. Biochem. Biophys.* 122(1):164-173.
132. Rohr U, Schatz J, & Sauer J (1998) Thio- and selenocarbonyl compounds as "superdienophiles" in [4+2] cycloadditions. *Eur. J. Org. Chem.* 1998(12):2875-2883.
133. Krief A (1988) *Organoselenium chemistry I : functional group transformations* (Springer-Verlag, Berlin).
134. Olszewska T, Pyszno A, Milewska MJ, Gdaniec M, & Polonski T (2005) Thioamides and selenoamides with chirality solely due to hindered rotation about the C-N bond: enantioselective complexation with optically active hosts. *Tetrahedron-Asymmetry* 16(22):3711-3717.
135. Murai T (2005) Thio-, seleno-, telluro-amides. *Chalcogenocarboxylic Acid Derivatives* 251:247-272.
136. Koketsu M & Ishihara H (2007) Synthesis and applications of chalcogenoamide: Thio-, seleno- and telluroamides. *Curr. Org. Synth.* 4(1):15-29.
137. Pilkington MJ, Slawin AMZ, Williams DJ, Wood PT, & Woollins JD (1990) The preparation and characterization of binary phosphorus–selenium rings. *Heteroat. Chem.* 1(5):351-355.
138. Gray IP, Bhattacharyya P, Slawin AMZ, & Woollins JD (2005) A new synthesis of (PhPSe2)2 (Woollins' reagent) and its use in the synthesis of novel P–Se heterocycles. *Chem. Eur. J.* 11(21):6221-6227.
139. Bhatacharyya P & Woollins JD (2001) Selenocarbonyl synthesis using Woollins reagent. *Tetrahedron Lett.* 42(34):5949-5951.

140.   Bethke J, Karaghiosoff K, & Wessjohann LA (2003) Synthesis of N,N-disubstituted selenoamides by O/Se-exchange with selenium–Lawesson's reagent. *Tetrahedron Lett.* 44(36):6911-6913.

141.   Niu S, Li GM, Zingaro RA, Reibenspies JH, & Ichiye T (2002) Planarity of acetamides, thioacetamides, and selenoacetamides: Crystal structure of N,N-dimethylselenoacetamide. *Heteroat. Chem.* 13(4):380-386.

142.   Mutoh Y, Murai T, & Yamago S (2007) Telluration of seleno- and chloroiminium salts leading to various telluroamides, and their structure and NMR properties. *J. Organomet. Chem.* 692(1-3):129-135.

143.   Murai T, Mizutani T, Kanda T, & Kato S (1995) Reactions of diselenoic acid esters with amines and X-ray crystal structure analyses of aromatic selenoamides. *Heteroat. Chem.* 6(3):241-246.

144.   Li GM, Zingaro RA, Segi M, Reibenspies JH, & Nakajima T (1997) Synthesis and structure of telluroamides and selenoamides. The first crystallographic study of telluroamides. *Organometallics* 16(4):756-762.

145.   Li Y, Hua GX, Slawin AMZ, & Woollins JD (2009) The X-Ray crystal structures of primary aryl substituted selenoamides. *Molecules* 14(2):884-892.

146.   Glendening ED & Hrabal JA (1997) Resonance in formamide and its chalcogen replacement analogues: a natural population analysis/Natural Resonance Theory viewpoint. *J. Am. Chem. Soc.* 119(52):12940-12946.

147.   Prasad BV, Uppal P, & Bassi PS (1997) Barrier to C-N rotation in selenoformamide: An ab initio study. *Chem. Phys. Lett.* 276(1-2):31-38.

148.   Jensen KA & Sandström.J (1969) Barriers to internal rotation in N,N-dimethylselenoamides. A complete line shape analysis. *Acta Chem. Scand.* 23(6):1911-1915.

149.   Milewska MJ & Połoński T (1999) Chiroptical spectra of bicyclic selenolactams. Optical activity of the singlet–triplet transition. *Tetrahedron: Asymmetry* 10(21):4123-4128.

150.   Milne J (1993) Chemical shift references for ^{77}Se NMR spectroscopy. Selenous acid. *Magn. Reson. Chem.* 31(7):652-655.

151.   Bethke J, Karaghiosoff K, & Wessjohann LA (2003) Synthesis of N,N-disubstituted selenoamides by O/Se-exchange with selenium-Lawesson's reagent. *Tetrahedron Lett.* 44(36):6911-6913.

152.   Hoeg-jensen T (1996) Review: endothiopeptides alias peptide thioamides. *Phosphorus, Sulfur Silicon Relat. Elem.* 108(1-4):257-278.

153.   Hussaini SR & Hammond GB (2008) Eschenmoser coupling reaction of selenoamides. Synthesis of enamino ester. *Arkivoc*:129-136.

154.   Zhao JZ, Micheau JC, Vargas C, & Schiene-Fischer C (2004) *cis/trans* photoisomerization of secondary thiopeptide bonds. *Chem. Eur. J.* 10(23):6093-6101.

155.   Walter W & Becker RF (1969) On the structure of thioamides and their derivatives, VII I). Acidity of aromatically substituted thioamides. *Liebigs Ann.* 727(1):71-80.

156.   Jensen K & Nielsen PH (1966) Infrared spectra of thioamides and selenoamides. *Acta Chem. Scand.* 20(3):597-629.

157.   Creswell CJ & Allred AL (1962) The strengths of hydrogen bonds formed by protium and deuterium. *J. Am. Chem. Soc.* 84(20):3966-3967.

158.   Martin DC & Butler JAV (1939) 291. The dissociation constants of some nitrophenols in deuterium oxide. *J. Chem. Soc.*:1366-1369.

159.   Nielsen EB & Schellman JA (1967) The absorption spectra of simple amides and peptides. *J. Phys. Chem.* 71(7):2297-2304.

160.   Lumbroso H & Curé J (1990) A dipole moment study of enamines, amides, amidines, hydrazones, triazenes and ureas. *J. Mol. Struct.* 239:219-233.

161.   Sheinblatt M (1970) Determination of an acidity scale for peptide hydrogens from nuclear magnetic resonance kinetic studies. *J. Am. Chem. Soc.* 92(8):2505-2509.

162.   Wildemann D, Drewello M, Fischer G, & Schutkowski M (1999) Extremely selective $Mg(ClO_4)_2$ mediated removal of Bpoc/Ddz moieties suitable for the solid phase peptide synthesis of thioxo peptides. *Chem. Commun. (Cambridge, U. K.)* (18):1809-1810.

163. Miwa JH, Margarida LA, & Meyer AE (2001) Improved acidolytic deprotection conditions for the Fmoc-based solid-phase synthesis of thioxo peptides. *Tetrahedron Lett.* 42(41):7189-7191.

164. Zacharie B, Sauve G, & Penney C (1993) Thioacylating agents − use of thiobenzimidazolone derivatives for the preparation of thiotuftsin analogs. *Tetrahedron* 49(46):10489-10500.

165. Shalaby MA, Grote CW, & Rapoport H (1996) Thiopeptide synthesis. alpha-amino thionoacid derivatives of nitrobenzotriazole as thioacylating agents. *J. Org. Chem.* 61(25):9045-9048.

166. Brain CT, Hallett A, & Ko SY (1997) Thioamide synthesis: Thioacyl-N-phthalimides as thioacylating agents. *J. Org. Chem.* 62(12):3808-3809.

167. Jahreis G. *unpublished work.*

168. Brown DW, Campbell MM, & Walker CV (1983) Endothiopeptides. *Tetrahedron* 39(7):1075-1083.

169. Lajoie G, Lépine F, Maziak L, & Belleau B (1983) Facile regioselective formation of thiopeptide linkages from oligopeptides with new thionation reagents. *Tetrahedron Lett.* 24(36):3815-3818.

170. Jensen OE & Senning A (1986) Studies on amino acids and peptides XII1: Synthesis of thiated analogues of Boc-S-Ala-Aib-S-Ala-OMe and Ac-S-Ala-Aib-S-Ala-OMe. *Tetrahedron* 42(23):6555-6564.

171. Brown DW, Campbell MM, Chambers MS, & Walker CV (1987) Mono- and dithionopeptide synthesis. *Tetrahedron Lett.* 28(19):2171-2174.

172. Pfeifer T*, et al.* (1997) Specific fragmentation of thioxo peptides facilitates the assignment of the thioxylated amino acid. *J. Mass Spectrom.* 32(10):1064-1071.

173. Duddeck H (1995) *Selenium-77 Nuclear Magnetic Resonance Spectroscopy* (Pergamon).

174. Gerothanassis IP, Vakka C, & Troganis A (1996) ^{17}O NMR studies of the solvation state of *cis/trans* isomers of amides and model protected peptides. *J. Magn. Reson. B.* 111(3):220-229.

175. Valentine B*, et al.* (1985) Oxygen-17 NMR of peptides. *Int. J. Pept. Protein Res.* 25(1):56-68.

176. Takahashi O, Kohno Y, & Nishio M (2010) Relevance of weak hydrogen bonds in the conformation of organic compounds and bioconjugates: evidence from recent experimental data and high-level *ab Initio* MO calculations. *Chem. Rev.* 110(10):6049-6076.

177. Steiner T & Koellner G (2001) Hydrogen bonds with π-acceptors in proteins: frequencies and role in stabilizing local 3D structures. *J. Mol. Biol.* 305(3):535-557.

178. Schutkowski M, Woellner S, & Fischer GS (1995) Inhibition of peptidyl-prolyl *cis/trans* isomerase activity by substrate analog structures: thioxo tetrapeptide-4-nitroanilides. *Biochemistry* 34(40):13016-13026.

179. Weiss MS, Metzner HJ, & Hilgenfeld R (1998) Two non-proline *cis* peptide bonds may be important for factor XIII function. *FEBS Lett.* 423(3):291-296.

180. Wedemeyer WJ, Welker E, & Scheraga HA (2002) Proline *cis−trans* isomerization and protein folding. *Biochemistry* 41(50):14637-14644.

181. Bader RFW, Cheeseman JR, Laidig KE, Wiberg KB, & Breneman C (1990) Origin of rotation and inversion barriers. *J. Am. Chem. Soc.* 112(18):6530-6536.

182. Englander SW & Kallenbach NR (1983) Hydrogen exchange and structural dynamics of proteins and nucleic acids. *Q. Rev. Biophys.* 16(04):521-655.

183. Perrin CL, Johnston ER, Lollo CP, & Kobrin PA (1981) NMR studies of base-catalyzed proton exchange in amides. *J. Am. Chem. Soc.* 103(16):4691-4696.

184. Dugave C (2006) Chemical aspects of the restricted rotation of esters, amides, and related compounds. *cis-trans Isomerization in Biochemistry*, (Wiley-VCH Verlag GmbH & Co. KGaA), pp 143-166.

185. Perrin CL, Lollo CP, & Hahn CS (1985) Imidate anions: stereochemistry, equilibrium, nitrogen inversion, and comparison with proton exchange. *J. Org. Chem* 50(9):1405-1409.

186. Perrin CL & Thoburn JD (1989) Mechanism of *E/Z* stereoisomerization of imidate anions. *J. Org. Chem* 54(4):764-767.

187. Arnér ESJ (2010) Selenoproteins—What unique properties can arise with selenocysteine in place of cysteine? *Exp. Cell Res.* 316(8):1296-1303.

188. Wawra S & Fischer G (2006) Amide *cis-trans* isomerization in peptides and proteins. *cis-trans Isomerization in Biochemistry*, (Wiley-VCH Verlag GmbH & Co. KGaA), pp 167-193.

189. Harrison RK & Stein RL (1990) Mechanistic studies of peptidyl prolyl *cis-trans* isomerase: evidence for catalysis by distortion. *Biochemistry* 29(7):1684-1689.

190. Reimer U, Mokdad NE, Schutkowski M, & Fischer G (1997) Intramolecular assistance of *cis/trans* isomerization of the histidine−proline moiety. *Biochemistry* 36(45):13802-13808.

191. Perrin CL, Lollo CP, & Hahn CS (1985) Imidate anions: stereochemistry, equilibrium, nitrogen inversion, and comparison with proton exchange. *J. Org. Chem.* 50(9):1405-1409.

192. Walter W & Schaumann E (1971) On the structure of thioamides and their derivatives, XI. NMR-spectroscopic studies and the mechanism of isomerization of thioamide anions. *Chem. Ber.* 104(1):4-10.

193. Iwaoka M (2011) Nucleophilic Selenium. *Organoselenium Chemistry*, (Wiley-VCH Verlag GmbH & Co. KGaA), pp 53-109.

194. Cainelli G, Giacomini D, Trerè A, & Boyl PP (1996) Efficient transamination under mild conditions: preparation of primary amine derivatives from carbonyl compounds via imine isomerization with catalytic amounts of potassium *tert*-butoxide. *J. Org. Chem* 61(15):5134-5139.

195. Guthrie RD, Meister W, & Cram DJ (1967) 1,3-Aymmetric induction in a transamination reaction. *J. Am. Chem. Soc.* 89(20):5288-5290.

196. Cram DJ & Guthrie RD (1966) Electrophilic substitution at saturated carbon. XXVII. Carbanions as intermediates in the base-catalyzed methylene-Azomethine rearrangement. *J. Am. Chem. Soc.* 88(24):5760-5765.

197. Guthrie Robert D, Jaeger DA, Meister W, & Cram DJ (1971) Electrophilic substitution at saturated carbon. XLVIII. High stereospecificity in a transamination reaction. *J. Am. Chem. Soc.* 93(20):5137-5153.

198. Pauling L (1932) The nature of the chemical bond. IV. The energy of single bonds and the relative electronegativity of atoms. *J. Am. Chem. Soc.* 54(9):3570-3582.

199. Teachout RR & Pack RT (1971) The static dipole polarizabilities of all the neutral atoms in their ground states. *At. Data Nucl. Data Tables* 3:195-214.

200. Politzer P (1987) A relationship between the charge capacity and the hardness of neutral atoms and groups. *J. Chem. Phys.* 86(2):1072-1073.

201. Sanderson RT (1952) An interpretation of bond lengths in alkali halide gas molecules. *J. Am. Chem. Soc.* 74(1):272-274.

202. Sanderson RT (1955) Partial charges on atoms in organic compounds. *Science* 121(3137):207-208.

203. Sanderson RT (1954) Electronegativities in inorganic chemistry. III. *J. Chem. Educ.* 31(5):238.

204. Parr RG, Donnelly RA, Levy M, & Palke WE (1978) Electronegativity: The density functional viewpoint. *J. Chem. Phys.* 68(8):3801-3807.

205. Donnelly RA & Parr RG (1978) Elementary properties of an energy functional of the first-order reduced density matrix. *J. Chem. Phys.* 69(10):4431-4439.

206. Politzer P & Weinstein H (1979) Some relations between electronic distribution and electronegativity. *J. Chem. Phys.* 71(11):4218-4220.

207. Nagle JK (1990) Atomic polarizability and electronegativity. *J. Am. Chem. Soc.* 112(12):4741-4747.

208. Lee H-K & Querijero G (1985) Kinetics and mechanisms of thioamide rotational isomerism: N-thionaphthoyl-N-methyl glycine derivative. *J. Pharm. Sci.* 74(3):273-276.

209. Hiraoka K, Yamdagni R, & Kebarle P (1973) Effects of halogen substituents on the intrinsic acidity of acetic acids determined by measurements of gas-phase ion equilibriums. *J. Am. Chem. Soc.* 95(20):6833-6835.

210. Wang WH & Cheng CC (1994) General base catalyzed proton exchange in amides. *Bull. Chem. Soc. Jpn.* 67(4):1054-1057.

211. Witanowski M, Stefaniak L, & Webb GA (1987) Nitrogen NMR spectroscopy. *Annu. Rep. NMR Spectrosc.*, ed Webb GA (Academic Press), Vol 18, pp 1-211.

212. Martin GJ, Gouesnard JP, Dorie J, Rabiller C, & Martin ML (1977) Advantages of nitrogen-15 NMR in studying delocalization and evaluating the energy barriers of carbon-nitrogen rotation process in amides, thioamides, and related compounds. *J. Am. Chem. Soc.* 99(5):1381-1384.

213. Wiberg KB & Laidig KE (1987) Barriers to rotation adjacent to double bonds. 3. The C-O barrier in formic acid, methyl formate, acetic acid, and methyl acetate. The origin of ester and amide "resonance". *J. Am. Chem. Soc.* 109(20):5935-5943.

214. Yamada S (1995) Relationship between C(O) N twist angles and ^{17}O NMR chemical shifts in a series of twisted amides. *Angew. Chem. Int. Ed.* 34(10):1113-1115.

215. Yamada S (1996) Effects of C(O)-N bond rotation on the C-13, N-15, and O-17 NMR chemical shifts, and infrared carbonyl absorption in a series of twisted amides. *J. Org. Chem.* 61(3):941-946.

216. Politzer P, Huheey JE, Murray JS, & Grodzicki M (1992) Electronegativity and the concept of charge capacity. *J. Mol. Struct. THEOCHEM* 259:99-120.

217. Choudhary A, Gandla D, Krow GR, & Raines RT (2009) Nature of amide carbonyl-carbonyl interactions in proteins. *J. Am. Chem. Soc.* 131(21):7244-7246.

218. Bartlett GJ, Choudhary A, Raines RT, & Woolfson DN (2010) n ->π* interactions in proteins. *Nat. Chem. Biol.* 6(8):615-620.

219. Jakobsche CE, Choudhary A, Miller SJ, & Raines RT (2010) n-π* interaction and n)(π Pauli repulsion are antagonistic for protein stability. *J. Am. Chem. Soc.* 132(19):6651-6653.

220. Hodges JA & Raines RT (2006) Energetics of an n-π* interaction that impacts protein structure. *Org. Lett.* 8(21):4695-4697.

221. Bretscher LE, Jenkins CL, Taylor KM, DeRider ML, & Raines RT (2001) Conformational stability of collagen relies on a stereoelectronic effect. *J. Am. Chem. Soc.* 123(4):777-778.

222. Matthew P. Hinderaker RTR (2003) An electronic effect on protein structure. *Protein Sci.* 12(6):1188-1194.

223. Burgi HB, Dunitz JD, & Shefter E (1973) Geometrical Reaction Coordinates 2. Nucleophilic Addition to a Carbonyl Group. *J. Am. Chem. Soc.* 95(15):5065-5067.

224. Vishwanatha TM, Narendra N, Chattopadhyay B, Mukherjee M, & Sureshbabu VV (2012) Synthesis of selenoxo peptides and oligoselenoxo peptides employing LiAlHSeH. *J. Org. Chem* 77(6):2689-2702.

225. Dyson HJ & Wright PE (2005) Intrinsically unstructured proteins and their functions. *Nat. Rev. Mol. Cell Biol.* 6(3):197-208.

226. Tompa P (2002) Intrinsically unstructured proteins. *Trends Biochem. Sci.* 27(10):527-533.

227. Dyson HJ (2011) Expanding the proteome: disordered and alternatively folded proteins. *Q. Rev. Biophys.* 44(04):467-518.

228. Neudecker P*, et al.* (2012) Structure of an intermediate state in protein folding and aggregation. *Science* 336(6079):362-366.

229. Tóth G, Murphy RF, & Lovas S (2001) Stabilization of local structures by π–CH and aromatic–backbone amide interactions involving prolyl and aromatic residues. *Protein Eng.* 14(8):543-547.

230. Tóth G, Watts CR, Murphy RF, & Lovas S (2001) Significance of aromatic-backbone amide interactions in protein structure. *Proteins: Struct., Funct., Bioinf.* 43(4):373-381.

231. Shi Z, Olson CA, & Kallenbach NR (2002) Cation−π interaction in model α-helical peptides. *J. Am. Chem. Soc.* 124(13):3284-3291.

232. Gallivan JP & Dougherty DA (2000) A computational study of cation−π interactions vs salt bridges in aqueous media: implications for protein engineering. *J. Am. Chem. Soc.* 122(5):870-874.

233. Ma JC & Dougherty DA (1997) The cation−π interaction. *Chem. Rev.* 97(5):1303-1324.

234. Tsuzuki S, Honda K, Uchimaru T, Mikami M, & Tanabe K (2000) Origin of the attraction and directionality of the NH/π interaction: comparison with OH/π and CH/π interactions. *J. Am. Chem. Soc.* 122(46):11450-11458.

235. Motohiro Nishio MH, Yoji Umezawa (1998) *The CH/π Interaction. Evidence, Nature, and Consequences* (Wiley).
236. Ganguly HK, Majumder B, Chattopadhyay S, Chakrabarti P, & Basu G (2012) Direct evidence for CH···π interaction mediated stabilization of Pro-*cis*Pro bond in peptides with Pro-Pro-aromatic motifs. *J. Am. Chem. Soc.* 134(10):4661-4669.
237. Umezawa Y, Tsuboyama S, Takahashi H, Uzawa J, & Motohiro (1999) CH/π interaction in the conformation of peptides. A database study. *Bioorg. Med. Chem.* 7(9):2021-2026.
238. Tóth G, Murphy RF, & Lovas S (2001) Investigation of aromatic-backbone amide interactions in the model peptide Acetyl-Phe-Gly-Gly-N-Methyl amide using molecular dynamics simulations and protein database search. *J. Am. Chem. Soc.* 123(47):11782-11790.

Appendix

Chemical shift values in some representative oxo, thioxo and selenoxo peptides.

Notes:

1. Chemical shifts values are in ppm; 2. Values from the phenyl ring are listed in "other H" or "other C" in the order H(2)/H(3)/H(4) for δ-^{1}H and C(1)/C(2)/C(3)/C(4) for δ-^{13}C. 3. All spectra are collected in 33 mM phosphate buffer (pH 6.5) at 20 °C except for those with other statements.

Table App1. Bz-Val-Gly-Ala-Ala-OMe.

residue	HN	CO	H$_\alpha$	C$_\alpha$	H$_\beta$	C$_\beta$	other H	other C
Bz		174.4					7.78/7.52/7.63	135.7/130.1/131.4/135.1
Val^1	8.64	177.4	4.28	63.6	2.20	32.5	1.06/1.03	20.9/21.1
Gly^2	8.84	173.8	3.96	45.2				
Ala^3	8.24	177.5	4.31	52.3	1.39	19.2		
Ala^4	8.55	177.7	4.39	51.5	1.41	18.6		
Me			3.71	55.5				

Table App2. Bz-Val-Gly-Ala-ψ[CS−NH]Ala-OMe.

residue	HN	CO	H$_\alpha$	C$_\alpha$	H$_\beta$	C$_\beta$	other H	other C
Bz		174.3					7.78/7.52/7.62	135.7/130.1/131.4/135.0
Val^1	8.63	177.4	4.28	63.5	2.20	32.5	1.06/1.02	20.8/21.1
Gly^2	8.84	173.5	3.96	45.3				
Ala^3	8.33	208.9 (C=S)	4.68	58.0	1.44	22.8		
Ala^4	10.20	176.6	4.84	57.3	1.52	18.1		
Me			3.71	55.6				

Table App3. Bz-Val-Gly-Ala-ψ[CSe–NH]Ala-OMe.

residue	HN	CO	H$_\alpha$	C$_\alpha$	H$_\beta$	C$_\beta$	other H	other C	Se
Bz		174.3					7.79/7.53/7.63	135.8/130.1/131.4/135.2	
Val[1]	8.64	177.3	4.30	63.6	2.21	32.6	1.06/1.03	20.9/21.2	
Gly[2]	8.85	173.4	3.98	45.4					
Ala[3]	8.40	215.3 (C=Se)	4.70	60.8	1.43	22.9			387.5
Ala[4]	10.89[a]	175.8	4.95	60.1	1.58	18.1			
Me			3.73	55.7					

[a] Value determined in 50 mM sodium acetate buffer at pH 6.0.

Table App4. Bz-Val-Gly-Ala-Phe-OMe.

residue	HN	CO	H$_\alpha$	C$_\alpha$	H$_\beta$	C$_\beta$	other H	other C
Bz		174.3					7.78/7.52/7.62	135.7/130.1/131.3/135.2
Val[1]	8.62	177.4	4.28	63.5	2.21	32.5	1.06/1.03	20.8/21.0
Gly[2]	8.78	173.7	3.93	45.1				
Ala[3]	8.18	177.3	4.25	52.3	1.26	19.2		
Phe[4]	8.45	175.9	4.70	56.8	3.21/3.04	39.1	7.24/7.33/7.28	138.9/131.9/131.4/129.8
Me			3.70	55.5				

Table App5. Bz-Val-Gly-Ala-ψ[CS–NH]Phe-OMe.

residue	HN	CO	H$_\alpha$	C$_\alpha$	H$_\beta$	C$_\beta$	other H	other C
Bz		174.4					7.78/7.52/7.62	135.8/130.1/131.4/135.1
Val[1]	8.61	177.3	4.30	63.5	2.20	32.6	1.06/1.03	20.8/21.1
Gly[2]	8.79	173.3	3.93	45.3				
Ala[3]	8.28	209.1 (C=S)	4.63	58.3	1.35	22.6		
Phe[4]	10.06	175.1	5.30	62.2	3.33/3.23	38.4	7.25/7.33/7.29	138.7/131.9/131.4/129.9
Me			3.69	55.6				

Table App6. Bz-Val-Gly-Ala-ψ[CSe–NH]Phe-OMe.

residue	HN	CO	H$_\alpha$	C$_\alpha$	H$_\beta$	C$_\beta$	other H	other C	Se
Bz		174.3					7.79/7.52/7.63	135.7/130.1/131.3/135.2	
Val[1]	8.62	177.4	4.31	63.5	2.21	32.7	1.06/1.03	20.9/21.2	
Gly[2]	8.80	173.2	3.94	45.3					
Ala[3]	8.33	215.5 (C=Se)	4.66	60.9	1.35	22.7			391.1
Phe[4]	10.74[a]	174.2	5.45	65.2	3.40/3.28	38.4	7.27/7.34/7.28	138.3/131.9/131.5/129.9	
Me			3.71	55.7					

[a] Value determined in 50 mM sodium acetate buffer at pH 6.0.

Table App7. Bz-Val-Gly-Ala-Pro-OMe with Pro[4] in *trans* conformation.

residue	HN	CO	H$_\alpha$	C$_\alpha$	H$_\beta$	C$_\beta$	other H	other C
Bz		174.4					7.79/7.53/7.63	135.7/130.0/131.3/135.1
Val[1]	8.64	177.3	4.27	63.6	2.20	32.5	1.06/1.03	20.9/21.1
Gly[2]	8.82	173.5	3.97	45.0				
Ala[3]	8.23	175.7	4.61	50.5	1.37	18.0		
*trans*Pro[4]	---	177.4	4.47	62.2	2.30/2.01	31.3	2.03/3.80/3.68	27.3/50.2
Me			3.74	55.7				

Table App7'. Bz-Val-Gly-Ala-Pro-OMe with Pro[4] in *cis* conformation.

residue	HN	CO	H$_\alpha$	C$_\alpha$	H$_\beta$	C$_\beta$	other H	other C
Bz		174.4					7.79/7.53/7.63	135.7/130.0/131.3/135.1
Val[1]	8.64	177.3	4.27	63.6	2.20	32.5	1.06/1.03	20.9/21.1
Gly[2]	8.82	173.5	3.97	45.0				
Ala[3]	8.13	175.6	4.52	50.1	1.29	19.2		
*cis*Pro[4]	---	*177.5*	4.76	62.3	2.33/2.24	33.4	1.98/1.88/3.61/3.47	24.3/49.8
Me			3.74	55.7				

Table App8. Bz-Val-Gly-Ala-ψ[CS–N]Pro-OMe with Pro[4] in *trans* conformation.

residue	HN	CO	H_α	C_α	H_β	C_β	other H	other C
Bz		174.3					7.79/7.52/7.63	135.7/130.2/131.4/135.1
Val[1]	8.63	177.2	4.31	63.5	2.20	32.6	1.06/1.03	20.9/21.2
Gly[2]	8.84	173.0	3.96	45.4				
Ala[3]	8.37	205.2 (C=S)	4.90	55.1	1.39	21.4		
*trans*Pro[4]	---	176.0	4.91	69.1	2.37/2.14	31.0	2.16/4.02/3.91	27.3/54.3
Me			3.72	55.7				

Table App8'. Bz-Val-Gly-Ala-ψ[CS–N]Pro-OMe with Pro[4] in *cis* conformation.

residue	HN	CO	H_α	C_α	H_β	C_β	other H	other C
Bz		174.3					7.79/7.52/7.63	135.7/130.2/131.4/135.1
Val[1]	8.63	177.2	4.31	63.5	2.20	32.6	1.06/1.03	20.9/21.2
Gly[2]	8.84	173.0	3.96	45.4				
Ala[3]	8.12	204.5 (C=S)	4.77	54.6	1.33	23.0		
*cis*Pro[4]	---	175.1	5.07	65.7	2.43/2.38	33.5	2.07/1.96/3.98/3.72	24.3/57.6
Me			3.75	56.3				

Table App9. Bz-Val-Gly-Ala-ψ[CSe–N]Pro-OMe with Pro[4] in *trans* conformation.

residue	HN	CO	H_α	C_α	H_β	C_β	other H	other C	Se
Bz		174.3					7.79/7.53/7.63	135.8/130.1/131.3/135.0	
Val[1]	8.63	177.2	4.32	63.4	2.20	32.5	1.06/1.03	20.9/21.1	
Gly[2]	8.85	173.0	3.97	45.4					
Ala[3]	8.44	210.9 (C=Se)	4.84	57.5	1.36	21.4			455.0
*Trans*Pro[4]	---	175.1	4.97	72.4	2.40/2.18	30.8	2.24/2.19/3.89/3.84	27.2/55.5	
Me			3.73	55.7					

Table App9'. Bz-Val-Gly-Ala-ψ[CSe–N]Pro-OMe with Pro[4] in *cis* conformation.

residue	HN	CO	H$_\alpha$	C$_\alpha$	H$_\beta$	C$_\beta$	other H	other C	Se
Bz		174.3					7.79/7.53/7.63	135.8/130.1/131.3/135.0	
Val[1]	8.64	177.1	4.35	63.3	2.22	32.6	1.06/1.03	20.9/21.1	
Gly[2]	8.89	172.0	4.00/3.89	45.4					
Ala[3]	8.15	209.6 (C=Se)	4.71	56.9	1.31	23.3			469.0
*cis*Pro[4]	---	173.9	5.03	66.6	2.44	33.4	2.10/2.01/3.99/3.71	24.1/61.3	
Me			3.76	56.2					

Table App10. Ac-Gly-Ala-ψ[CSe–NH]Ala-OMe.

residue	HN	CO	H$_\alpha$	C$_\alpha$	H$_\beta$	C$_\beta$	Se
Ac		174.3					
Gly[1]	8.39	173.7	3.93	45.3			
Ala[2]	8.53	215.3 (C=Se)	4.72	60.7	1.44	22.8	380.8
Ala[3]	10.94	175.7	4.99	60.4	1.59	18.1	
Me			3.76	55.7			

Table App11. Bz-Val-Gly-Ala-Phe-ψ[CSe–NH]Ala-OMe [a].

residue	HN	CO	H$_\alpha$	C$_\alpha$	H$_\beta$	C$_\beta$	other H	other C
Bz		174.2					7.77/7.50/7.61	130.0/131.3/135.1/135.6
Val[1]	8.62	177.2	4.32	63.4	2.20	32.7	□1.05/1.02	20.8/21.1
Gly[2]	8.77	173.1	3.95/3.87	45.2				
Ala[3]	8.37	215.3 (C=Se)	4.69	61.9	1.35	22.7		
Phe[4]		174.0	5.09	66.6	3.27	39.2	7.24/7.35/7.30	131.7/131.5/130.0/138.0
Ala[5]	8.56	180.3	4.10	52.2	1.13	19.0		
NH$_2$	7.41/7.16							

[a] Spectra were collected in 20 mM Gly-NaOH buffer (pH 7.0) at 20 °C.

Table App11'. Bz-Val-Gly-Ala-Phe-ψ[CSe–NH]Ala-OMe [a].

residue	HN	CO	H$_\alpha$	C$_\alpha$	H$_\beta$	C$_\beta$	other H	other C
Bz							7.74/7.47/7.58	130.0/131.4/135.1
Val[1]			4.28	63.4	2.16	32.8	1.01/0.98	20.8/21.1
Gly[2]			3.92/3.84	45.3				
Ala[3]			4.59	61.9	1.27	22.6		
Phe[4]			5.05	67.6	3.21	39.5	7.20/7.31/7.26	131.7/131.4/129.8
Ala[5]			4.09	52.2	1.12	19.1		
NH$_2$								

[a] Spectra were collected in 20 mM Gly-NaOH buffer (pH 9.0) at 20 °C.

Table App12. Ac-Val-Ala-ψ[CS–NH]Phe-Gly-Gly-Ala-ψ[CSe–NH]Phe-OMe [a].

residue	HN	CO	H$_\alpha$	C$_\alpha$	H$_\beta$	C$_\beta$	other H	other C
Ac			2.02	24.8				
Val[1]	8.22		4.21	62.1	2.13	32.7	0.92	21.7/20.3
Ala[2]	8.48		4.74	58.8	1.32	23.1		
Phe[3]	9.80		5.35	62.3	3.41/.3.25	39.2	7.30/7.27/7.21	131.9/130.8/129.1
Gly[4]	8.30		3.95.3.90	45.4				
Gly[5]	8.11		3.93/3.79	45.1				
Ala[6]	8.17		4.86	60.2	1.36	23.7		
Phe[7]	10.94		5.38	65.2	3.31	38.7	7.31/7.31/7.25	131.9/130.8/129.1
OMe			3.68	54.6				

[a] Spectra were collected in DMF solution.

Acknowledgements

First, I would like to give my deepest gratitude to my supervisor Prof. Dr. Gunter Fischer, for giving me the chance to work on this interesting project "selenoxo peptide chemistry" in Max Planck Research Unit for Enzymology of Protein Folding. Your unflagging enthusiasm and conscientious attitude on science have inspired me immensely and will be of great benefit to my whole career.

I also thank Dr. Günther Jahreis for your leading to the selenoxo peptide synthesis and for your kind help on my work and my life in the last four years. You are always available when I need any help.

I am grateful to Dr. Christian Lücke for your work on NMR experiments, for your intensive discussion on the NMR analysis of the chalcogen-substituted peptides and for your precious time and effort to carefully read and correct my thesis. It cannot be completed without your help.

I would like to acknowledge Dr. Dirk Wildemann for your help on the photoswitching experiments, and Dr. Angelika Schierhorn and Christina Gersching for measuring mass spectra. I also thank Suzanne Roß and Dirk Tänzler for providing hCyp18.

I greatly appreciate Alexander Rentzsch for your academic discussion and kind help in the lab and my life. I also appreciate Ilona Kunze, Birgit Hökelmann and other members in the chemical group for your help in the lab and for sharing of happy time.

I am grateful to Dr. Christian Beyer and Jean-Philippe Demers for carefully reading this thesis.

I greatly appreciate my colleagues in Max Planck Research Unit for Enzymology of Protein Folding for your help, friendship and providing a heart-warming environment to a foreigner.

I thank my friends Miaomiao Shi, Qi Zhang, Jun Li, Xueqin Zeng and Yang Yang for your company and friendship.

Last, but not least, I would like to give infinite thanks to Guohua Lv and my parents for your love and understanding.

Curriculum Vitae

Personal data

Name	Yun Huang
Date and place of birth	June 13, 1982, Ganzhou, China
Email	huangy2005@gmail.com

Education and Position

10/2008 –	**Max Planck Research Unit for Enzymology of Protein Folding**, Halle(Saale) Germany PhD candidate in Biochemisty Supervisor: Prof. Gunter Fischer Dissertation: *Selenoxo Modulation of Oligopeptide Backbone: Synthesis, Photoisomerization and Electronic Effects*
9/2005 – 7/2008	**Lanzhou University**, Lanzhou, China M.S. in Biochemistry and Molecular Biology Supervisor: Prof. Shouliang Dong Thesis: *A Photoswitchable Thioxo Analog of Insect Kinin: Synthesis, Characterization, and Conformation-Activity Relation-ship Study*
4/2004 – 9/2005	**Hangzhou Jiuyuan Gene Engineering Co., Ltd**, Hangzhou, China Technician for Protein Renaturation and Purification
8/2002 – 8/2003	**Yingcai High School**, Nanchang, China Biology Teacher.
9/1999 – 7/2002	**Jiangxi Institute of Education**, Nanchang, China College Diploma in Biotechnology
9/1996 – 7/1999	**Ganxian Middle School**, Ganzhou, China

Publications Related to This Dissertation

1. ***Yun Huang***, Günther Jahreis, Christian Lücke, Dirk Wildemann, Gunter Fischer*. Modulation of the Peptide Backbone Conformation by the Selenoxo Photoswitch. ***J. Am. Chem. Soc.*** 2010, **132**: 7578–7579.

2. ***Yun Huang***, Günther Jahreis, Gunter Fischer*, Christian Lücke*. Atomic Polarizability Dominates the Electronic Properties of Peptide Bonds upon Thioxo and Selenoxo Substitution. ***Chem. Eur. J.*** 2012, **18**: 9841–9848. (*Selected as VIP article*)

3. ***Yun Huang***, Günther Jahreis, Christian Lücke, Gunter Fischer*. Rapid Nitrogen Inversion Pathway in the *cis/trans* Isomerization of Selenoxo Peptide Bonds. ***Chem. Eur. J.*** *Under review*

4. ***Yun Huang***, Christian Lücke, Günther Jahreis, Gunter Fischer*. Multiple Photocontrol of *cis*/*trans* Isomerization by Thioxo and Selenoxo Dual Modification. *In preparation*

Posters

1. ***Yun Huang***. One Atom (O→Se) Substitution on Peptide Bond: Synthesis and Properties Focusing on Photoisomerization and Tautomerization. In *EMBO Conference Series-Chemical Biology 2010*. 22-25 Septermber 2010. EMBL Heidelberg, Germany.

Eidesstattliche Erklärung

Hiermit erkläre ich, dass ich die vorliegende Arbeit selbstständig und ohne fremde Hilfe verfasst sowie keine anderen als die angegebenen Quellen und Hilfsmittel benutzt habe. Die den benutzten Werken wörtlich oder inhaltlich entnommenen Stellen wurden als solche von mir kenntlich gemacht.

Halle, den 30.10.2012

Yun Huang